DOI: 10.14750/ME.2022.010

Ph.D. Dissertation

Edina Reizer

2021

DOI: 10.14750/ME.2022.010

Témavezetői ajánlás

Edina Reizer

Growth Mechanisms of Polycyclic Aromatic Hydrocarbon –
A Case Study of Benzo(a)pyrene

című PhD értekezéséhez

Örülök annak, hogy az utóbbi nagyjból négy év során egy kiemelkedően szorgalmas és érdeklődő doktorjelölttel, Reizer Edinával dolgozhattam együtt. A Miskolci Egyetemen végzett doktori tanulmányai során policiklikus aromás szénhidrogének (PAH-ok) különböző reakcióit vizsgálta számítógépes kémiai módszerek segítségével. A PAH-ok komoly globális problémát jelentenek számos különféle káros hatásuk miatt, s ezért Edina kutatási eredményei nem csak a szűk tudományos közösség, hanem mindenki számára érdekesek és hasznosak lehetnek.

Edina sikeresen meghatározta az ún. „parent" PAH-ok növekedési mechanizmusainak kezdőpontjait. Továbbá sikerült feltárnia egy erősen rákkeltő PAH, a benzo(a)pirén képződésének elemi lépéseit. A doktori témájából eddig összesen három első szerzős közlemény (ezek közül egy D1, egy Q1, egy pedig Q2-es minősítésű) került elfogadásra egy további pedig beküldés előtt áll. Számos hazai és nemzetközi konferencián is bemutatta eredményeit, amelyek közül kiemelném a *Visegrad Symposium on Structural System Biology*-t, ahol 2019-ban a legjobb poszternek járó díjat is kiérdemelte.

Minden eredmény, amelyek Edina publikációiban és a doktori értekezésében közlésre kerültek, illetve a tézisek között olvashatók, az Ő saját eredményei, és önálló tudományos munkáját fémjelzik. A közös munka nem volt zökkenőmentes és sok esetben ütköztünk nehézségekbe, de ezeket sikerült együtt legyűrnünk és Edina megmutatta, hogy kutatóként megállja a helyét. Nem csak motivált és lelkiismeretes, hanem képes hatékonyan együtt dolgozni másokkal. Témavezetőként is elkezdte szárnyait bontogatni, s bízom benne, hogy ezt a készséget is tökélyre tudja fejleszteni.

Mindezek alapján kijelenthetem, hogy Reizer Edina doktorjelölt alkalmas önálló kutatási tevékenység végzésére és javaslom számára a PhD fokozat odaítélését.

Miskolc, 2021. november 3.

Dr. Fiser Béla

DOI: 10.14750/ME.2022.010

Growth Mechanisms of Polycyclic Aromatic Hydrocarbons – A Case Study of Benzo(a)pyrene

Ph.D. Dissertation

Edina Reizer

Supervisor:
Dr. Béla Fiser

Antal Kerpely Doctoral School of Materials Science & Technology at the Faculty of Materials Science & Engineering

Institute of Chemistry
University of Miskolc

2021

DOI: 10.14750/ME.2022.010

Preface

The undeclared purpose of the industrial society was that everything we can produce manually we should manufacture in huge quantity irrespectively of how much waste we are producing at the same time. Similarly, we should burn everything possible irrespectively of how many chemical compounds we produce, even if they are extremely dangerous to the environment as well as to human beings. The present work is dedicated to the thorough study of the reaction mechanisms of cancer-causing polycyclic aromatic hydrocarbons that are formed during incomplete combustion.

DOI: 10.14750/ME.2022.010

Table of Contents

DOI: 10.14750/ME.2022.010

DOI: 10.14750/ME.2022.010

Acknowledgment/ Köszönetnyilvánítás

This research was supported by the European Union and the Hungarian State, co-financed by the European Regional Development Fund in the framework of the GINOP-2.3.4-15-2016-00004 project, which aimed to promote the cooperation between the higher education and the industry. The GITDA (Governmental Information-Technology Development Agency, Hungary) is gratefully acknowledged for allocating computing resources used in this work.

Ez a dolgozat nem jöhetett volna létre, ha nincs egy olyan remek témavezetőm mint *Dr. Fiser Béla*, ezért elsősorban neki szánom köszönetemet. Amellett, hogy azonnal elvállalta a témavezetésemet, nyitottsággal, jókedvvel és főleg kreatívitással vezetett be a számítógépes kémia elbüvölő világába. Köszönöm, hogy mind a szakmai, mind a személyes kérdések megválaszolásában mentorom volt. Hálás vagyok a törődésért és a figyelemért, amelyeket nyújtott az évek során, valamint azért, hogy velem együtt örült a sikereimnek. Türelmes magyarázatait és bátorító szavait biztosan magammal viszema szakmai pályámon.

Köszönöm *Dr. Viskolcz Bélának*, hogy a Kémiai Intézet legelfoglaltabb embereként is időt szánt a kutatásomra és végig támogatta a doktori munkámat.

Hálás a szívem, amiért sikerült megismernem a reakciómechanizmusok atyját Dr. Csizmadia Imre Gyulát. Köszönöm a személyes és virtuális konzultációkat egyaránt valamint azt, hogy ha bármilyen nehézségbe ütköztem egy reakciók kapcsán, ő azonnal segített. Örök bölcsességeivel és a jövőről alkotott elméleteivel igazán gazdagította nézeteimet.

Köszönöm a *Kémiai Intézet dolgozóinak*, hogy befogadtak és a legszürkébb hétköznapokban is vidám és kedves hangulatot teremtettek. Nekik köszönhetően egy csodálatos környezetben dolgozhattam, okos és nyitott emberekkel magam körül.

Köszönöm *Zsuzsa* vidámságát, *Gábor* főztjeit, *Jutka* segítőkészségét és *Laci* vidám köszöneseit. Hálás vagyok, doktorandusz társaimnak *Zsófinak*, *Zsanettnek* és *Rachidnak*,

DOI: 10.14750/ME.2022.010

a tudományos beszélgetésekért, a társasjátékos programokért és hogy ott voltak, amikor baráti tanácsra volt szükségem.

Szeretnék köszönetet mondani a *Tüzeléstani Intézet dolgozóinak*, amiért a doktori tanulmányaim első évében lelkesen mutatták be a Műszaki Anyagtudományi Kart. Köszönöm, hogy támogattak, segítettek, hasznos szakmai és baráti tanácsokkal láttak el.

Ezúton szeretném megköszönni a szüleimnek *Reizer Ferencnek* és *Reizer Ildikónak*, a nővéremnek *Hanus-Reizer Helgának* és *családjának,* az én drága unokahúgomnak *Hanus Natalienak*, *nagyszüleimnek*, *keresztszüleimnek* és *unokatestvéreimnek*, hogy távollétemben támogattak, finom ételekkel elláttak, aggódtak és mindig szeretettel vártak haza. Hálás vagyok az értem elmondott imákért és a lelkierőért, amelyet távollétemben nyújtottak. Remélem büszkék rám.

Utoljára de nem utolsó sorban, szeretném hálámat kifejezni jegyesemnek Belza Róbertnek, a Miskolcon eltöltött évekért. Köszönöm, hogy csatlakozott hozzám, hogy őszinte társként támogatott és jóban-rosszban mellettem állt.

List of Figures

DOI: 10.14750/ME.2022.010

List of Tables

DOI: 10.14750/ME.2022.010

1. Introduction

In the 18th century, the use of communal and industrial energy resulted in rapid economic growth that culminated in the 21st century and led to advanced infrastructure and a high standard of living. A primary goal of humankind is facilitating and ensuring the sustainable well-being of successive generations. This goal is closely linked to the concept of sustainable development, the first principle of which, according to the Bruntland Commission [1], is meeting the needs of the present without hindering future generations from being able to fulfill their own needs. Everyday modern existence relies on energy-centric needs, and meeting those needs is essential. The balance of energy supply is governed by the rules of economic and energy policy, but the unequal distribution of energy sources is a consequence of the alternation of natural and geological times. In recent decades, a huge proportion of the energy demand has been provided by fossil fuels, although the use of unconventional energy reserves has also been increasing. At present, however, the vast majority of global energy consumption is still covered by oil, gas, and coal assets. At this point, the second principle of sustainable development should be mentioned, according to which energy supply must be provided without depleting the environment and minimizing pollution. Thus, conscious and environmentally friendly management of energy supplies must be the top priority of all human activities. However, during the thermal decomposition of carbon-based energy sources, countless pollutants are formed, and thus, enter all spheres of our environment, causing innumerable problems. Among these, air pollution represents the leading health and environmental risk factor, estimated to cause between four to nine million deaths globally [2] and which results in such worrying effects as global warming, climate change, acid rain, or smog. In the background of these effects, complicated chemical processes take place, resulting in the formation of countless harmful compounds. The present doctoral dissertation contributes to the understanding of the formation processes of such harmful species, with the investigation of the reaction mechanisms of highly carcinogenic

benzo(a)pyrene, and with the research made on the reaction initiation points of polycyclic aromatic hydrocarbons.

1.1. Polycyclic Aromatic Hydrocarbons

Polycyclic aromatic hydrocarbons (PAHs) consist of a set of several thousand ubiquitous pollutants in the environment and belong to the persistent organic pollutants (POPs) class [3]–[5]. Their structure is composed of multiple aromatic rings, with a pair of carbon atoms shared between them [6]. PAHs are formed during the incomplete combustion of organic material, thus, they can be emitted during natural processes like forest fires and volcanic eruptions [7], [8]. However, the most predominant emissions originate from anthropogenic activities such as biomass burning, coke production, thermal industrial processes, vehicle use, waste burnings, *etc.* [9]–[13]. The mutagenic and teratogenic effects of PAHs are thoroughly proven. They can react with DNA, inducing thereby mutations in the lung, liver, and skin [14], [15]. An essential feature of PAHs is that they play an important role in the formation of combustion-generated particles. They are considered precursors for soot, initiating the soot formation by their inception and through their further reactions (**Figure 1** Schematic representation of soot formation.)[16]–[21][22]. Nevertheless, PAHs with lower vapor pressure can reside in a significant amount of fine air particulate matter, ($PM_{2.5}$) which can penetrate human lungs, causing problems in the respiratory system [3], [23].

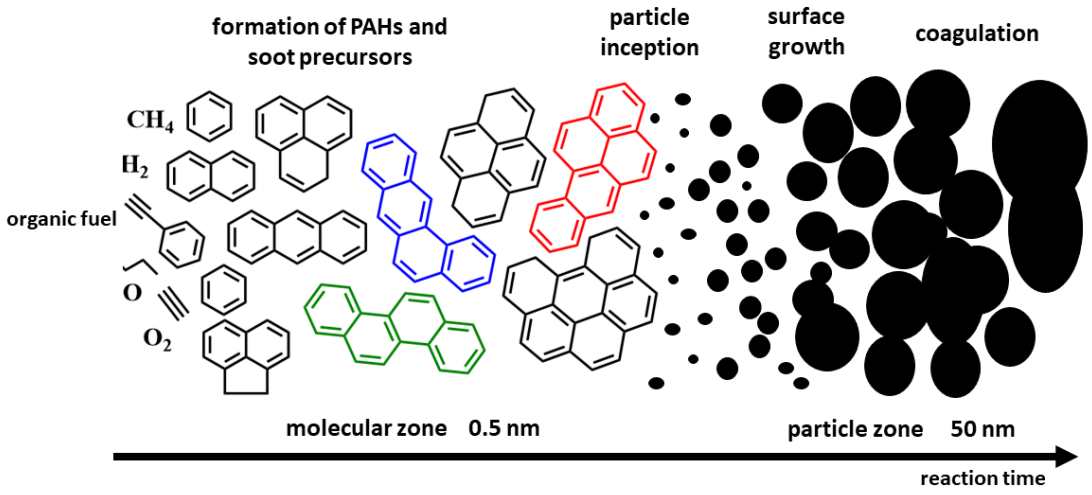

Figure 1 *Schematic representation of soot formation.*

DOI: 10.14750/ME.2022.010

The continuous production/emission of PAHs represents a constant concern to people's health [24], [25]. The first challenge in the task to reduce or to predict the combustion generated soot emission is to model correctly the PAH chemistry [18]. The monitoring of polycyclic aromatic hydrocarbons in the environment started more than 40 years ago with the appearance of a list of 16 priority PAHs, (often called "parent PAHs", Error! Reference source not found.) issued by the U.S. Environmental Protection Agency (EPA) in 1976 [26], [27]. Up until now, the parent PAH molecules are regarded by researchers as being representatives for all the PAHs.

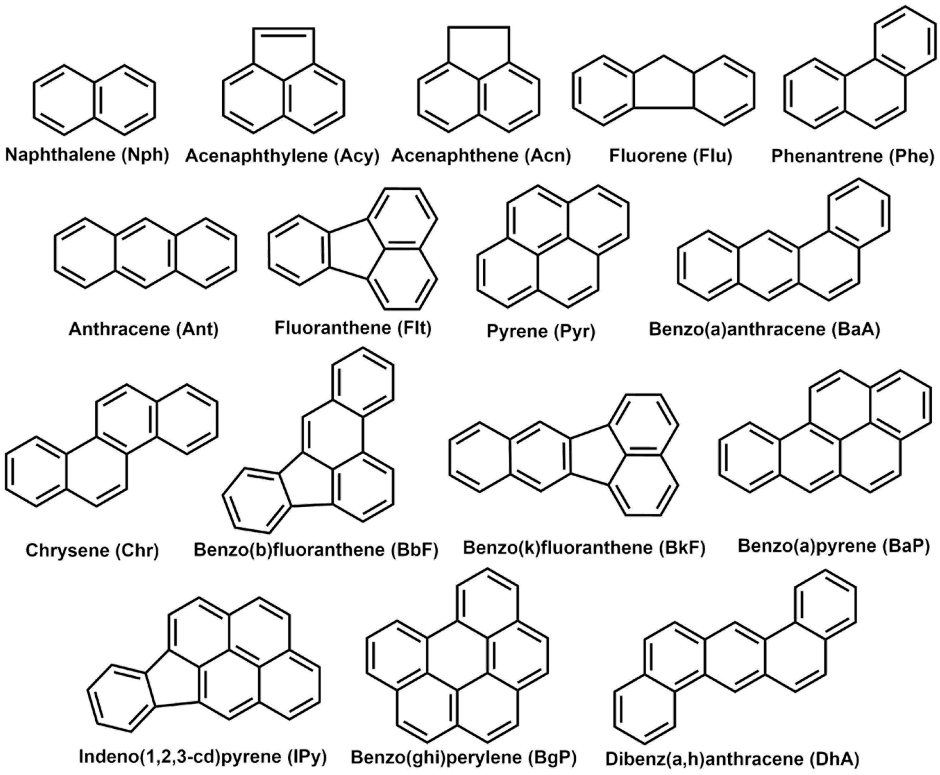

Figure 2 *2D representation of the 16 priority PAHs or "parent PAHs".*

However, some recent studies strongly suggest further modification of the list to be able to cover the wide range of polycyclic aromatic components that occur in any studied samples [28]–[30]. These 16 PAHs have different carcinogenic properties [23], [25], [31], [32]. In general, the carcinogenic potency of PAHs increases with the number of aromatic rings [33]–[35]. Benzo[a]pyrene (BaP) is one of the most carcinogenic PAHs among the priority PAHs and it has been identified by the International Agency for Research on Cancer as a class I carcinogen [36]. BaP, therefore, is chosen as an indicator of PAHs pollution, and other PAHs are ranked according to cancer potency, relative to BaP, using

the toxic equivalence factor [33], [37]. The priority PAHs have also been included in the Convention of Long-range Transboundary Air Pollution Protocol on Persistent Organic Pollutants [38]. The global total annual atmospheric emission of the 16 PAHs in 2007 was 504 Gg [39]. Shen *et al*., in their simulational work revealed that from 2009 to 2030 the PAH emissions in developed and developing countries would decrease by 46–71% and 48–64%, respectively [39]. Although the global emission of the parent PAHs is in a slightly descending trend, their emission quantity is still too large. Because of the different energy-producing technology systems of the countries, the dominant PAH emission sources are also different. Over 80% of the emission has been attributed to developing countries and more than half has originated from biomass and coal burning. However, emissions in developed regions are significant as well, having the combustion of motor fuels in means of transportation and domestic and industrial heating systems as major sources [39]. PAHs have strong relevance in astrochemical and astrophysical studies as well since they are linked for being the source of unidentified infrared emission bands (UIR) (3.3, 6.2, 7.7, 8.6, 11.3, and 12.7 μm) detected in planetary nebulae (NGC 7027; BD+30°3639) and external galaxies (M82) [40], [41] and in diffuse interstellar bands (DIBs), whose absorption features are seen in the spectra of reddened stars throughout the Galaxy extending from the ultraviolet region to near-infrared [42]–[44]. Moreover, ≲15% of the interstellar carbon and up to 20% of the total infrared emission of the Milky Way and star-forming galaxies is attributed to PAHs [45], [46]. Thus, the presence of both peri-condensed (pyrene, benzo(ghi)perylene, coronene, *etc.*) and cata-condensed PAHs (phenanthrene, chrysene, pentacene, *etc.*) in space are supported by observational and laboratory experiments [47]–[49]. In this regard, PAHs are now recognized as essential components of the interstellar medium (ISM – space between stars) of the Milky Way and external galaxies and play an important role in many aspects of astrophysics (*i.e.* starlight absorption) [45]–[48], [50].

Even though PAHs consists of numerous aromatic rings, the formation of the first aromatic ring (benzene, phenyl) is also important and under continuous discussion within the scientific community and thus, numerous formation mechanisms are

DOI: 10.14750/ME.2022.010

proposed based on experimental and computational studies, involving several different reactants and reaction mechanisms [51]–[57] (Error! Reference source not found.).

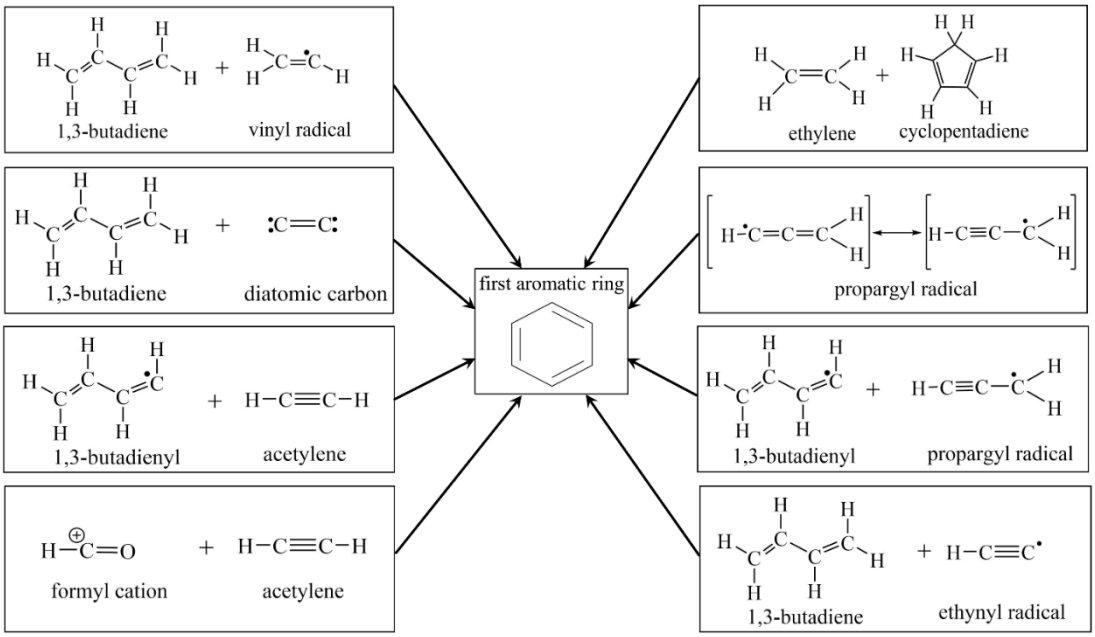

Figure 3 *The most well-known reactant pairs involved in the formation of the first aromatic ring of PAHs.*

The most well-known reactions leading to the formation of the first aromatic ring of the PAH structure are the following:

- the reaction of vinyl radical ($^{\bullet}C_2H_3$) and 1,3-butadiene (1,3-C_4H_6) followed by hydrogen elimination [51]
- reaction between propargyl ($^{\bullet}C_3H_3$) and 1,3-butadienyl [52]
- the reaction of 1,3-butadienyl radical (1,3-$^{\bullet}C_4H_5$) with acetylene (C_2H_2) followed by hydrogen elimination [53]
- the reaction between ethylene (C_2H_4) and cyclopentadiene (C_5H_6) [54]
- recombination of propargyl radicals ($^{\bullet}C_3H_3$) [55]
- ionization reactions between formyl cation (HCO^+) and acetylene (C_2H_2) [56]
- reaction between 1,3-butadiene (1,3-C_4H_6) and ethynyl ($^{\bullet}C_2H$) [56]
- the reaction of diatomic carbon ($^{\bullet}C_2$) with 1,3-butadiene (1,3-C_4H_6) [57]

After the formation of the first aromatic ring, the expansion of the structure occurs through various mechanisms and polycyclic aromatic structures develop. PAH formation and growth processes are highly dependent on the carbon source and the corresponding environmental conditions, and thus to understand the mechanisms, a complex approach

DOI: 10.14750/ME.2022.010

is inevitable within which all the important factors must be considered. In the following sections, the most important PAH formations are described and divided into groups based on the involved reactants, but various additional factors are also presented and discussed.

1.2. PAH Formation Mechanisms

In the last few decades, strong efforts have been made to create an appropriate model for the growth of PAHs, drawing numerous researchers to this topic from the fields of theoretical chemistry, environmental science, combustion chemistry, material science, cancer research, space chemistry, *etc.* [58]–[62]. In a general view of the history of PAH growth model development, researchers usually try to fill the blanks in the giant map of aromatic species. Various models are developed and validated with a large array of possible reactions due to the diversity of molecules and radicals that are present in significant concentrations in hydrocarbon flames [22]. This part is intended to provide a comprehensive picture of the already investigated growth mechanisms of PAHs, paying particular attention to those in which at least one of the 16 priority PAHs are formed or involved. It is also important to mention that all the presented reaction mechanisms have a "bottom-up" type of structure under which the growth of larger PAHs from smaller molecules is understood. However, in both astrophysical and combustion environments "top-down" PAH formation can also occur. The fragmentation of bulk amorphous carbon material by grain–grain collisions in interstellar shocks, or the oxidation-induced fragmentation of soot particles in thermal treatments are possible processes for "top-down" PAH formation [42], [63]–[65]. Almost all the proposed and studied reaction mechanisms and models for PAH growth and formation are summarized chronologically (**Figure 4** and **Figure 5**) from 1981 to 2021 [17], [21], [53], [58]–[61], [66]–[115]. Based on this huge set of literature data, it can be seen that experimental and theoretical studies are carried out and go hand in hand to understand PAH formation (**Figure 4** and **Figure 5**).

DOI: 10.14750/ME.2022.010

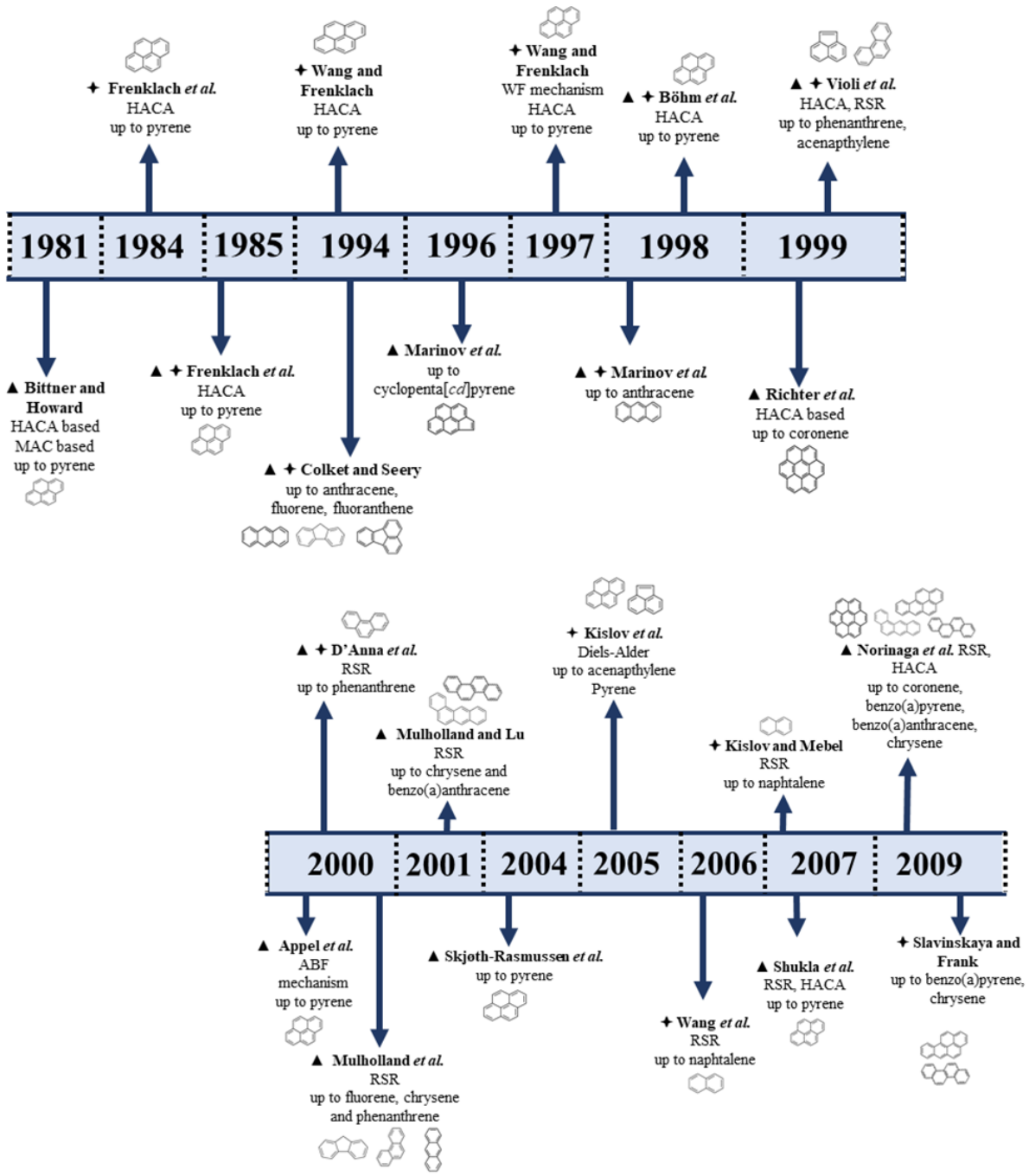

Figure 4 *Experimental (▲) and computational (✦) studies of polycyclic aromatic hydrocarbons (PAHs) published between 1981-2009.*

DOI: 10.14750/ME.2022.010

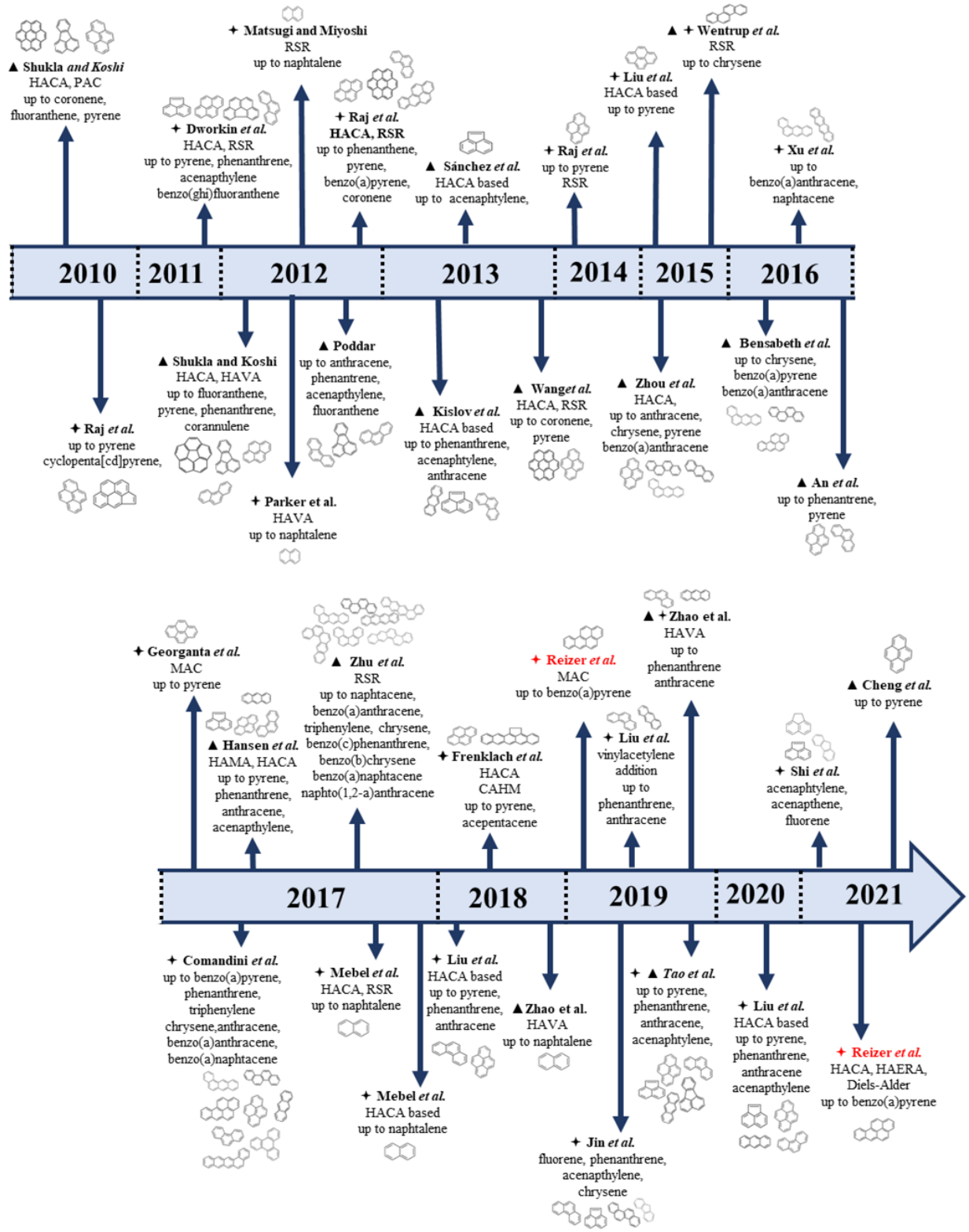

Figure 5 *Experimental (▲) and computational (✦) studies of polycyclic aromatic hydrocarbons (PAHs) published between 2010-2021.*

DOI: 10.14750/ME.2022.010

1.2.1 PAH formation mechanisms with acetylene (C_2H_2) additions

1.2.1.1. HACA - Hydrogen Abstraction and Acetylene or Carbon Addition

The most classical reaction mechanism for the growth of polycyclic aromatic hydrocarbons is hydrogen abstraction and acetylene or carbon addition (HACA). This mechanism was originally proposed by Frenklach *et al.* [53], [114] and represents a two-step process, which is based on the repetitive sequence of hydrogen abstraction, to activate the aromatic molecule, and on the subsequent acetylene (C_2H_2) addition to the radical site, formed in the hydrogen abstraction step (**Figure 6**).

The term „HACA" was introduced by Frenklach and Wang in 1990 [116]. The initial

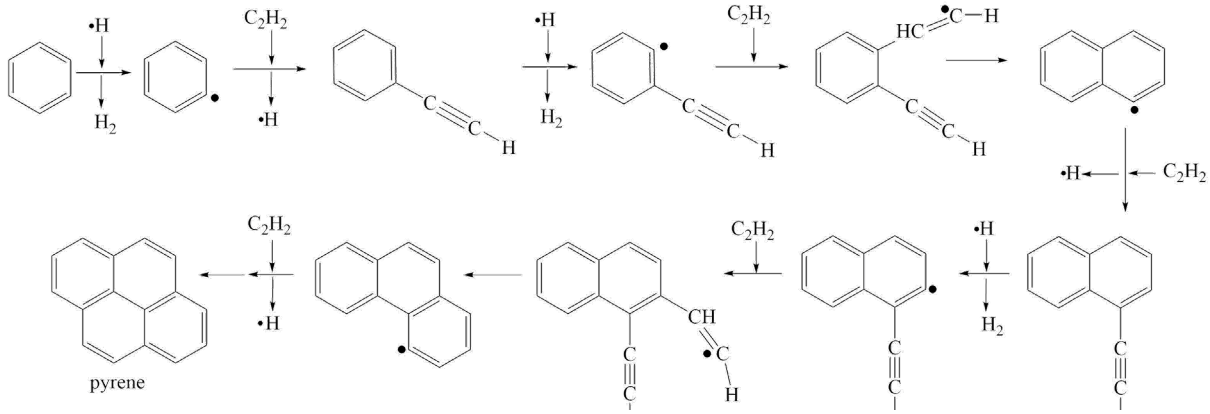

Figure 6 *Schematic representation of the hydrogen abstraction and acetylene or carbon addition (HACA) reaction.*

framework was proposed as a mechanism for pyrene and cyclopenta(cd)pyrene formation starting from benzene, and it was established to describe the further growth of PAHs in flames fueled by C_2 hydrocarbons (ethane, ethylene, and acetylene) [116]. Over the past few decades, the HACA mechanism has become a central topic among PAH growth processes, drawing increasing attention to it [88], [103], [117], [118]. One of the most significant observations regarding HACA is that it accelerates the formation of benzenoid PAHs, thus, it is associated with the contribution of the surface growth of soot mass through acetylene addition. The advantageous and also critical intrinsic feature of HACA is based on the accordance between reaction reversibility and kinetic driving force [119]. The low degree of reversibility in the acetylene addition step and the high reaction affinity of hydrogen atoms results in the continuous growth of PAHs. Furthermore, the reaction steps involved in HACA have relatively low reaction barriers and high

exothermicities. These facts explain why the energy barriers during the HACA reactions can be easily overcome [119]. For acetylene additions to PAH radicals, the predicted barriers are usually within ~8-30 kJ/mol and the exothermicities are ~120-160 kJ/mol, whereas the ring closure steps normally exhibit a barrier of ~8-20 kJ/mol and exothermic up to a range of ~125-200 kJ/mol [88]. The acetylene additions are also exergonic in the work of Reizer *et al.*, but the reactions are barrierless with ~70 kJ/mol energy release on average [120]. Nevertheless, the ring closures showed a barrier of ~22 kJ/mol on average which is very close to the previously mentioned values [88][120].

It is also important to mention that the basic reactant molecule of HACA, acetylene, is abundant in various types of aliphatic and aromatic flames such as methane, ethane, ethylene, dimethyl ether, phenylacetylene, heptane, gasoline mixtures, butadiene, butane, benzene, toluene, and also polymers [87], [121]–[127], which underlines its significance in PAH formation, and increases its chance of occurrence. The characteristics of the HACA mechanism are explored in numerous experimental and theoretical studies [88], [101], [128]–[130]. For instance, Peng *et al.* [128], studied the site effect on PAH formation in the HACA reaction framework and concluded that the H abstraction and C_2H_2 addition reactions on the ortho positions and armchair surface site are kinetically unfavorable (had relatively high energy barrier compared to other site options, such as zig-zag, free-edge, and armchair surface). An investigation of the PAH growth mechanisms under exhaust gas recirculation revealed that the HACA pathway should account for temperature effects on the formation [129]. The combustion of premixed ethylene-oxygen flame is also studied, and it is concluded that HACA controls the formation of PAHs in fuel-rich and pure pyrolytic conditions [71]. However, in the oxidative environment, resonantly stabilized radicals (RSR) have a central role [71]. It is important to mention that the investigations on HACA often led to distinctive and controversial results as well. The work of Parker *et al.* [130] on the reaction of 1- and 2-naphthyl radicals and acetylene at combustion-like temperatures showed that the dominant product via HACA is acenaphthylene, and not anthracene or phenanthrene. Mebel *et al.* [101] discussed the branching ratio of products in a benzene - acetylene

DOI: 10.14750/ME.2022.010

reaction system, and their results confirmed that naphthalene is the dominant product of the HACA framework over a wide temperature range. In addition, the work of Kislov *et al*. [88] showed that in the HACA mechanism, the five-membered ring growth on PAH molecules is more dominant than the six-membered. Similarly, the experimental results on acetylene pyrolysis of Shukla and Koshi [58] pointed out that the HACA products are mainly polyacetylenes, polyene derivatives, and cyclopentafused-PAHs (CP-PAHs). The speed of HACA is also an essential feature regarding the growth of aromatic compounds. According to the interpretation of some experimental investigations, if HACA is considered, the results underpredict the concentrations of PAHs in flames and it is considered slow, compared to the fast process of PAH formation [87]. This is also supported by the fact that during HACA, the mass of product species is increased by 24 atomic units (au), which comes from acetylene addition (+C_2H_2, +26) and hydrogen molecule elimination (-H_2, -2 au) (*e.g.* the formation of acenaphthylene ($C_{12}H_8$, 152 au) from naphthalene ($C_{10}H_8$, 128 au) or the formation of pyrene ($C_{16}H_{10}$, 202 au) from phenanthrene ($C_{14}H_{10}$, 178 au). Other similar reaction pathways to HACA are also proposed, such as the Bittner–Howard's process [113]. It is based on acetylene addition as well, but differs from HACA in the place of the addition of the second acetylene molecule, which is added to the first one to form a C_4H_4 chain, and leads to an additional ring by the subsequent ring closure (**Figure 7**).

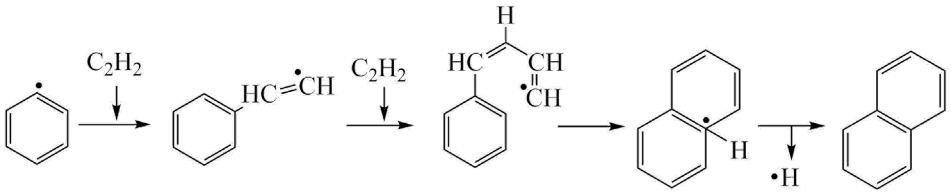

Figure 7 *Bittner–Howard's reaction route.*

However, the work of Mebel *et al.* [101] on the examination of naphthalene reaction mechanisms, revealed that the probability of the Bittner–Howard's reaction is greatly limited compared to the original HACA, due to the unlikely presence of unstable C_8H_7 radicals (**Figure 7**, second structure) in flames at high temperatures (1600 K and higher). All in all, since acetylene represents the most abundant hydrocarbon in the sooting regions of flames [131], studying its properties and reactions is crucial in the

understanding of PAH growth, and thus further research is inevitable regarding acetylene addition-based mechanisms.

1.2.1.2. Diels-Alder mechanism

Aromatic compounds are frequently synthesized in laboratories through Diels-Alder (DA) reactions [132]. In the traditional Diels-Alder process, butadiene is reacted with an olefin, which will lead to a cyclic compound. Morokuma has published a theoretical study on Diels-Alder-type reactions of acetylene and butadiene within which 1,4-cyclohexadiene is formed [133]. The same type of DA reaction can also occur between acetylene and a PAH (**Figure 8**).

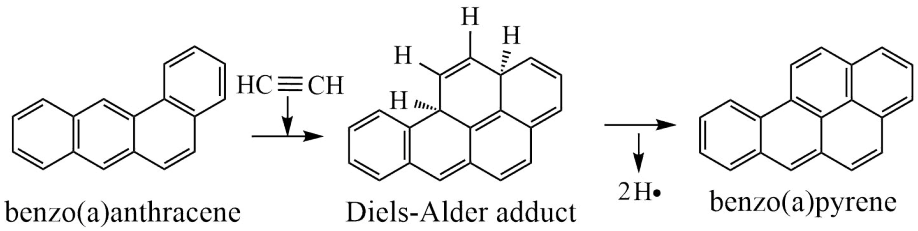

Figure 8 *Diels-Alder reaction mechanism for pyrene formation.*

Siegmann and Sattler proposed the two-part benzogenic Diels-Alder mechanism as the dominant route for PAH growth in which acetylene closes the bay region of PAH structures (**Figure 8**). The reaction begins with the cycloaddition of acetylene producing the Diels-Alder adduct and ends with the loss of hydrogen atoms. In this methane combustion experiment, the benzogenic Diels-Alder mechanism proved to be highly advantageous to achieve compact peri-condensed PAHs [134], because it explains well the growth on bay-type structures. As soon as the most condensed PAH with all closed bays have formed, the growth of larger particles can continue with coagulation mechanisms. Thus, the benzogenic Diels-Alder mechanism can be considered as a viable route in addition to HACA. However, a study on the possible pathways of HACA and DA mechanisms leading to naphthalene, acenaphthylene, phenanthrene, and pyrene concluded that the Diels-Alder process cannot compete with the hydrogen abstraction and acetylene addition reaction, because of its high barriers and low reaction rates [135].

1.2.1.3. Environmental considerations of the HACA and DA mechanisms

The occurrence of acetylene-based mechanisms (HACA and DA) under the combustion of different organic materials are proven. In this sense, PAHs can be formed via HACA and DA in anthropogenic (*e.g.* wood heating, coal-fired power plants, transport, waste incineration [136]–[139]) and natural events (savannah fires, diagenetic and volcanic eruptions [140]) as well. PAHs are often distinguished into pyrogenic (combustion and pyrolysis) and petrogenic (oil spills and oil exploitation) PAHs based on their origin [141]. The temperatures at which the pyrogenic processes occur are ranging from about 600 K to 1500 K. However, crude oils containing petrogenic PAHs are formed at temperatures as low as 373 - 423 K over millions of years. In the work of Shukla and Koshi [83], the growth of aromatic products started from 1274 K in the case of acetylene pyrolysis. In this respect, knowing that HACA is operating primarily at elevated temperatures, its role is more significant in combustion and pyrogenic processes. HACA can be linked to the formation of PAHs also in biological processes. Perylene (PAH with 5 six-membered rings) is considered to originate from anaerobic diagenesis of organic matter [142], and at the same time, its formation via the HACA mechanism is proved [143]. It is also important to mention the probability of occurrence of HACA and DA in extraterrestrial environments where much more extreme physical and chemical conditions prevail than on Earth [144]. In astrophysical environments, the excitation of interstellar dust by UV radiation can be considered as an energy supply process (like combustion) through which chemical compounds like PAHs can be formed. The investigation of the space-formed PAHs is much complicated, therefore, the mechanisms already established in combustion chemistry are often borrowed by the astrochemical community. However, the essential differences between the two environments should be always taken into account. The molecular oxygen necessary for combustion is not relevant neither in the diffuse interstellar medium (DIM) nor in carbon rich Asymptotic Giant Branch stars (AGB) or nebula (*i.e.* CRL 618 proto planetary nebula) [56]. Since the abundance of acetylene in interstellar environments is 100 times less than those detected

in carbon rich circumstellar mediums, HACA and DA are probably efficient in PAH formations in the atmosphere of carbon stars [56], [145]. Even though carbon stars are often thought to be PAH producers, concrete PAH emission has not yet been detected from these [42]. Acetylene is considered to have an important role in the formation of benzene rings as well, which are the simplest building block of PAHs. For instance, in the work of Wood *et al.*, the benzene formation under the conditions of CRL 618 PPN involving relatively large fractional abundances of C_2H_2 and HCO^+ is much more efficient than in interstellar clouds or cool circumstellar shells around AGB stars ($HCO^+ \rightarrow C_2H_3^+ \rightarrow C_4H_3^+ \rightarrow C_6H_5^+ \rightarrow C_6H_6$) [56]. However, Titan's harsh astrochemical conditions (*i.e.* low-temperature 70–200 K) challenges the HACA and DA mechanisms because of the unsurmountable entrance barriers (20 kJ mol^{-1}) both for the H abstraction and for acetylene addition steps, which make them unlikely to be a significant source of PAHs [108], [146]. It is also important to mention, that the condensation process of carbon dust from acetylene in the outflow from carbon rich red giants is considered very similar to that occurring during the gas phase pyrolysis of hydrocarbon molecules which leads to the formation of PAHs [147]. HACA has a possible role in space in the formation of other stable allotropic carbon-based structures, such as in the formation of carbon nanotubes (CNTs) [148]–[150]. The feasibility of HACA in the formation of CNTs in space has been verified computationally [148], [149]. Since the examined CNTs exhibited intense vibrational transitions in the IR (infrared), their presence in the ISM can be further investigated [148].

1.2.2. PAH formation with vinyl acetylene (C_4H_4) addition (HAVA)

The possible role of vinyl acetylene (VA) as a logical four-carbon intermediate unit in the formation of tars appeared already in the work of Badger *et al*. [151]. Since then, it has been proven that VA successfully facilitates PAH formation reactions, and the corresponding mechanism is called hydrogen abstraction vinyl acetylene addition (HAVA). There is a high probability that the HAVA will occur, due to the abundance of VA (C_4H_4) in the combustion environment of various types of flames [72], [100], [152]. Its

advantage is that a new benzene ring can be achieved relatively simply since the second addition of other carbon species is not required in the reaction (**Figure 9**).

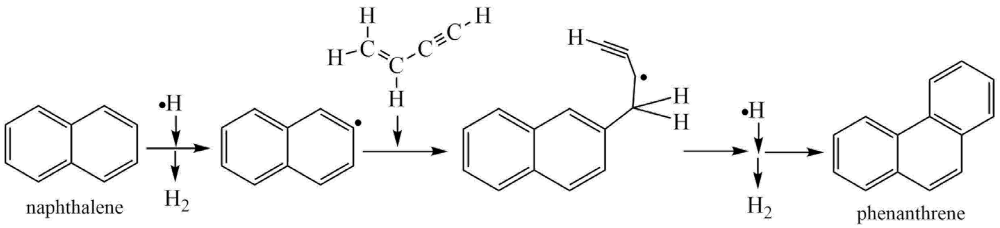

Figure 9 *Formation of phenanthrene starting from naphthalene via the hydrogen abstraction vinyl acetylene addition (HAVA) mechanism.*

In the HAVA mechanism, after a PAH radical is formed, a new ring can be achieved in two steps, which include the addition of C_4H_4 (VA) to the radical and the subsequent cyclisation (**Figure 9**). The double and triple bonds in VA make its carbon atoms very active, which is used in the attack on the C atoms of PAHs. The synthesis of naphthalene at elevated temperatures (1600 K) is studied by considering the HAVA framework [100], [104]. HAVA plays a key role in PAH formations during CVD (chemical vapor deposition) processes and in interstellar medium as well since in cold molecular clouds (10 K) naphthalene can be achieved through HAVA via a barrierless bimolecular route [61], [85], [115], [116]. The formation of anthracene from vinyl acetylene and naphthyl radicals is proposed by Tao *et al.* based on the obtained experimental results of C_2H_2 pyrolysis, but a detailed analysis of the reaction steps is not given [109]. On the contrary, Zhao *et al.* investigated the barrierless reactions between C_4H_4 and naphthyl radicals towards anthracene and phenanthrene formation under the atmospheric conditions of Titan (low temperatures 70–180 K) using computational chemistry tools [108]. The reaction channels are exoergic with a total energy change of -277 kJ/mol and -257 kJ/mol in the case of phenanthrene and anthracene formation, respectively. Moreover, the possibility of further reactions towards more complex PAHs ($C_{14}H_{10}$) via the HAVA mechanism is also proposed [108]. The addition reaction of C_4H_4 to PAH radicals to obtain phenanthrene is further investigated by Liu *et al.* [107] considering the zig-zag and free edge surfaces as well [107]. The sensitivity of the reaction pathway was also analyzed and showed that the new benzene rings are more likely to be formed starting from the zig-zag edge surface site

compared to the free edge. Using the available zig-zag type structure HAVA can have a possible role in the formation of for CNTs in space. Zhao *et al*. presented the formation of pentacene ($C_{22}H_{14}$) - a fundamental molecular building block in CNTs - by the reaction of vinylacetylene (C_4H_4) with 2-tetracenyl radical ($^{\bullet}C_{18}H_{11}$) through a low temperature barrierless gas phase reaction mechanism [154]. Their result highlighted the possible formation of PAHs in cold molecular clouds like TMC-1 and OMC-1 using the hydrogen abstraction vinyl acetylene addition mechanism [154]. In addition, it is demonstrated through molecular dynamic simulations that zig-zag single-walled carbon nanotubes could be formed from linear, cata-condensed PAHs [149]. Overall, it can be observed that the importance of HAVA lies in the fact that PAH formations can be achieved through this mechanism at very different conditions (*e.g.* combustion, interstellar medium [42], Titan's atmosphere [155], carbon stars [156], cold molecular clouds [154], comets [49]).

1.2.3. PAH Formation Mechanisms with Radicals

1.2.3.1. Reaction mechanism with methyl radical - Methyl addition cyclization (MAC)

Among the different chemical species, radicals have a particular role in PAH growth. Based on the nature of radicals, different reaction mechanisms are possible by involving less or more stable carbon-centered radicals. Methyl radical represents one of the simplest but at the same time the most common alkyl radical in the flames of aliphatic or aromatic fuels. The possible role of methyl radicals in PAH growth is first mentioned by Weissman and Benson in the experimental study on the polymerization of methane [157]. Later Shukla also underlined the importance of methyl radicals in the formation mechanisms, because in their experiment made on the pyrolysis of toluene/acetone the mass spectra of PAHs are separated by 14 au, which represents a methyl addition ($+C_1H_3$, +15 au) followed by hydrogen abstraction (-H, -1 au) [158]. Thus, they assumed that a methyl addition and hydrogen atom elimination reaction occur [158]. Based on their results, a new PAH growth mechanism was proposed, the methyl addition cyclization mechanism (MAC). As its name suggests, the MAC mechanism involves the addition of

DOI: 10.14750/ME.2022.010

two or three methyl radicals to form ethyl or propyl chains on the corresponding PAHs (Error! Reference source not found.), accompanied by hydrogen eliminations and cyclization to create new aromatic rings.

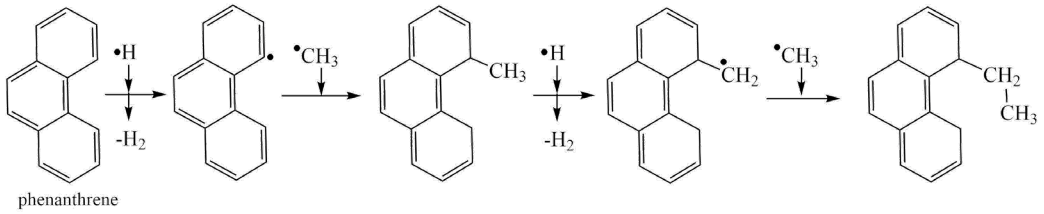

Figure 10 *The formation of an ethyl chain on phenanthrene through the MAC mechanism.*

An essential feature of the MAC mechanism is the capability of expanding cyclopentafused-PAHs into benzenoid rings (**Figure 11**).

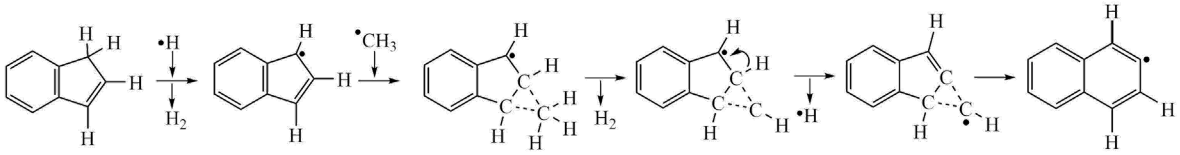

Figure 11 *Formation of a six-membered ring through the MAC mechanism.*

The growth of five-membered rings on the polyaromatic hydrocarbon framework is also discussed in the work of Shi *et al*., in which the formation of fluorene from biphenyl through the MAC mechanism involves four steps is described [111]. The role of methyl radicals is investigated in the mechanistic and flame simulation work of Georganta *et al.* [60] for pyrene formation from phenanthrene. In their results, it turned out, that C_2H_2 occupies faster the radical sites on the armchair position of phenanthrene than methyl which indicates that the MAC mechanism is not competitive with the HACA. However, the MAC mechanism is still an important piece within the continuously expanding puzzle of PAH growth due to the prevalence of methyl radicals. It is important to mention that besides combustion processes, the occurrence of MAC is also probable in astrophysical environments, since methyl is present in a large abundance in the interstellar medium, and methyl-PAHs are considered photolitically more stable than others with alkyl (ethyl, propyl) or unsaturated alkyl chains. In addition, as it is mentioned before the unidentified infrared emission features at 3.4 μm, detected in different astrophysical regions in the Milky Way and nearby galaxies as well, it is often considered that they are carried by aliphatic groups attached to aromatic systems. The computational work of Yang *et al*. carried out on the IR vibrational spectra of a range of PAHs with methyl side chain,

indicated that the computed band intensities overestimated the gas-phase experimental values [159]. On the contrary, a good agreement between the measured and computed C–H stretch vibrational frequencies is achieved in all cases, for all the molecules at all levels [159].

1.2.3.2. Reaction mechanism with ethynyl radical

A radical alternative of HACA is the one that involves ethynyl radical instead of acetylene [160], [161]. Ethynyl (or hydrodicarbon, $^{\bullet}C_2H$) is formed in a carbon-rich environment from the decomposition of acetylene and it also can be found in high density in the interstellar medium [162]. Since PAHs represent 20 percent of the carbon material in the universe, consequently the role of ethynyl radicals in PAH growth mechanisms has become more significant from this point of view. Mebel *et al.* proposed the ethynyl addition mechanism (EAM) [160] and a similar reaction mechanism which involves hydrogen abstraction ethynyl radical addition (HAERA) has been proposed recently to model BaP formation from chrysene [120] (**Figure 12**).

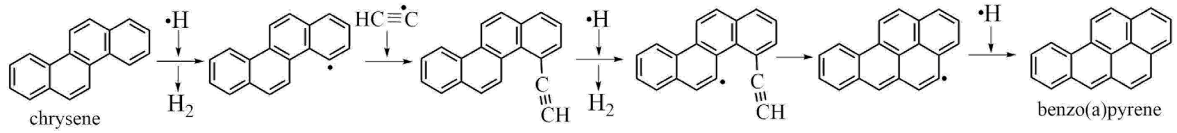

Figure 12 *Formation of benzo(a)pyrene from chrysene via the hydrogen abstraction ethynyl radical addition (HAERA) mechanism.*

It has also been demonstrated that benzene (precursor of PAHs) can be formed under single collision conditions via the gas phase reaction of ethynyl radicals with 1,3-butadiene [163]. Electronic structure calculations predicted that phenylacetylene molecule (C_9H_6) can be synthesized with benzene and ethynyl radical in an exoergic, barrierless reaction [160]. Moreover, the reaction can reach naphthalene if the phenylacetylene reacts with two additional ethynyl radicals including ring closures and hydrogen atom emission steps [160], [163]. Such neutral–neutral reactions (benzene or naphthalene with ethynyl radicals) could be a possible route to reach PAHs at temperatures as low as 10 K, as they are present in cold molecular clouds [163].

1.2.3.3. PAH formation with vinyl radicals (HAVA*)

PAHs can also be formed through vinyl radical ($^{\bullet}C_2H_3$) additions before which a hydrogen abstraction occurs (hydrogen abstraction vinyl radical addition, HAVA*). To the best of our knowledge, this mechanism was first proposed in the experimental work of Shukla and Koshi [83] within which PAH growth processes were analyzed by the addition of C_2H_x species. In their results on ethylene pyrolysis, the detected mass spectra appeared in 26 mass number sequences which strongly indicated the role of $^{\bullet}C_2H_3$ in PAH formations (+ $^{\bullet}C_2H_3$, +27 au; -H, -1 au). HAVA* has been declared to be particularly suitable for the formations of CP-PAHs such as fluoranthene ($C_{16}H_{10}$) (**Figure 13**) or corannulene ($C_{20}H_{10}$) [83].

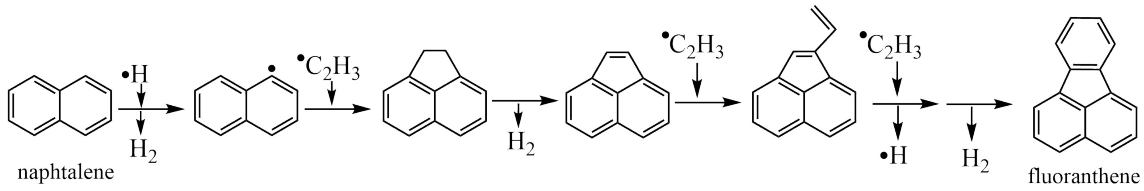

Figure 13 *Formation of fluoranthene from naphthalene via the hydrogen abstraction vinyl radical addition (HAVA*) reaction mechanism.*

It is also observed that during aliphatic hydrocarbon pyrolysis at least up to moderate temperature (1300 K) HAVA* is more promising for producing PAHs, than HACA [83]. Thus, HAVA* has a well-deserved place at the table of PAH growth mechanisms. It is also observed that during aliphatic hydrocarbon pyrolysis at least up to moderate temperature (1300 K) HAVA* is more promising for producing PAHs, than HACA [83]. In addition, the dominant temperature of HAVA* is in the middle of the temperature range of combustion and pyrolitic processes (which is about 600 K - 1500 K [3], [83]). Consequently, its role is more significant in the formation of pyrogenic than petrogenic PAHs and has a well-deserved place at the table of PAH growth and formation mechanisms.

1.2.3.4. Phenyl addition cyclization mechanism

During an experimental study on toluene pyrolysis, Shukla *et al*. [117] observed several PAH species with a mass difference of ~76 au. Based on this observation, they suggested a phenyl-addition-cyclization (PAC) mechanism [117], within which a phenyl radical (+

DOI: 10.14750/ME.2022.010

•C_6H_5, + 77 au) was added to a molecule, and this step was followed by hydrogen abstraction (-H, -1 au). Thereafter, with increasing temperatures, dehydrocyclization took place (-H_2, -2 au) under which the conversion of thermally unstable phenyl-PAHs into stable condensed PAHs occurred (**Figure 14**).

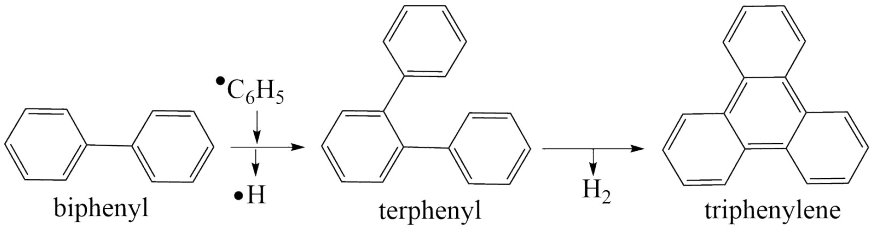

Figure 14 *Formation of triphenylene from biphenyl.*

However, it has been shown that the condensation of phenyl radicals (•C_6H_5) on aromatics may not be a competitive route in comparison to HACA, due to the low concentration of benzene in flames compared to C_2H_2 [17]. Although, this may vary if other fuels are used for the flames. In another experimental work done on the pyrolysis of toluene with and without the addition of benzene to acetylene, the PAC mechanism appeared to be more efficient over the HACA [164]. Furthermore, PAC is proposed as an efficient PAH growth mechanism in circumstellar envelopes of carbon stars [165]. However, PAC is unable to produce symmetrical PAHs like coronene or corannulene, but it is considered highly efficient if phenyl radicals are present, because it ensures an endless growth of PAHs by creating additional triple fusing sites in each step [124]. Knowing that the PAC mechanism leads to the formation of asymmetrical structures, which are more characteristics of protoplanetary nebulae (PPN), this mechanism might have relevance in the PAH formation in PPN [159]. Furthermore, the occurrence of PAC mechanism in astrochemical environments is probable, since the solar ultraviolet radiation can penetrate deep into *e.g.* Titan's atmosphere, and thus photodissociation of benzene to phenyl radical and atomic hydrogen can occur [166]. However, the barrierless formation of larger PAHs than naphthalene at low temperatures is not validated yet [166].

DOI: 10.14750/ME.2022.010

1.2.3.5. Reaction mechanisms with resonantly stabilized radicals

The role of resonantly stabilized radicals (RSR) in PAH growth is also significant. These radicals can be present in high concentrations in flames due to their relatively stable nature [61] and they can participate in radical-radical and radical-neutral recombination reactions. A series of PAH mechanisms are proposed and calculated which involve RSRs, and among them the most well-known pathways include propargyl [55], [61], [167]–[169], cyclopentadienyl [74], [78], [79], [99], [170]–[175], and indenyl [106], [176]–[180] radicals (**Figure 15**).

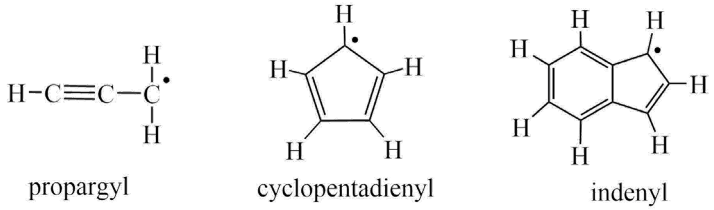

Figure 15 *2D structures of the propargyl, cyclopentadienyl, and indenyl radicals.*

Regarding the environmental occurrence, the mechanisms with RSRs are relatively more likely to occur in combustion processes. For instance, the self-recombination of propargyl radical to form benzene (a central building block of PAHs) is followed by isomerization and stabilization via a third-body collision [181]. However, in cold molecular clouds, such collision complexes cannot be stabilized by a third-body collision as those processes are extremely rare to occur. Consequently, even though the self-recombination of propargyl radical reaction has no entrance barrier it is still not expected to happen in cold molecular clouds.

DOI: 10.14750/ME.2022.010

2. Methods

2.1. Schrödinger equation

The study of the PAH growth reaction mechanisms can be accomplished by using a wide range of toolkits for computational chemistry. In the following section, the applied methods are presented as well as the theoretical foundations behind them. The studied reaction mechanisms of PAH growth consist of numerous elementary reactions steps involving chrysene and benzo(a)anthracene as reactants, several transition states, intermediate structures, and benzo(a)pyrene as the final product. All of the corresponding structures involved in the studied reaction mechanisms have a particular molecular structure to which a specific energy value is assigned. The determination of the energy value of a molecule begins with Schrödinger's famous *wavefunction equation* (**Eq. 1**) [182]–[185].

$$\widehat{H}\Psi = E\Psi \qquad \textbf{Eq. 1}$$

Following the *first postulate* of quantum mechanics, a wavefunction represents the momentary state of a quantum chemical system by describing the probability distribution of its measurable properties. Since the energy of the ground state of a molecular system does not depend on time, the non-relativistic time-independent Schrödinger equation can be applied within which $\widehat{H}$ is the Hamiltonian operator, E is the energy and Ψ is the wavefunction of all the spatial coordinates of nuclei and spatial and spin coordinates of electrons (**Eq. 1**). Correspondingly to the *second postulate* of quantum mechanics, the linear Hermitian operator is represented by the Hamiltonian operator, which gives the total energy of a system. Since a Hermitian operator always has real eigenvalues and expectation values, this criterion is also valid to the time-independent Schrödinger equation, which in mathematical terms represents an Eigenvalue equation, having Ψ as the eigenfunction and E as the eigenvalue (**Eq. 1**). According to the *third postulate* of quantum mechanics, the eigenvalues of the $\widehat{H}$ operator is equal to the measurable energy values. The *fourth postulate* describes the general expectation value of a given physical observable (**Eq. 2**),

DOI: 10.14750/ME.2022.010

$$\langle A \rangle = \int_{-\infty}^{+\infty} \Psi^* \hat{A} \Psi dt \qquad \textbf{Eq. 2}$$

where Ψ^* is the conjugate form of the normalized wavefunction Ψ, and $\hat{A}$ is the corresponding operator [186]. The *fifth postulate* of quantum mechanics declares that the state of a microsystem is described by the time-dependent Schrödinger equation (**Eq. 3**):

$$i\hbar \frac{\partial \psi(\tau, t)}{\partial t} = \hat{H}\psi(\tau, t) \qquad \textbf{Eq. 3}$$

where $\hbar$ is the reduced Planck constant $\left(\hbar = \frac{h}{2\pi}\right)$, and $\hat{H}$ is the total energy Hamiltonian operator. If a state of a system does not change in time, the time-independent Schrödinger equation shall be applied (**Eq. 1**). The *sixth postulate* of quantum mechanics is also called the antisymmetry principle within which the Pauli exclusion principle can be directly deduced. By means of the sixth postulate, the wave function of a microsystem must be antisymmetric for the exchange of all coordinates of identical particles with half-integer spin (fermion) and symmetric for the exchange of all coordinates of identical particles with integer spin (bozon).

As we know in classical physics, the total energy includes kinetic and potential energy terms. This is also true in quantum mechanics and it can be seen in the expanded version of the Hamiltonian. It includes the sum of all possible interactions between electrons and nuclei, where the first two terms correspond to the kinetic energy of all the electrons and nuclei, the third and fourth term represents the Coulomb repulsion between electrons and nuclei respectively, and the fifth term is the Coulomb attraction between nuclei and electrons ( ).

$$\hat{H} = -\sum_{i=1}^{N_{el}} \frac{\nabla_i^2}{2} - \sum_{A=1}^{M} \frac{\nabla_A^2}{2M_A} + \sum_{i=1}^{N_{el}} \sum_{j>i}^{N_{el}} \frac{\mathbf{1}}{|\boldsymbol{r_i} - \boldsymbol{r_j}|} + \sum_{A=1}^{M} \sum_{B>A}^{M} \frac{Z_A Z_B}{|R_A - R_B|} + \sum_{i=1}^{N_{el}} \left(\sum_{A=1}^{M} \frac{-Z_A}{|r_i - R_A|} \right) \qquad \textbf{Eq. 4}$$

where, M_A is the ratio of the mass of nucleus A to the mass of an electron,

Z_A is the atomic number of nucleus *A,*

∇_i^2 and ∇_A^2 are the Laplacian operators which give the sum of second partial derivatives of a function.

Since the introduction of the wavefunction, huge efforts are made in science to simplify it. A significant reduction in its complexity resulted from the work of Max Born and

DOI: 10.14750/ME.2022.010

Robert J. Oppenheimer, by introducing the famous *Born-Oppenheimer approximation* [187] in which the nucleus and electrons are treated separately. The possibility for the dynamic decoupling of the nucleus and electrons is supported by the fact that the nuclei are much heavier than the electrons, consequently, the timescale of the response of the electrons is a few orders of magnitude faster than that of the nuclei. In this sense, nuclei can be treated as static particles concerning electrons, which eliminates the second term of **Eq. 4**. At the same time the repulsion between nuclei (fourth term), can be treated as a constant for a fixed configuration of the nuclei. In this sense the Hamiltonian after the Born-Oppenheimer approximation, will contain terms that are ”electron related”, and thus it is called the *electronic Hamiltonian* (**Eq. 5**):

$$\hat{H}_e = -\sum_{i=1}^{N_{el}} \frac{\nabla_i^2}{2} + \sum_{i=1}^{N_{el}} \sum_{j>i}^{N_{el}} \frac{\mathbf{1}}{|\boldsymbol{r_i} - \boldsymbol{r_j}|} - \sum_{i=1}^{N_{el}} \sum_{A=1}^{M} \frac{Z_A}{|r_i - R_A|} \qquad \textbf{Eq. 5}$$

In the electronic Hamiltonian, the electron-electron term causes the biggest concern in the solution of the Schrödinger equation (**Eq. 1**). The individual electron wavefunction cannot be found without simultaneously considering that the individual electron wavefunctions are associated with all the other electrons. This problem is also known as the *many-body problem.* The solution of the time-independent many-body electronic Schrödinger equation is highly difficult and time-consuming for systems with more than a few electrons, even for smaller molecules. For example, carbon dioxide with its 22 electrons and 3 nuclei in a three-dimensional coordinate system would have 75 variables, and the complexity further increases with the size of the molecular system.

2.2. Computational Chemistry

The practical use of quantum chemistry is realized through computational chemistry. With the development of computer technology, it became possible to achieve an approximate solution of the Schrödinger equation with very good accuracy and to predict molecular properties in a precision that is comparable to experiments, and thus the elucidation of ambiguous or unclear experimental data became possible and short-lived, unstable intermediates and transition states could be described. Through the application of the Born-Oppenheimer approximations, potential energy can be defined by the position of nuclei in space. In this sense, the Coulomb attraction between nuclei and electrons is considered as external potential. At this point, it is important to introduce the concept of the *potential energy surface* (PES) which is a mathematical representation that gives the total energy of a molecule as a function of its geometrical coordinates. Since a molecule has 3N-6 degrees of freedom (where N is the number of atoms if N>2), the corresponding PES is also multidimensional. The most significant chemical concepts can be represented on a 3D, or just a 2D section of it, which is called a potential energy curve (PEC). A PEC helps to visualize and compare the energy levels of the reactants, intermediates, transition states, and products, and thus the preferable pathways of a reaction can be determined.

The 3D PES can be considered as a geomorphological map, where critical points (minima, maxima, transition states) can be defined. In order to investigate the reaction mechanism of PAHs, the reactants, products, intermediates, and transition states have to be found on the potential energy surface or potential energy curve. For both minima and maxima the first derivative (gradient) of the energy with respect to all internal coordinates (q, q_0) is zero, so they are stationary points (**Eq. *6*** and **Eq. *7***).

$$E = E_0 + \frac{1}{2}|k|(q - q_0)^2, \ \frac{\partial E}{\partial q} = 0 \qquad \textbf{Eq. 6}$$

$$E = E_0 - \frac{1}{2}|k|(q - q_0)^2, \ \frac{\partial E}{\partial q} = 0 \qquad \textbf{Eq. 7}$$

In **Eq. *6*** and **Eq. *7*** k represents the force constant. The types of the critical points can be determined from the second derivative, which is positive for a minimum $\frac{\partial^2 E}{\partial q^2} = |k| > 0$,

and negative for a maximum $\frac{\partial^2 E}{\partial q^2} = -|k| < 0$. Besides minima and maxima, first-order saddle points can also occur, which are a maximum in one direction and minimum in all other directions, corresponding to transition state structure.

A computational chemistry calculation begins with **geometry optimization**, in which the first step is to choose an initial molecular geometry. This can be done with different software using the known properties of a molecular structure (bond length, dihedral angles, *etc*.) but in many cases, this step relies only on chemical intuition. The local minimum can be determined by changing the coordinates of nuclei and calculating the corresponding electronic energy and nuclei-nuclei repulsion energy. The sum of the beforementioned two energy terms gives the total energy (E_{tot}). In reality, geometry optimization and the corresponding energy calculations are time-consuming and complex and they are realized with specific quantum chemical software, which often requires a supercomputer. In this study, all the quantum chemical calculations are carried out by using the Gaussian09 program package [188]. During a geometry optimization with the Gaussian09 program package, the minimum energy of a molecular structure is found when the (i) maximum remaining force, (ii) the average mass-weighted force (RMS - root mean square force), (iii) the maximum displacement (maximum structural change of one coordinate), and the (iv) average (RMS) change over all structural parameters fall below the threshold value. Once the beforementioned four convergence criteria are fulfilled, the optimization is considered complete.

After the optimization, **frequency calculation** can be carried out at the optimized geometry of the predicted structure. It is important to confirm that the structure indeed is a true stationary point (minimum or saddle point) and corresponds to the studied reaction pathway. Frequency calculations consider the nuclear vibration in the molecular systems as if they are in their equilibrium states. If the geometry is optimized to a minimum, the gradient is zero, and the force constant matrix determines the behavior of the system under small displacements.

The vibration energy of a given molecule can be approached by the harmonic oscillator approximation using the following equation (**Eq. 8**):

$$E_\upsilon = hc\upsilon_i\left(\upsilon + \frac{1}{2}\right) \qquad \textbf{Eq. 8}$$

where υ_i is the vibrational frequency wavenumber (**Eq. 9**),

$$\upsilon_i = \frac{1}{2\pi c}\sqrt{\frac{k}{\mu}} \qquad \textbf{Eq. 9}$$

υ_i is the vibrational quantum number, h is the Planck constant ($6.62 \cdot 10^{-34}$ J·s), k is the force constant, μ is the reduced mass, and c is the speed of light ($2.99 \cdot 10^8$ m/s):

2.3. Thermodynamic parameters

To understand the reaction mechanisms of PAHs, it is important to determine the experimentally most important thermodynamic properties. The reaction enthalpy ($\Delta_r H°$), Gibbs free energy ($\Delta_r G°$), entropy ($\Delta_r S$) can be obtained by using the toolkit of *statistical thermodynamics*, with the help of *partition functions* [q(V,T)] which tell how the probabilities are partitioned among the different microstates (transition, rotation, vibration, electronic state). Through the partition functions, the thermodynamic state functions [G(T,p), E_0, S(T,p), H(T)] can be derived for each molecule participating in the reaction, and then, the corresponding thermodynamic properties of the reaction can be obtained (**Figure 16**).

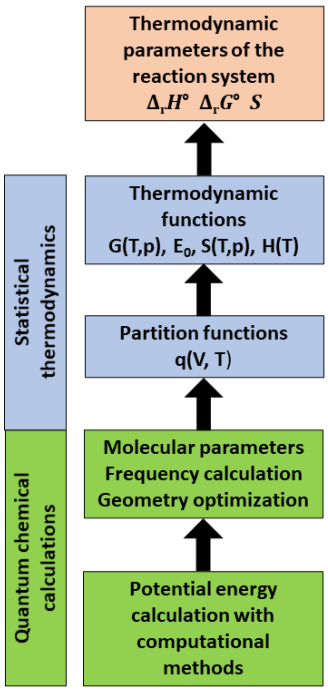

Figure 16 *Schematic representation of the steps to compute the thermodynamics of a reaction starting from the potential energy of individual structures.*

DOI: 10.14750/ME.2022.010

At a microscopic scale, the atomic dimensions are considered and it is specified by the number of particles in each energy state. This approach is known as *statistical thermodynamics* which represents a bridge between the molecular properties and macroscopic thermodynamic properties (**Figure 16**).

The energy distribution of the molecules can be given by the Boltzmann distribution, and the partition function [q(V,T)] shows how the probabilities are partitioned among the different microstates. The *total energy of a microstate* of a molecule can be calculated as a sum of the translational (ε_{tr}), rotational (ε_{rot}), vibrational (ε_{vib}), and electronical energy (ε_{elec}) (**Eq. 10**).

$$\varepsilon = \varepsilon_{tr} + \varepsilon_{rot} + \varepsilon_{vib} + \varepsilon_{elec} \qquad \textbf{Eq. 10}$$

Similarly, the *molecular partition function* (q) can be calculated (**Eq. 11, Table 1**):

$$q = q_{tr} + q_{rot} + q_{vib} + q_{elec} \qquad \textbf{Eq. 11}$$

Table 1 *Contribution of translation, rotational, vibrational, and electronic motions to the partition and state functions.*

Translation motion	**Rotational motion**	**Vibrational motion**	**Electronic motion**
$\boldsymbol{q_t = \left(\frac{2\pi m k_B T}{h^2}\right)^{3/2} V}$	$\boldsymbol{q_r = \frac{1}{\sigma_r}\left(\frac{T}{\Theta_r}\right)}$ $\boldsymbol{q_r = \frac{\pi^{1/2}}{\sigma_r}\left(\frac{T^{3/2}}{\sqrt{\Theta_{r_1x}\Theta_{r_1y}\Theta_{r_1z}}}\right)}$	$\boldsymbol{q_{v,K} = \frac{e^{\Theta_{v,K}/2T}}{1 - e^{-\Theta_{v,K}/T}}}$	$\boldsymbol{q_e = \omega_0}$
m = molecular mass *k_B=Boltzmann Constant 1.3807 × 10^{-23} J·K^{-1}* *T = temperature* *h = Planck Constant 6.62˙10^{-34} J·s* *V = volume*	$\Theta_{r_1x} = hc\, B_{0,x}/k_B$ *characteristic temperature* *$B_{0,x}$: rotational constant in x direction* $B_0 = \frac{h}{4\pi\mu R^2 c}$	$\theta_{\upsilon,K} = hc\tilde{\upsilon}_K/k_B$ *characteristic temperature* *$\tilde{\upsilon}_K$: K_{th} vibrational wavenumber*	*degeneracy of the electronic energy level* *ω_0: multiplicity*

Internal energy (*E*), entropy (*S*), Gibbs free energy (*G*), enthalpy (*H*), derived from the partition function can describe quantitatively an equilibrium state of a thermodynamic system, irrespectively of how the system arrived in that state.

Entropy (*S*) is a state function originally introduced to explain why part of the total energy is unavailable to do useful work. It is equal to the Boltzmann's constant (k_B =1.38065 × 10−23 J/K) multiplied with the natural logarithm of the number of possible quantum states (*W*) (**Eq. 12**):

DOI: 10.14750/ME.2022.010

$$S = k_B \ln W \qquad \textbf{Eq. 12}$$

Through partition functions the entropy contribution would be (**Eq. 13**):

$$S = Nk_B + Nk_B \ln\left(\frac{q(V,T)}{N}\right) + Nk_B \mathrm{T}\left(\frac{\partial \ln \mathrm{q}}{\partial \mathrm{T}}\right)V \qquad \textbf{Eq. 13}$$

where N is the particle number of molecules as a dimensionless quantity.

The enthalpy (H) is equivalent to the total heat content of the system and it is equal to the internal energy of the system plus the product of the pressure and volume (**Eq. 14**). Being a state function enthalpy depends only on the prevailing equilibrium state identified by the variables of the internal energy, pressure, and volume.

$$H(T) = E(T) + pV \qquad \textbf{Eq. 14}$$

By means of partition functions the enthalpy would be (**Eq. 15**):

$$H - H(0) = \left(\frac{\partial \ln \mathrm{Q}}{\partial \beta}\right)_{\mathrm{V}} + \mathrm{kTV}\left(\frac{\partial \ln \mathrm{Q}}{\partial \mathrm{V}}\right)_{\mathrm{T}} \qquad \textbf{Eq. 15}$$

where β represents the most probable populations of the states of the system, which strongly suggests that it is related to the temperature: $\beta = \frac{1}{kT}$, Q is the partition function of the system and q is the molecular partition function. If the molecules are independent (for distinguishable molecules, *e.g.* solids) $Q = qN$. For indistinguishable molecules (*e.g*: gases) $Q = \frac{qN}{N!}$ where $q = \frac{V}{\Lambda^3}$ with Λ = thermal wavelength $\Lambda = \left(\frac{h}{2\pi mkT}\right)^{\frac{1}{2}}$.

The Gibbs free energy G(T,p) tells the maximum or reversible work that may be performed by a thermodynamic system at a constant temperature (T) and pressure (p) (**Eq. 16**).

$$G(T,p) = H(T) - TS(T,p) \qquad \textbf{Eq. 16}$$

where S refers to the entropy of the *system*. Expressing the Gibbs free energy from the partition function we get (Eq. **17**):

$$G - G(0) = -\mathrm{nRT}\ln\frac{\mathrm{q}}{\mathrm{N}} \qquad \textbf{Eq. 17}$$

DOI: 10.14750/ME.2022.010

2.4. Computational Chemistry Methods

As the solution of the Schrödinger equation is extremely difficult, various approximations are developed over the years. The two most important method types are the wavefunction-based and density functional-based methods (**Figure 17**). Both wavefunction and density functional-based methods have different advantages and disadvantages. Among the wavefunction-based methods, the coupled-cluster (CC) technique is often considered as the theoretical gold standard, but its biggest downside is that its computational cost increases severely with the system size. At this level, even the computation of a few tens of electrons represents an issue for the world's largest computers and most efficient algorithms [189].

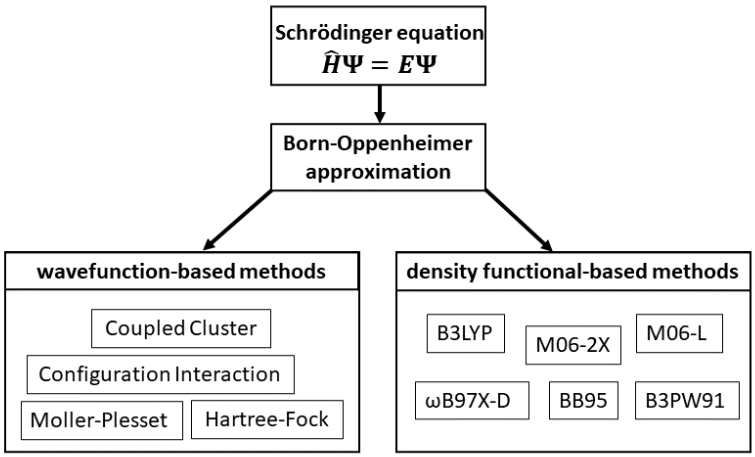

Figure 17 *Classification of different approximate solutions of the Schrödinger equation with specific examples of wavefunction-based and density functional-based methods.*

In contrast to this, the density functional-based methods are capable of dealing with systems with thousands or even more electrons. Regarding accuracy, DFT methods yield very good results if those are used for the appropriate types of systems. However, the abundance of DFT methods makes the selection difficult. In addition, between CC and DFT methods CC should be the reference.

2.4.1. *Ab Initio*

The methods through which the Schrödinger equation can also be approximated based on whether or not they include an empirical or measured term. Those which are only

based on fundamental laws of quantum mechanics and use a variety of mathematical transformation and approximation techniques to solve the equations are called *ab initio* methods. The most widely used *ab initio* approximation in quantum chemistry is the Hartree-Fock (HF) method, which is based on the assumption that the Slater determinant wavefunction of an electron cloud can be constructed from the corresponding spin-orbital product and this can be extended to any number of electrons, and thus can be used to approximate the multi-electron wavefunction of the system [190], [191]. The HF *ab initio* method does not address electron correlation within the system, which leads to a low computational time, but also a lower computational accuracy. To achieve higher accuracy, so-called post-Hartree-Fock *ab initio* methods are developed, within which the electron correlation has also been included. A great example of these methods is the Møller–Plesset family (*e.g.* MP2, MP3, MP4, MP6) which operates based on the Møller–Plesset perturbation theory at a relatively low computational cost [192]–[194].

2.4.2. Density Functional Theory

The Density Functional Theory (DFT) is introduced by Pierre Hohenberg and Walter Kohn [195]. The fundamental concept of DFT is that the n-electron wavefunction can be replaced with the much simpler electron density ($n(r)$). In this respect, regardless of how many electrons a system has, the density remains three-dimensional. The density of the electrons ($n(r)$) at a particular position is expressed by **Eq. *18***, which shows the probability that an electron in an individual wavefunction $\Psi_i(r)$ is located at a given position (r). The 2 multiplier refers to the Pauli exclusion principle that states that each electronic wavefunction can be occupied by two separate electrons with different spins.

$$n(\mathrm{r}) = 2\sum_{\mathrm{i}} \Psi_{\mathrm{i}}^{*}(\mathrm{r})\Psi_{\mathrm{i}}(\mathrm{r}) \qquad \textbf{Eq. 18}$$

Hohenberg and Kohn expressed the electronic Hamiltonian for a fixed number of electrons and arbitrary external potential through two key theorems:

1. there is a one-to-one correspondence between the external potential and the electron density (**Eq. *18***).

2. the electron density that minimized the energy is the true electron density which corresponds to the full solution of the Schrödinger equation.

In DFT the *external potential* is the Coulomb attraction between nuclei and electrons (third term in the electronic Hamiltonian (**Eq. 19**), because due to the Born-Oppenheimer approximation the nuclei are considered "external" fixed objects, which exert their Coulomb potential to the electrons. Simply the electronic Hamiltonian of the system can be written as:

$$\hat{H}_e = \hat{\mathrm{V}}_{\mathrm{k}}(\mathrm{n}) + \hat{\mathrm{V}}_{\mathrm{ee}}(\mathrm{n}) + \hat{\mathrm{V}}_{\mathrm{ext}}(\mathrm{n}) \qquad \textbf{Eq. 19}$$

where $\hat{\mathrm{V}}_{\mathrm{k}}$ and $\hat{\mathrm{V}}_{\mathrm{ee}}$ are the kinetic and electron-electron interaction operators, and $\hat{\mathrm{V}}_{\mathrm{ext}}$ is the external potential, which can be expressed explicitly as a function of the ground state electron density (**Eq. 20**):

$$\hat{\mathrm{V}}_{\mathrm{ext}}(\mathrm{n}) = \int \mathrm{n}\,(\mathrm{r})\Psi^{*}(\mathrm{r})\Psi(\mathrm{r})\mathrm{dr} \qquad \textbf{Eq. 20}$$

This implies that the total energy is a functional of the density because density determines the Hamiltonian, and thereby the wavefunction. This unique functional relation is denoted with *F* and consist of the two other terms from **Eq. 21** ($\hat{\mathrm{V}}_{\mathrm{k}}(\mathrm{n})$ and $\hat{\mathrm{V}}_{\mathrm{ee}}(\mathrm{n})$). Consequently, the energy will be:

$$E = \int \hat{\mathrm{V}}_{\mathrm{ext}}(\mathrm{n})\ \mathrm{n}(\mathrm{r}) + \mathrm{F}[\mathrm{n}(\mathrm{r})] \qquad \textbf{Eq. 21}$$

So the first theorem states that a functional relation exists between the ground state wavefunction and the ground state electron density, but it tells nothing about what the functional actually is. However, based on the second theorem if the true functionals are known, then the electron density could be varied until the energy from the functional is be minimized. For this, the variational principle method is applied.

The practical applicability of Density Functional Theory became feasible with the work of Kohn and Sham [195]. They showed that the electron density can be expressed by solving a set of equations, which all involve a single electron. Theoretically, through these equations, the exact electron density can be obtained, and hence the total energy.

In the Kohn and Sham approximation, a virtual non-interacting system is introduced and it is assumed that its ground-state electron density is equal to the real interacting system.

DOI: 10.14750/ME.2022.010

The ground-state electron density is defined at a location by the following expression (**Eq. 22**):

$$n(\mathrm{r}) = \sum_{\mathrm{i}=1}^{\mathrm{n}} \left|\varphi_{\mathrm{i}}^{\mathrm{KS}}(\mathrm{r})\right|^2 \qquad \textbf{Eq. 22}$$

where $\varphi_i^{KS}(r)$ are the Kohn-Sham orbitals. Consequently, the ground state of the system is defined as (**Eq. 23**):

$$\hat{\mathrm{h}}^{\mathrm{KS}}(\mathrm{i})\varphi_{\mathrm{i}}^{\mathrm{KS}} = \varepsilon_{\mathrm{i}}^{\mathrm{KS}}\varphi_{\mathrm{i}}^{\mathrm{KS}} \qquad \textbf{Eq. 23}$$

where $\hat{h}^{KS}(i)$ is the Kohn-Sham Hamiltonian, and ε_i^{KS} is the corresponding energy of the Kohn-Sham orbital. The Hamiltonian of the interacting (real) system is given by the sum of the external potential term $\hat{V}_{ext}^{vir}[\mathrm{n(r)}]$, the kinetic energy term $\hat{V}_k^{vir}[n(r)]$, the electron-electron repulsion term $\hat{V}_{ee}^{vir}[n(r)]$ and corrections of the last two terms ($\Delta_k^{corr}[\mathrm{n(r)}] + \Delta_{ee}^{corr}[\mathrm{n(r)}]$) which represents the difference between the virtual and real system (**Eq. 24**).

$$\hat{\mathrm{h}}^{\mathrm{KS}}(\mathrm{i}) = \hat{\mathrm{V}}_{\mathrm{ext}}^{\mathrm{vir}}[\mathrm{n(r)}] + \hat{\mathrm{V}}_{\mathrm{k}}^{\mathrm{vir}}[\mathrm{n(r)}] + \Delta_{\mathrm{k}}^{\mathrm{corr}}[\mathrm{n(r)}] + \hat{\mathrm{V}}_{\mathrm{ee}}^{\mathrm{vir}}[\mathrm{n(r)}] + \Delta_{\mathrm{ee}}^{\mathrm{corr}}[\mathrm{n(r)}] \qquad \textbf{Eq. 24}$$

The sum of the corrections in **Eq. 24** ($\Delta_k^{corr}[\mathrm{n(r)}] + \Delta_{ee}^{corr}[\mathrm{n(r)}]$) is the exchange-correlation energy functional (which are corresponding to the exchange ($E^X[n(r)]$) and correlation energy terms ($E^C[n(r)]$). The E^Xrepresents the interactions between electrons of the same spin, while E^C is associated with the electron-electron interactions with opposite spin. Consequently, the Kohn-Sham Hamiltonian can be expressed as the sum of four major terms (**Eq. 25**):

$$\hat{\mathrm{h}}^{\mathrm{KS}}(\mathrm{i}) = \hat{\mathrm{V}}_{\mathrm{k}}[\mathrm{n(r)}] + \hat{\mathrm{V}}_{\mathrm{ee}}[\mathrm{n(r)}] + \hat{\mathrm{V}}_{\mathrm{ext}}[\mathrm{n(r)}] + \hat{\mathrm{V}}_{\mathrm{XC}}[\mathrm{n(r)}] \qquad \textbf{Eq. 25}$$

where $\hat{V}_k[n(r)]$ is the kinetic energy term, $\hat{V}_{ee}[n(r)]$ is the electron-electron repulsion term, $\hat{V}_{ext}[n(r)]$ is the external potential term, and $\hat{V}_{XC}[n(r)]$ is the exchange-correlation term. The exchange-correlation functional has an exact form just for the uniform electron gas, but this case seldom appears in real life. In other words, DFT remains exact just in principle, but in practice, it needs an approximation for the electron exchange and correlation interactions. By now, there is an almost endless list of approximated functionals with varying levels of complexity. A very illustrative way of categorizing the density functional methods (how DFT's are handling the $V_{XC}[n(r)]$) was created by

DOI: 10.14750/ME.2022.010

Perdew and is known as Jacob's ladder of DFT, where the functionals are grouped according to their complexity on rungs of a ladder [196] (**Figure 18**).

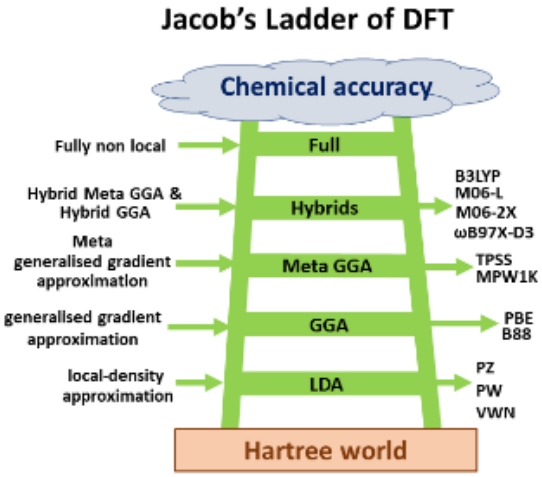

Figure 18 *Jacob's ladder of density functional approximations.*

Besides that, the functionals can be categorized as *non-empirical* (formulated only by satisfying some physical rules) and *empirical* (made by fitting to the known results of atomic or molecular properties) methods.

In the *local density approximation* (LDA), a real inhomogeneous system is divided into infinite volumes, and the electron density in each of the volumes is considered constant. The exchange-correlation energy for the density within each volume is obtained from the uniform electron gas model [189]. Thus, the total exchange-correlation energy of the system can be written as (**Eq. 26**)

$$\mathrm{E_{XC}^{LDA}(n)} = \int n(\mathrm{r})\mathrm{dr}\, E_{\mathrm{XC}}^{\mathrm{unif}}(\mathrm{n(r)})\ \mathrm{dr} \qquad \textbf{Eq. 26}$$

where $E_{\mathrm{XC}}^{\mathrm{unif}}$ is the exchange-correlation energy per particle of the interacting uniform electron gas, which has an electron density n(r). The analytical expression for the exchange energy is known as (**Eq. 27**):

$$\mathrm{E_X^{LDA}(n)} = -\frac{3}{4}\left(\frac{3}{\pi}\right)^{1/3} \int \mathrm{n}^{4/3}(\mathrm{r})\mathrm{dr} \qquad \textbf{Eq. 27}$$

and the correlation energy is obtained by mathematical fitting [197], [198]. Modern LDA functionals differ only in how their correlation contributions are fitted to the many-body free electron gas data. LDA works well for metals but gives insufficient results for weakly bonded systems, such as Van der Waals and H-bonded systems. The most common LDA

functionals are the Perdew-Zunger (PZ), Perdew-Wang (PW), and the Vosko-Wilk-Nusair (VWN) functionals [199]–[201].

It was observed that the use of the uniform density at each given point does not serve as a reasonable approximation for the rapidly varying electron densities of many materials. To correct this, various gradients of the density ($\nabla n(r)$, $\nabla^2 n(r)$, etc.) are introduced, but these seldom improved the LDA results [202]. It was found that instead of power-series-like gradient expansions, more general functions of $n(r)$ and $\nabla n(r)$ could be applied. These functionals represent the second rung of Jacob's ladder (**Figure 18** Jacob's ladder of density functional approximations.) known as GGA (Generalised Gradient Approximations) functionals, with the following general form (**Eq. 28**):

$$E_X^{GGA}(n) = \int f^{GGA}\left(n(r), \nabla n(r)\right) dr \qquad \textbf{Eq. 28}$$

For geometries and ground state energies GGAs could yield better results than the LDAs. Especially for covalent bonds and weakly bonded systems. The functional form of f^{GGA} is taken as a correction to the LDA exchange and correlation (**Eq. 29**):

$$E_X^{GGA}(n) = \int n(r) E_X^{unif}\left(n(r)\right) F_X^{GGA}(s) dr \qquad \textbf{Eq. 29}$$

where F_X^{GGA} is the exchange enhancement factor and tells how much exchange energy is enhanced over the LDA value for a given $n(r)$ and s is the gradient. The most well-known gradient corrected correlation functionals are the Perdew-Burke-Ernzerhof (PBE), Lee-Yang-Parr (LYP), and Becke88 (B88) [203]–[205] which have the following forms (**Eq. 30**, and **31**):

$$F_X^{PBE} = 1 + k - \frac{k}{(1 + \mu s^2/k)} \qquad \textbf{Eq. 30}$$

$$F_X^{B88} = 1 + \frac{\beta x(s)^2}{C[1+6\beta x(s) sinh^{-1}(x(s))]}, x(s) = 2(6\pi^2)^{1/3} s \qquad \textbf{Eq. 31}$$

where k and μ are non-empirical constraints, while C and β are parameters obtained from empirical fitting. In the case when the density gradient is zero, the LDA exchange is obtained. The functional form to the gradient corrected correlation energy E_C^{GGA} is also expressed as a complex function of *s*. The application of GGAs is inevitable to a reasonable description of hydrogen bonds [118–120].

The third rung of Jacob's ladder represents the *meta-GGA functionals*, whose specialty is the usage of the second derivative of the density, $\nabla^2 n(r)$, and/or kinetic energy densities $\tau_\sigma(n) = \frac{1}{2}\sum_i \left|\nabla_{\varphi i}(n)\right|^2$ as additional degrees of freedom (**Figure 18**). In gas-phase studies of molecular properties meta-GGAs such as the TPSS functional is shown to offer improved performance over LDAs and GGAs [189], [196], [206].

The fourth rung of Jacob's ladder represents the *hybrid functionals*. Among them, B3LYP is the most well-known method containing the linear combination of BLYP and LDA functionals (**Eq. 32**).

$$E_{XC}^{B3LYP} = E_X^{LDA} + a_0(E_X^{HF} - E_X^{LDA}) + a_x(E_X^{GGA} - E_c^{LDA}) + a_x(E_C^{GGA} - E_c^{LDA}) \qquad \textbf{Eq. 32}$$

The functional name of B3LYP is an abbreviation in which, B3 refers to Becke's 3 parameter exchange-correlation functional [207], and LYP is the Lee-Yang-Parr correlation functional [205] that recovers the dynamic electron correlation. B3LYP is used in numerous studies and has become a default choice for many researchers [61], [88], [102], [208], [209]. In terms of calculation time, the B3LYP is generally faster than most of the post-Hartree-Fock methods and usually provides sufficiently good results. In the B3LYP-D3 method, a correction for long-range dispersion interactions is incorporated as well.

Another popular hybrid functional group worth mentioning here is the Minnesota Functionals (Myz) introduced by Prof. Donald Truhlar and his co-workers [210], [211]. Among them, M06-L and M06-2X are the most well-known functionals with 0% and 54% HF exchange, respectively [212]–[215]. Furthermore, the hybrid GGA range-separated (RSH) functionals are also important which include the semi-empirical ωB97 and ωB97X-D [216]. The former two are introduced by Head-Gordon and co-workers with 0% and 15.77% short-range exact exchange, and with ω =0.4 and ω = 0.3 empirical values, respectively [217]. ωB97X-D works with 22% of HF exchange and its specific feature is the capability of capturing both short-range and long-range interactions. Besides, in the comparative study of Mardirossian and Head-Gordon, the ωB97X-D is qualified as one of the most promising among 200 other functionals [218].

DOI: 10.14750/ME.2022.010

2.4.3. Basis sets

A basis set is a collection of mathematical functions used to represent the quantum mechanical wavefunction of a molecular system. All of the previously mentioned methods require a certain basis set. Altogether, in computational chemistry this is called the level of theory (method/basis set). In principle larger basis sets with a relatively high number of mathematical functions give a more accurate description of the electronic structure. However, this also requires more computational time. The most common minimal basis sets are part of the STO-*n*G family, where *n* indicates the number of primitive Gaussian functions that comprise a single basis function. For instance in the STO-3G minimal basis set each atomic orbital (either core or valence) is treated as a single slater type orbital (STO), which is approximated by a linear combination of 3 Gaussian functions (3G)[219][122]. Consequently, the 1s orbital in the hydrogen atom will be approximated by three Gaussian functions. However, for a carbon atom 15 Gaussian functions will be used (Error! Reference source not found.).

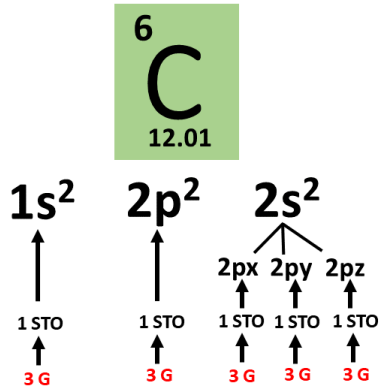

Figure 19 *The meaning of the STO-3G basis set in the case of a carbon atom.*

The basis set can be more accurate by increasing the number of basis functions per atomic orbital. The basis sets in which two, three or more basis functions are used to describe the atomic orbitals are supplemented by the term of double-, triple-zeta or *N*-zeta. For example 6-31G is a split-valence double-zeta basis set, in which the core orbitals are made of 6 primitive Gaussian functions, while the valence orbitals are described by two basis functions (double-zeta) each of them made from three Gaussians and one Gaussian [220]. The basis sets can be further improved by adding *polarization* (* - in

Pople's notation) and *diffuse* (+ - in Pople's notation) functions, which are more sensitive for the description of weak interactions or anionic systems [186].

Another important basis set class is the def2 which was developed by Aldrichs *et al*. [221] [222] and referred by the SV, SVP, TZV, TZVP keywords. The def2-TZVP is a newer version of the TZVP basis set [223] [224] which was used as it is implemented in the Gaussian 09 program package.

2.4.4. Composite methods

In order to achieve high accuracy at a relatively low computational cost, composite methods are introduced. As its name suggests the composite methods are a combination of several computational chemistry methods. They are also called thermochemical recipes and are commonly used to calculate the thermodynamic properties of molecules in chemical reactions. Nowadays, the CBS (Complete Basis Set, *e.g.* CBS-4M and CBS-APNO) and Gaussian-n (n≤4, *e.g.* G3, G3MP2, G3MP2B3) families are applied in most cases [225]–[227]. In the case of the G3MP2B3 composite method, the geometries and zero-point energies are obtained at the B3LYP/6-31G(d) level of theory and the frequencies are scaled with 0.96. Furthermore, additional single point energy calculations are also included in the procedure at the following levels of theory: MP2/6-31G(d); MP2/G3MP2large and QCISD(T)/6-31G(d). The high accuracy of this method is achieved by using additional corrections (E(HLC) and E(SO)) determined by experimental and theoretical methods.

2.5. Applied levels of theory

Considering the computational cost, the size of the molecular system as well as the features of the previously discussed methods and basis sets in this study the B3LYP [205][207], B3LYP-D3 [205][207][228], B97D3 [228], M06-2X [212]–[214], M06L-D3 [215] and ωB97X-D [217] density functional methods were used, in combination with the 6-31G(d), 6-31+G(d,p), 6-311++G(d,p) [220], and def2-TZVP [223] [224] basis sets.

DOI: 10.14750/ME.2022.010

All of the methods are used in some points of the investigations but not all of them at the same time (**Figure 20**).

	Levels of theory used for results discussion		Levels of theory used for preliminary calculations	Representation of the levels of theory applied in BDE study
	ωB97X-D/6-311++G(d,p)	M06-2X/6-311++G(d,p)	B3LYP/6-31+G(d,p)	
BDE	✓	✗	✓	
HAERA	✓	✗	✓	
HACA	✓	✗	✓	
DA	✓	✗	✓	
MAC	✗	✓	✓	

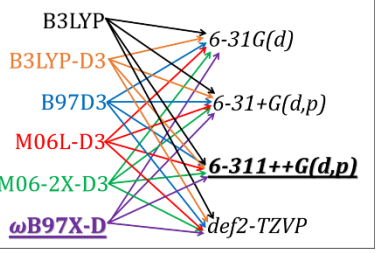

Figure 20 The applied level of theories.

DOI: 10.14750/ME.2022.010

3. Results and Discussion

3.1. Reaction initiation points of polycyclic aromatic hydrocarbons

In the following chapter the reaction initiation points of the 16 priority polycyclic aromatic hydrocarbons (PAHs) are determined and compared by calculating all the different C-H bond dissociation enthalpy (BDE) values. All in all, six density functional theory methods (B3LYP, B3LYP-D3, B97D3, M06-LD3, M06-2X-D3, and ωB97X-D) in combination with 4 basis sets (6-31G(d), 6-31+G(d,p), 6-311++G(d,p), def2-TZVP) are applied, and the most feasible combination is selected. The strength of the carbon-hydrogen bonds (C-H bonds) is a crucial parameter and can define the starting point of the reactions. Nevertheless, the occurrence of a given reaction mechanism is strongly influenced by the corresponding barrier height of the rate-determining step. Bond dissociation enthalpy (BDE) is an appropriate thermodynamic property to measure bond strength. It determines the enthalpy change associated with bond breaking and is equivalent to the difference between the sum of the enthalpy of the formed radicals (in this case a PAH radical ($H^0_{fPAHrad}$) and atomic hydrogen (H^0_{fH})) and the initial PAH structure (H^0_{fPAH}) (**Eq. 33**).

$$BDE = (H^0_{f_{PAH_{rad}}} + H^0_{f_H}) - H^0_{f_{PAH}} \qquad \textbf{Eq. 33}$$

In order to determine the BDE for each studied carbon-hydrogen bond ($BDE_{C\text{-}H}$) of the 16 priority PAHs (Error! Reference source not found.), 104 radicals, 16 molecules, and 1 hydrogen are calculated with each method, and thus in total 2904 calculations are performed [(104 radical + 16 reactants + 1 hydrogen)•24]. In the selection of the studied C-H bonds, the symmetry of the structures is taken into consideration, and thus positions that lead to identical radicals are excluded from the study (**Figure 21**). Method tests are also performed through which the selected DFT methods combined with the above mentioned four basis sets are compared to experimental values to provide the best DFT/basis set combination for future studies.

DOI: 10.14750/ME.2022.010

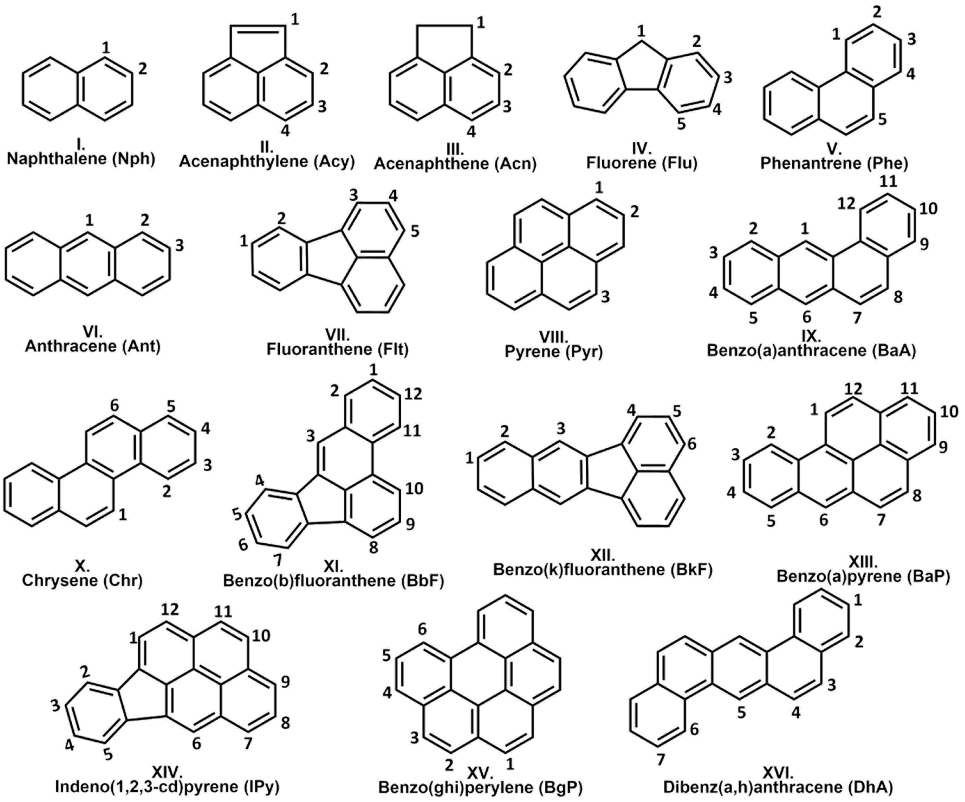

Figure 21 *2D structures of the priority PAHs. C-H bonds for which bond dissociation enthalpies (BDEs) are computed are indicated and marked by numbers.*

3.1.1. Validation

BDE values of Nph-2 (second hydrogen of naphthalene, and Acy-1 (the first hydrogen of acenaphthylene, are calculated with every combination of methods and basis sets and compared to experimental data (**Table 2**). It can be seen that in the case of naphthalene (Nph-2) each DBDEs is below 4 kJ/mol (within chemical accuracy). However, regarding acenaphthylene (Acy-1) the difference between the calculated and experimental BDE values is >4 kJ/mol, except in the case of the ωB97X-D/6-311++G(d,p) level of theory [229]. Taking into consideration the experimentally measured (BDE_{EXP}) and the calculated (BDE_{CALC}) values, it can be concluded that the best agreement is obtained with the ωB97X-D/6-311++G(d,p) level of theory, as the deviations (BDE_{EXP}-BDE_{CALC}) are only 0.07.

Table 2 *The deviations between the calculated (BDE_{CALC}) and experimental (BDE_{EXP}) [229] bond dissociation enthalpy values (in kJ/mol) for naphthalene (Nph-2) and acenaphthylene (Acy-1).*

$\Delta BDE = BDE_{EXP}-BDE_{CALC}$ / kJ/mol								
	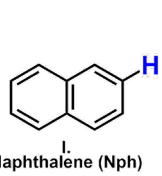 I. Naphthalene (Nph) 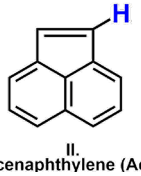 II. Acenaphthylene (Acy)							
Basis set	*6-31G(d)*		*6-31+G(d,p)*		*6-311++G(d,p)*		*def2-TZVP*	
Method	Nph-1	Acy-1	Nph-1	Acy-1	Nph-1	Acy-1	Nph-1	Acy-1
B3LYP	4.65	8.24	1.72	5.10	4.39	7.64	5.92	9.17
B3LYP-D3	2.52	5.80	1.58	4.45	1.58	4.45	3.77	6.66
B97D3	5.74	8.61	2.51	5.05	1.79	4.41	8.10	10.43
M06L-D3	22.78	27.43	18.01	22.43	17.58	22.14	21.12	25.36
M06-2X-D3	0.20	6.57	1.48	4.40	2.61	8.44	2.75	7.87
ωB97X-D	0.34	4.33	20.14	18.75	**0.07**	**3.87**	2.35	6.27

In addition, the extensive work of Mardirossian and Head-Gordon made on the analysis of 200 density functionals showed that ωB97X-D is the best hybrid GGA functional [218]. The results of ωB97X-D/6-311++G(d,p) are compared with the other DFT/basis set combinations (**Figure 22**).

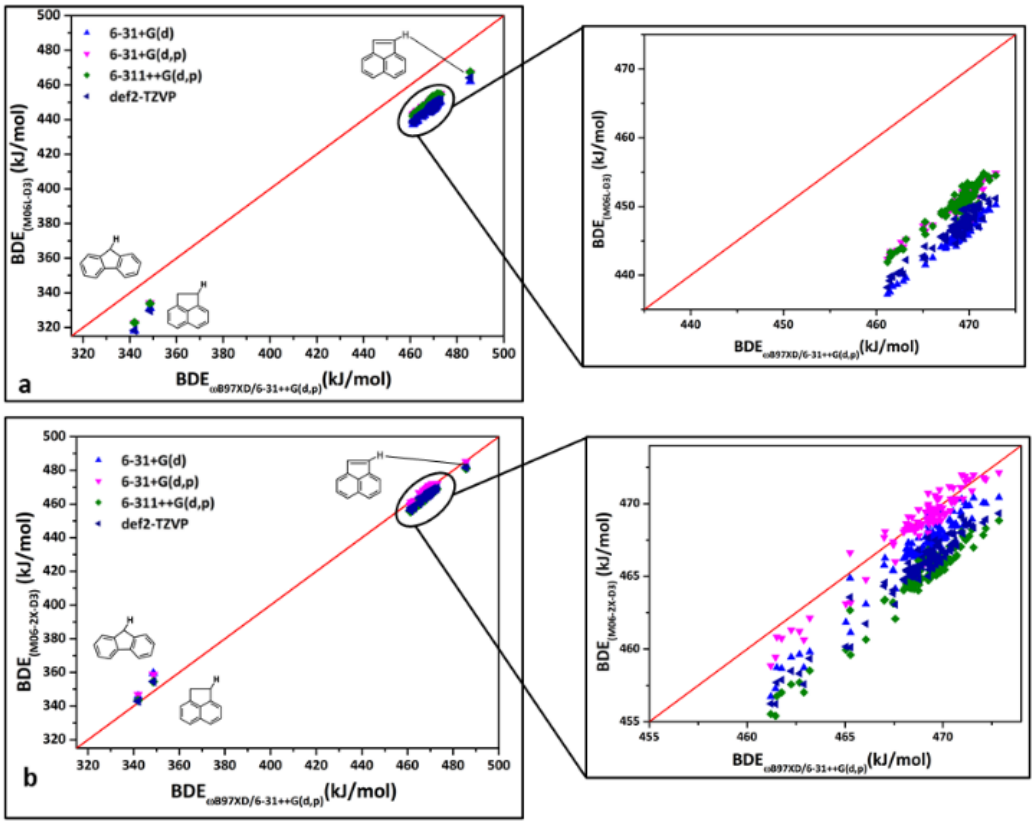

Figure 22 *Comparison of bond dissociation enthalpy (BDE, in kJ/mol) values computed at various theoretical levels.*

If the data of ωB97X-D/6-311++G(d,p) is considered as a reference (red line on **Figure 22**), the other DFT values usually underestimate these. The deviation is the highest (<20.34 kJ/mol on average) between the M06-LD3 and ωB97X-D/6-311++G(d,p) values. Not surprisingly, the ωB97X-D/6-31+G(d) data is very close to the reference. The difference between them is just 0.27 kJ/mol on average, which is well below the chemical accuracy (4 kJ/mol), and can be attributed to the difference of the diffuse and polarization functions (+, ++; (d), (d,p)) involved in the basis sets. In addition, among the values obtained with different methods, the M06-2X-D3 values are the closest to the ωB97X-D/6-311++G(d,p) values, as the deviation is just 2.5 kJ/mol. Thus, the ωB97X-D/6-31+G(d) and ωB97X-D/6-311++G(d,p) level of theories are both suitable for similar studies, but as the latter is slightly better, it is selected and applied in the analysis.

3.1.2. Structural and energetics considerations based on the results of the ωB97X-D/6-311++G(d,p) level of theory

The studied hydrogen atoms are categorized based on their position or chemical properties (**Figure 23**).

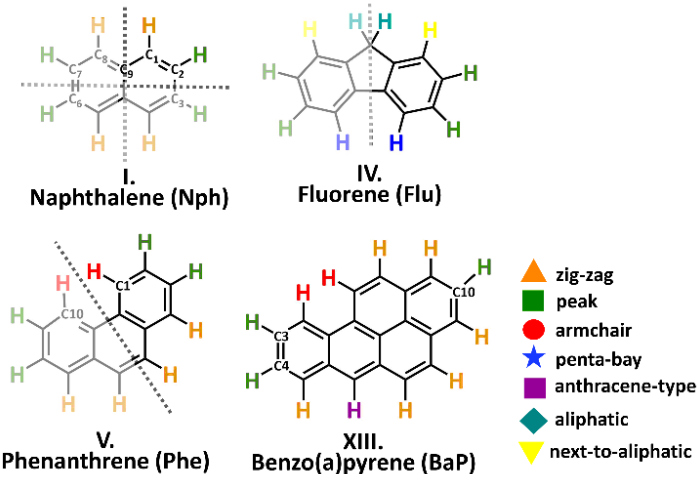

Figure 23 *Categorization of the H atoms of the studied PAHs introduced by using specific examples.*

Seven categories are identified and all of the hydrogens are assigned to one of the following groups taking into account the symmetry of the molecular structures as well: zig-zag (noted with an orange triangle), peak (marked with a green square), armchair (red circle), penta-bay (blue star) anthracene type (purple square), aliphatic (blue rhombus) and next-to-aliphatic (yellow triangle) (**Figure 23**). Hydrogens in zig-zag

positions are most easily represented on naphthalene, as the hydrogens attached to a connected section of 4 carbon atoms (for example C7–C8–C9–C1 zig-zag chain) between the C2 - C3 and C7 – C6 midpoints constituent symmetry plane. The next category is the peak, where the hydrogen is attached to a carbon and the neighboring C atoms also hold H atoms (**Figure 23**, C3, C4, C10, BaP). The hydrogen that is in armchair position belongs to a carbon around a bay region (between C1 and C10 carbons of phenanthrene, a prototype of a "bay region", **Figure 23**). Numerous PAHs have this structural feature (DhA, Chr, BaA, BaP), with additional fused aromatic rings. This type of arrangement has significance in cancer research since the bay region is preserved within the most carcinogenic PAHs (benzo(a)anthracene, benzo(a)pyrene-7,8-dihydrodiol-9,10-epoxide) and is considered as a critical structural feature for the formation of carcinogenic and mutagenic cells [230]. Hydrogens in penta-bay category are in similar positions to the hydrogens in the armchair group, but here the two benzene rings at the edge of the structural unit are fused with a five-membered ring in the middle (fluorene, **Figure 23**). The anthracene-type hydrogens are found on the middle ring of three linearly connected benzene rings (BaP, **Figure 23**). The last two categories are related to the aliphatic structural moieties of the PAHs. Aliphatic hydrogens are on the aliphatic unit of the molecules (Acn-1, Flu-1, **Figure 23**), while hydrogens which are on an aromatic six-membered ring connected to the aliphatic part of the species (Acn-2, Flu-2) belong to the next-to-aliphatic group. The computed BDE and the corresponding bond length values are plotted and analyzed (**Figure 24**)**.** By comparing all the obtained values, it can be seen that the minimum and maximum values belong to two molecules. Flu-1 has both the lowest BDE value and the longest bond length value at the same time with 342.01 kJ/mol and 1.10 Å respectively. However, Acy-1 (the first hydrogen on acenaphthylene, **Figure 24**) has the shortest bond length value with 1.08 Å, and the highest BDE value with 485.63 kJ/mol. Plotting the BDEs as a function of the corresponding bond lengths, three subgroups are observed (marked with roman numbers, **Figure 24, a**). The results of Acy-1 (the first hydrogen of acenaphthylene) define a special case due to the highest BDE value (485.63 kJ/mol) and to the relatively short bond length value (1.082 Å).

DOI: 10.14750/ME.2022.010

Consequently, Acy-1 stays separately from the first and third groups and basically would represent alone the first subgroup of the BDE vs bond length diagram (**Figure 24**, **a**, **I.**).

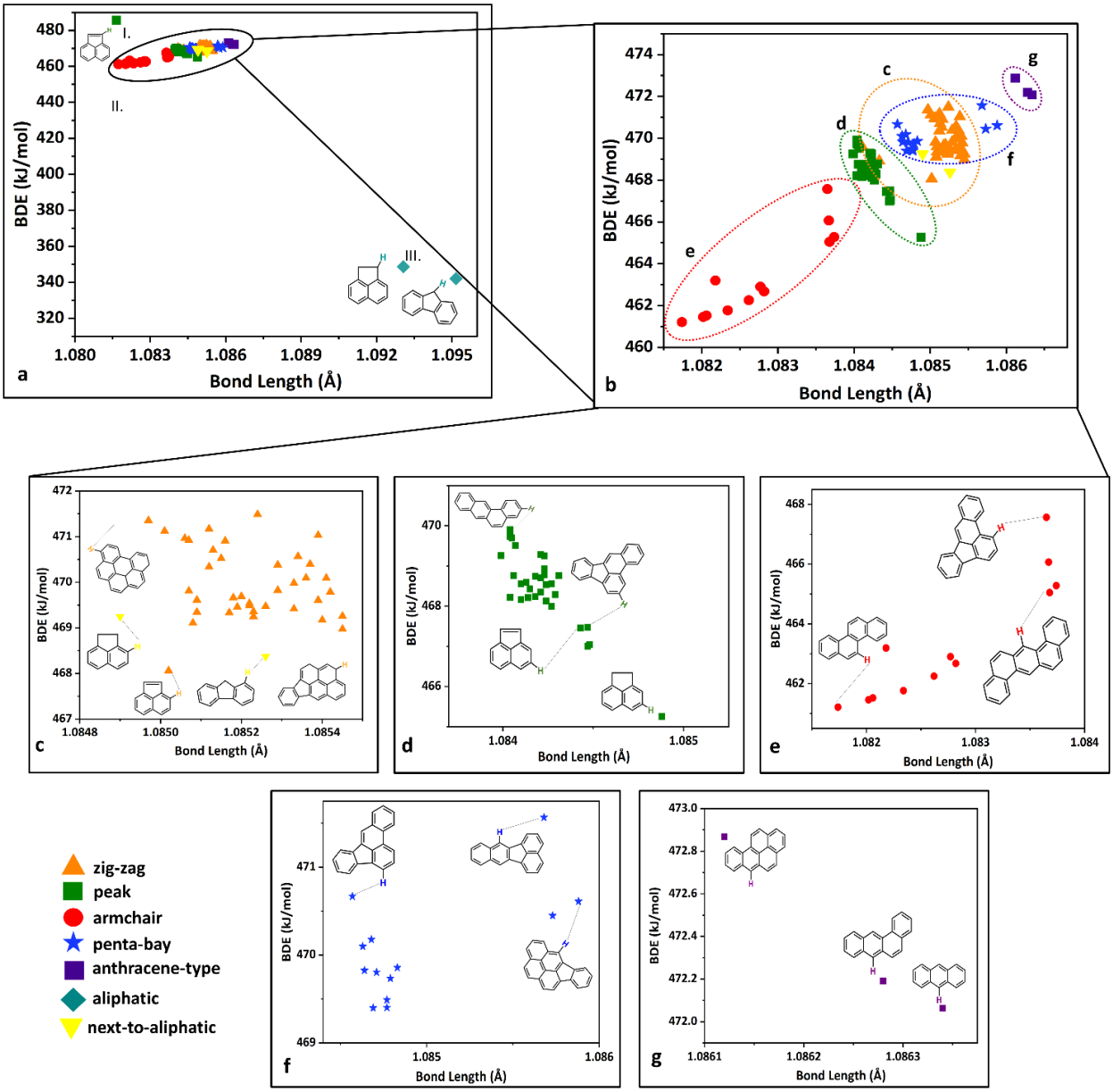

Figure 24 *Calculated bond dissociation enthalpy (BDE, in kJ/mol) values as a function of the corresponding C-H bond lengths and the categories of the H atoms.*

This can be explained by its special position since it is bound to a carbon atom involved in a five-membered ring which is fused with two six-member rings. Two data points of Flu-1 and Acn-1 represent the third major group (**Figure 24 a, III.**), with 342.01 kJ/mol and 348.68 kJ/mol BDE values respectively. These two points have a BDE value well below the average (466.56 kJ/mol) which can be explained by their aliphatic nature. Furthermore, if all the data are compared it can be seen that the longest C-H bond values

belong to these with 1.01 Å. Most of the data points (101 from 104) can be found in the second group (**Figure 24, a,** II.) with a bond length and BDE value range between 1.08 Å (Chr-1) and 1.09 Å (Ant-1) and 461.21 kJ/mol (Chr-1) and 472.87 kJ/mol (BaP-6), respectively. The positions of the hydrogens are also noted according to the categorization mentioned earlier (**Figure 23**). Thirty-eight hydrogens are in **zig-zag** position (within II.) so this type of arrangement is the most prevalent. In this group, the average BDE value is 469.98 kJ/mol, in a range between 468.06 kJ/mol (Acy-2) to 471.49 kJ/mol (Ipy-9). Regarding the bond lengths, the average is 1.085 Å with a minimum of 1.0850 Å (Phe-3) and a maximum of 1.0855 Å (BkF-2). 33 hydrogens can be identified as **peak** (within II.), with a 468.44 kJ/mol BDE and 1.08 Å bond length, on average. The maximum BDE value appeared on the tenth hydrogen of benzo(a)anthracene (BaA-10) with 469.90 kJ/mol and the minimum is obtained on Acn-3 with 465.25 kJ/mol. The longest C-H bond is located on the same molecule (Acn-3) within the peak category with 1.0849 Å. However, the minimum bond length is obtained on the first hydrogen of benzo(b)fluoranthene (BbF-1) with 1.0840 Å. 12 hydrogens within the II. group are in **armchair** arrangement (**Figure 24**). Interestingly both the minimum BDE and bond length values belong to Chr-1 with 461.21 kJ/mol and 1.082 Å, respectively. The maximum BDE value in **armchair** position is attributed to BbF-10 (benzo(b)fluoranthene) with 467.57 kJ/mol. The longest bond length belongs to BaA-1 with 1.084 Å. There are 13 hydrogens in the **penta-bay** group. Among them, indeno(1,2-cd)pyrene represents the minimum BDE and the longest bond length values with 469.40 kJ/mol (Ipy-1) and 1.086 Å (Ipy-6), respectively. The highest BDE is attributed to the third hydrogen of benzo(k)fluoranthene (Bkf-3), and the shortest bond length to benzo(b)fluoranthene. The fifth category in the second group is **anthracene-type,** which includes only three hydrogens (Ant-1, BaP-6, and BaA-6). Based on the results, it can be observed that the BDE and bond length values are changing inversely proportional with the growth of benzene rings. Ant-1 being the simplest prototype in this category has the longest bond length value (1.0863 Å) with the lowest BDE value (472.06 kJ/mol). The sixth hydrogen on benzo(a)pyrene (BaP-6) consists of two additional benzene rings than

anthracene, has the highest BDE value (472.87 kJ/mol), and the shortest bond length value (1.0861 Å) in this category. Being in concordance with previous observations the results of BaA-6 are between the results of Ant-1 and BaP-6, obtaining a 472.19 kJ/mol and a 1.08 Å of BDE and bond length values, respectively. Among the 13 hydrogens located in the **penta-bay** category the first and third hydrogens on indeno(1,2-cd)pyrene represent the minimum bond length and maximum BDE value with 1.086 Å and 469.40 kJ/mol, respectively. The maximum BDE is found at BkF-3 with 471.57 kJ/mol, and the minimum bond length corresponds to BbF-8 with 1.085 Å. The two hydrogens of Acn-2 and Flu-2 represent the last group that bears the **next-to-aliphatic** name. The BDE values here are 469.25 kJ/mol (Acn-2) and 468.37 kJ/mol (Flu-2), while the bond length values are ~1.08 Å. Based on the obtained BDEs, potential reaction initiation points can be determined on each molecule (**Figure 25**). For 7 molecules (Phe, BaA, Chr, BaP, BbF, DhA, BgP) from the 16 parent PAHs the most reactive hydrogens are in an armchair position and the most reactive molecule in this respect is chrysene (Chr) due to its slightly lower BDE value (461.21 kJ/mol) than the others. The hydrogens in peak positions represent the second most reactive subgroup (**Figure 25**). Among them, the most reactive molecule is acenaphthylene (Acy) which has a 468.06 kJ/mol BDE value. Thus, under a given mechanism the further growth of PAHs probably will start with the formation of the PAH radicals by the removal of hydrogens from these positions.

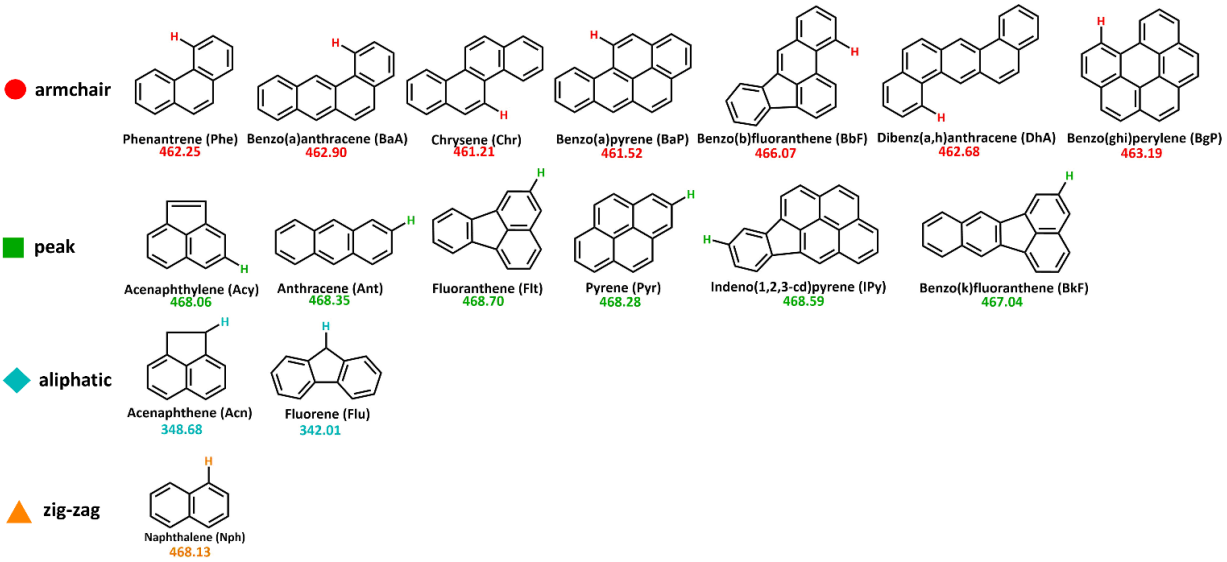

Figure 25 *Reaction initiation points of the 16 priority PAHs along with the corresponding bond dissociation enthalpy (BDE, in kJ/mol) values.*

DOI: 10.14750/ME.2022.010

3.1.3. Conclusion

Bond dissociation enthalpies (BDEs) of the 16 priority PAHs are calculated for each unique C-H bond. The calculations are carried out by using six density functional theory methods (B3LYP, B3LYP-D3, B97D3, M06-LD3, M06-2X-D3, and ωB97X-D) in combination with 4 basis sets (6-31G(d), 6-31+G(d,p), 6-311++G(d,p), def2-TZVP). The results compared with experimental values and the best method/basis set combination, the ωB97X-D/6-311++G(d,p) level of theory, has been selected. The hydrogens are categorized by using structural and chemical properties. Seven categories are defined, zig-zag, peak, armchair, penta-bay, anthracene type, aliphatic, and next-to-aliphatic. Most of the H atoms are in zig-zag positions. The BDE and bond length values for the C-H bonds within the 16 priority PAH are in a range between 342.01 – 485.63 kJ/mol and 1.08 – 1.10 Å, respectively. The minimum and maximum BDE and bond length values belong to fluorene and acenaphthylene, where the corresponding hydrogens are in the aliphatic and peak subgroup. The BDE values are used to determine potential reaction initiation points on each molecule. Most of these initiation points are hydrogens in an armchair (7 of them) or peak position (6 of them). Further growth of the structures would start with the removal of hydrogens from these points. This can be used to study the feasibility of potential growth mechanisms.

DOI: 10.14750/ME.2022.010

3.2. Benzo(a)pyrene formation - HACA, HAERA, & Diels-Alder mechanisms

Studying the reaction initiation point of PAHs (previous chapter) it was found that in the chrysene and benzo(a)anthracene molecules the hydrogen removal is most probable from armchair positions. Taking into account these results, in the following chapter, 10 reaction pathways are presented for benzo(a)pyrene formation, starting from the armchair positions of chrysene and benzo(a)anthracene. The reactants can be formed during combustion from phenanthrene by the addition of a new benzene ring utilizing the appropriate fusing sites (**Figure 26**).

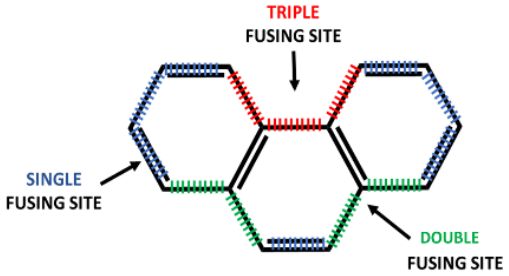

Figure 26 *The three types of fusing sites (new ring addition points) in the case of phenanthrene: single (blue), double (green) and triple (red).*

The more dangerous molecule, benzo(a)pyrene, can be reached with the addition of a second benzene ring to the triple fusing sites of chrysene and benzo(a)anthracene. The present chapter is focusing on the mechanism of this last step. The studied reaction mechanisms for benzo(a)pyrene formation include 36 elementary steps (**Figure 27**). All quantum chemical calculations are carried out by using the Gaussian09 program package [188]. The structures (reactants, intermediates, products, and transition states) are optimized by three density functional theory (DFT) methods. For preliminary calculations, the B3LYP/6-31+G(d,p) level of theory is used [231]. In order to improve the accuracy, DFT calculations with the ωB97X-D/6-311++G(d,p) level of theory are also performed. Based on the results obtained through the validation performed in the previous chapter (**Table 2**) the ωB97X-D/6-311++G(d,p) level of theory is selected and results with that discussed during the analysis.

Critical stationary points are characterized by vibrational frequency calculations at both levels of theories. Moreover, intrinsic reaction coordinate (IRC) analysis is carried out

DOI: 10.14750/ME.2022.010

[232] to ensure that the located transition states connect the appropriate starting structures and products at the level of ωB97X-D/6-311++G(d,p). The reference levels of the two benzo(a)pyrene formation reaction channels corresponded to chrysene (Chr) and benzo(a)anthracene (BaA). Atomic balance is considered, and the number of carbon and hydrogen atoms are kept the same by using additional species (hydrogen atoms, hydrogen molecules, and ethynyl radicals) (**Table 3**).

Table 3 *Atomic balance considered and the number of carbon and hydrogen atoms kept the same by using additional species (hydrogen atoms, hydrogen molecules, acetylene and acetylene radicals) in each step of benzo(a)pyrene formation.*

[HAERA]	**Chr**	**TS1**	**a**	**b**	**TS2**	**c**	**TS3**	**d**	**TS4**	**BaP**
nr C	18	18	18	20	20	20	20	20	20	20
nr H	12	13	11	12	13	11	11	11	13	12
•C$_2$H	1	1	1	0	0	0	0	0	0	0
H•	3	2	2	2	1	1	1	1	1	2
H$_2$	0	0	1	1	1	2	2	2	1	1

[HACA]	**Chr**	**TS1**	**a**	**e**	**TS5**	**f**	**TS6**	**BaP**
nr C	18	18	18	20	20	20	20	20
nr H	12	13	11	13	13	13	13	12
C$_2$H$_2$	1	1	1	0	0	0	0	0
H•	2	1	1	1	1	1	1	2
H$_2$	0	0	1	1	1	1	1	1

Diels-Alder	**Chr**	**TS7**	**g**	**TS8**	**BaP**
nr C	18	20	20	20	20
nr H	12	14	14	12	12
•C$_2$H	1	1	1	0	0
H$_2$	0	0	1	1	1

DOI: 10.14750/ME.2022.010

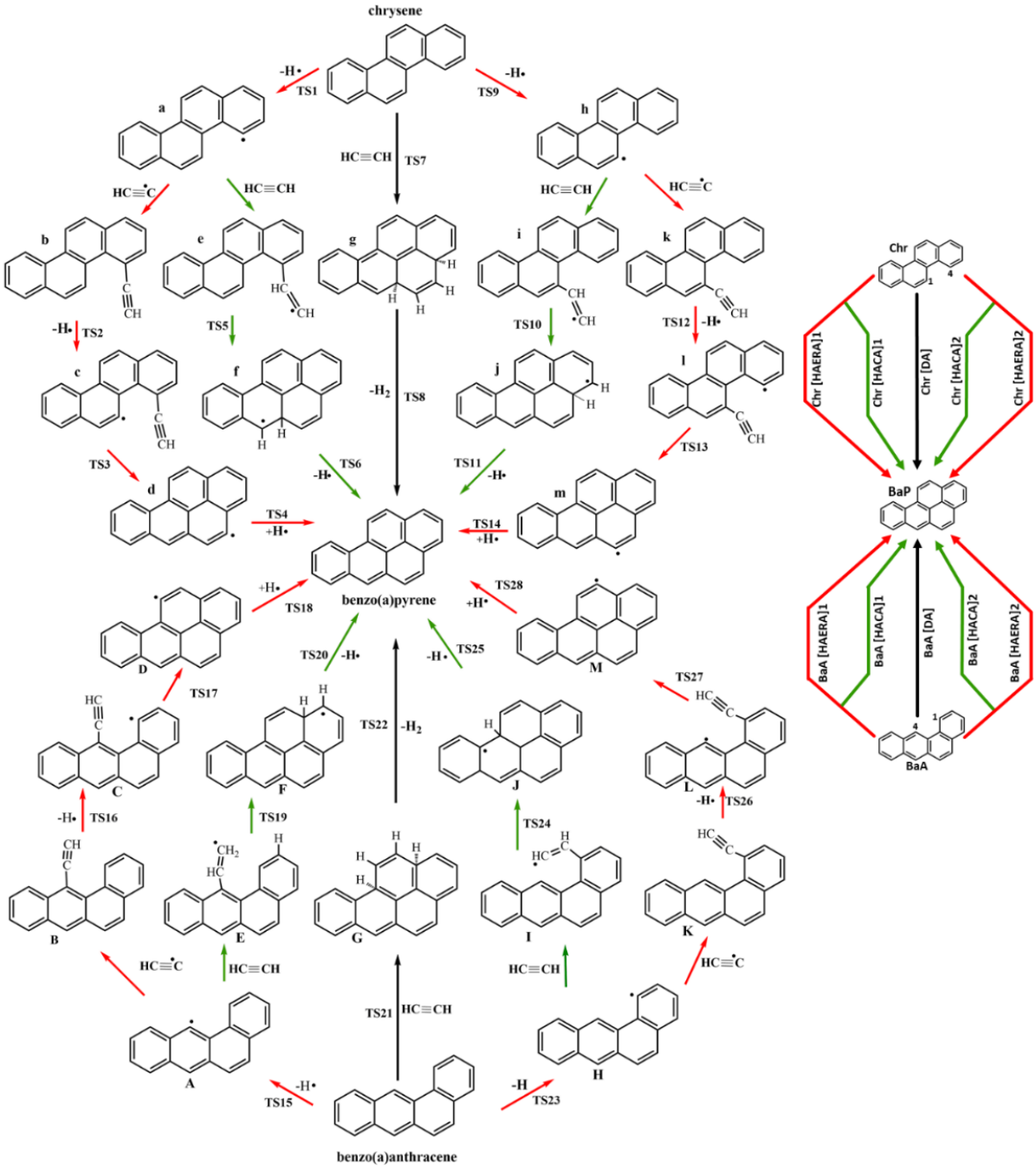

Figure 27 *The reaction pathways of benzo(a)pyrene formation starting from chrysene or benzo(a)anthracene. HACA - hydrogen abstraction acetylene addition, HAERA - hydrogen abstraction ethynyl radical addition, DA - Diels-Alder reaction mechanism.*

DOI: 10.14750/ME.2022.010

3.2.1. Description of the reactions pathways

The difference between the HAERA1 and HAERA2 routes as well as between the HACA1 and HACA2 pathways is the position where the first hydrogen abstraction took place (armchair site denoted with 1 and 4 in (**Figure 27**) which will lead to the formation of either **a**, or **h**, and **A** or **H** radical intermediates, respectively. The first steps are the same for both HAERA and HACA mechanisms (**Figure 27**). The reactions start with a hydrogen abstraction from chrysene or benzo(a)anthracene. This can occur by involving radicals, ($H^{\bullet}$, $^{\bullet}OH$, $^{\bullet}CH_3$, *etc.*) which can be present in high concentrations in flames. The type of radical which removes the hydrogen atom influence the energetics as well. However, the goal is to study the chosen mechanisms through the simplest systems, therefore we limited our consideration to H radicals. In the case of the Diels-Alder type mechanism, the first step is the direct addition of acetylene to either chrysene or benzo(a)anthracene (**Figure 27**). Furthermore, the reaction is shorter compared to the other routes and will reach the product within two steps.

3.2.1.1. HAERA reaction mechanism

In the HAERA reaction mechanism the first intermediate species are obtained by endoergic hydrogen abstraction reactions (**a**, **A**, **h**, **H**) and all four have similar reaction energy values in a range of 29.73 to 32.08 kJ/mol (**Figure 28 a**). The reactions are continued with barrierless additions of ethynyl radicals on the free radical sites of **a**, **A**, **h**, **H** to form **b, k**, **B**, **K** structures (**Figure 27**). These steps occurred with similar relative energy values in a range from -554.06 to -562.14 kJ/mol. The reactions continue with the second hydrogen abstraction. All of them represented a slightly endoergic reaction step. To overcome the energy barriers the following activation energy values are required, $\Delta E_0^{\ddagger}$(**TS2**) = 69.24 kJ/mol, $\Delta E_0^{\ddagger}$(**TS12**) = 67.44 kJ/mol, $\Delta E_0^{\ddagger}$(**TS16**) = 70.75 kJ/mol and $\Delta E_0^{\ddagger}$(**TS26**) = 75.31 kJ/mol.

DOI: 10.14750/ME.2022.010

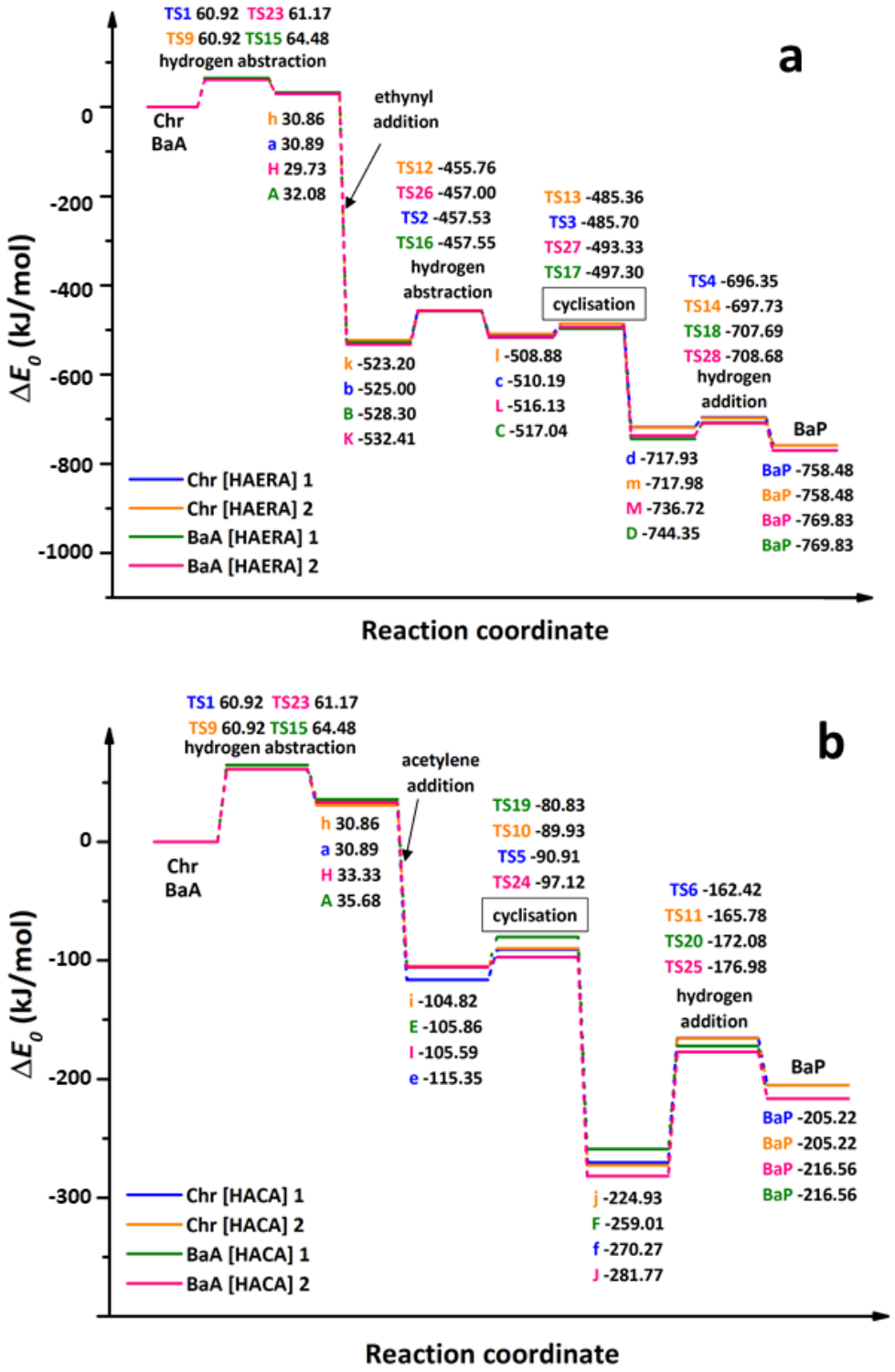

Figure 28 *Reaction energy profile (zero-point corrected) of the HAERA (a) and HACA (b) reaction pathways leading to the formation of benzo(a)pyrene (BaP) calculated at the ωB97X-D/6-311++G(d,p) level of theory. The chrysene pathways are indicated with blue and orange (solid and dotted) lines. In the case of benzo(a)anthracene, the reaction routes are represented with green and pink (solid and dotted) lines. The unimolecular steps are indicated with black frames.*

Table 4 *Zero-point corrected electronic energy (ΔE, kJ/mol) values of the corresponding conformer structures and their differences obtained in the HAERA reaction mechanism with the addition of ethynyl radical.*

Computational method	Transition state structure	Reaction pathway	Conformer type	
			S	R
B3LYP	TS2	Chr [HAERA]1	-494.98	-495.10
	TS12	Chr [HAERA]2	-493.58	-493.40
	TS16	BaA [HAERA]1	-493.20	-485.41
	TS26	BaA [HAERA]2	-494.21	-486.53
M062X	TS2	Chr [HAERA]1	-494.62	-493.98
	TS12	Chr [HAERA]2	-492.45	-492.03
	TS16	BaA [HAERA]1	-493.82	-493.98
	TS26	BaA [HAERA]2	-493.63	-494.04
ωB97X-D	TS2	Chr [HAERA]1	-457.53	-456.79
	TS12	Chr [HAERA]2	-455.76	-455.73
	TS16	BaA [HAERA]1	-57.55	-457.18
	TS26	BaA [HAERA]2	-457.10	-457.33

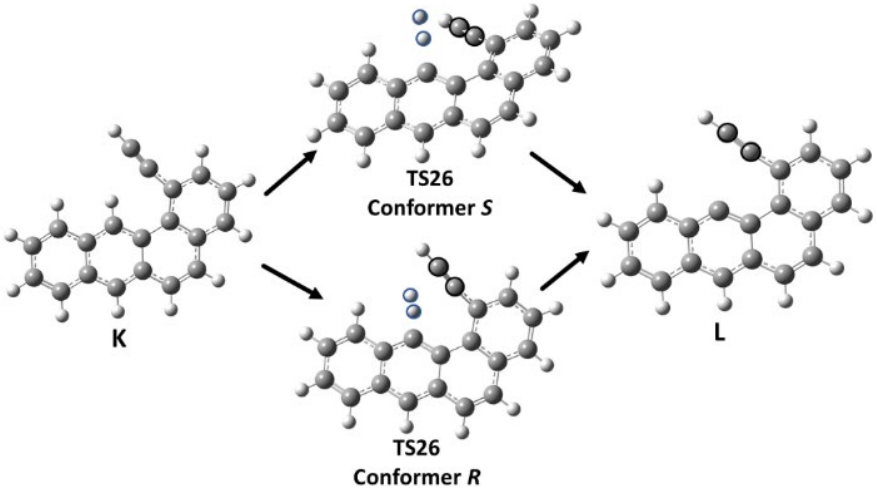

Figure 29 *Conformers of the TS26 structure.*

It is important to mention that the H_2 formation can take place on either side of the plane of the aromatic ring (**Table 4, Figure 29**). This geometrical difference will lead to a pair of chiral structures that could be assigned as *R* and *S* configurations with equal energies (**Figure 29**). The temporary chirality of the TS will disappear with the formation of all four intermediates (**c**, **l**, **C**, **L**) which do not contain a chiral center anymore. The reactions

are continued with cyclizations in order to obtain the fifth aromatic ring in the **d, m**, **M,** and **D** radicals. The ring closures occurred by the attack of the 1 or 4 carbon, which is carried out by the pendulous ethynyl group in the cases of [HAERA]1 and [HAERA]2 reaction pathways, respectively. For both chrysene and benzo(a)anthracene reaction routes this represents the only unimolecular step in the HAERA reaction mechanisms and corresponds to the second most exoergic reaction step with a reaction energy value lower than -207 kJ/mol. Among the unimolecular steps **TS17** in BaA[HAERA]1 has the lowest activation energy ($\Delta E_0^{\ddagger}$ (**TS17**) = 19.74 kJ/mol). The other three unimolecular steps, **TS3**, **TS13**, and **TS27** have higher, but very similar activation energy values 24.49, 23.53, and 22.79 kJ/mol, respectively. In the last step, exoergic hydrogen addition occurs in all four reaction routes to reach benzo(a)pyrene. The corresponding activation energy values are in the range of 20.25 kJ/mol and 36.65 kJ/mol. In the HAERA reaction routes the final product is the most stable structure with -758.48 kJ/mol and -769.83 kJ/mol in the Chr and BaA routes, respectively.

3.2.1.2. HACA reaction pathways

In total four HACA pathways (Chr[HACA]1; Chr[HACA]2; BaA[HACA]1; BaA[HACA]2) are leading to BaP and starting either from chrysene or benzo(a)anthracene (**Figure 27**). The first hydrogen abstractions are the rate-determining steps and these are the same as in the HAERA routes as well. The corresponding barrier heights are in a range of 60.92 and 64.48 kJ/mol (**Figure 28, b**). Energetically the two pairs of HACA routes starting from Chr and BaA are very similar to each other. The highest deviation between the corresponding steps (Chr[HACA]1; Chr[HACA]2 and BaA[HACA]1; BaA[HACA]2) are 11.53 kJ/mol and 22.77 kJ/mol, respectively. After the formation of the first intermediate species (**a**, **h**, **A**, **H**) the reactions are followed by the second most exoergic steps, which is the barrierless addition of acetylene whereupon **e**, **i**, **E**, **I** structures are reached. The relative reaction energy values are between -138.92 and -147.24 kJ/mol. The reaction pathways continue with cyclizations and thus, the fifth six-membered rings will be

achieved when **f**, **j**, **F** and **J** structures are formed. These steps represent the only unimolecular and most exoergic steps, placing the resulting intermediates between the -259.01 and -281.77 kJ/mol energy levels. The corresponding energy barriers are relatively low (>8.47 kJ/mol and <25.47 kJ/mol). Both *cis* and *trans* isomers of the **e**, **E**, **i** and **I** intermediates are calculated (**Table 11**). However, the cyclization could not occur through the *trans* structure and thus, only the *cis* isomers are considered in the reaction mechanism (**Figure 30**). In the last step, hydrogen atom abstraction occurs to reach benzo(a)pyrene with a -205.22 kJ/mol and -216.56 kJ/mol reaction energy in the cases of chrysene and benzo(a)anthracene reaction routes, respectively.

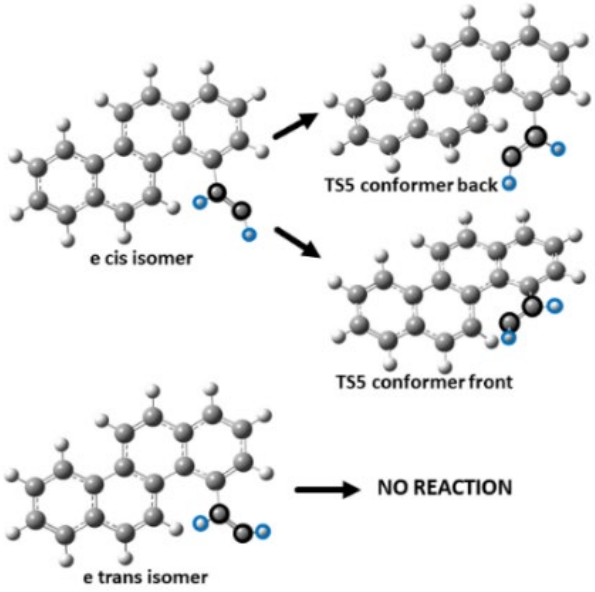

Figure 30 *Cis and trans isomers of the e intermediate structure on the left-hand side, and the back and front isomers of the TS5 structure.*

3.2.1.3. Diels-Alder-type pathways

The formation of benzo(a)pyrene through the Diels-Alder mechanism is much simpler compared to the HACA and HAERA mechanisms. The reaction pat hways consist of only one intermediate and two transition state structures (**Figure 27** and **Figure 31**). The reaction starts with the acetylene cycloadditions to the armchair sites of chrysene or benzo(a)anthracene, in order to form **g** or **G** structures, respectively (**Figure 31**)**.** The Diels-Alder adduct (**g** and **G**) formation is followed by a hydrogen elimination. The first steps in both routes have a high energy barrier with an activation energy of 220.07

kJ/mol and 164.61 kJ/mol, for **TS7** and **TS21**, respectively. The **g** intermediate is formed endoergically, while the **G** structure reached exoergically. The reaction continues with the exoergic hydrogen molecule elimination, which will lead to the benzo(a)pyrene formation. The activation energy values of the second transition states are 62.04 kJ/mol and 97.48 kJ/mol for the chrysene and benzo(a)anthracene routes, respectively (**Figure 31**). The final product, BaP is the most stable structure in both cases with a relative energy of -205.21 and -216.57 kJ/mol in the case of Chr and BaA, respectively.By comparing the two Diels-Alder pathways, it can be seen that the BaA[DA] is energetically more feasible than the Chr[DA] reaction route. A similar trend is obtained in the theoretical study of Kislov *et al.* [135] carried out on Diels-Alder-type reactions for pyrene formation. In their work the first step has a high barrier and is endothermic but the second one is strongly exothermic and exhibits at least 2 times lower barriers, similarly to our Chr[DA] reaction route [135].

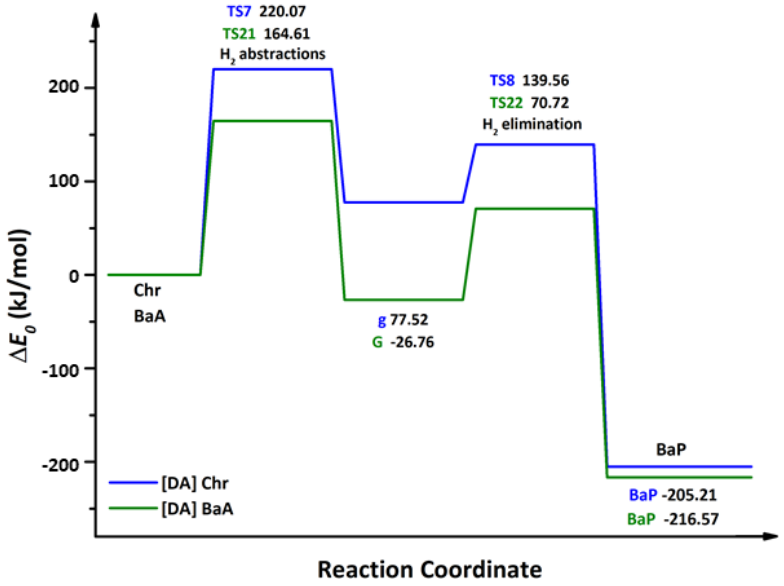

Figure 31 *Reaction energy profile (zero-point corrected) of the two Diels-Alder reaction pathways with acetylene addition leading to the formation of benzo(a)pyrene (BaP) calculated at the ωB97X-D/6-311++G(d,p) level of theory. The reaction pathways are indicated with blue and green (solid and dotted) lines for chrysene and benzo(a)anthracene, respectively.*

DOI: 10.14750/ME.2022.010

3.2.2. Conclusion

In this work, new reaction pathways leading to benzo(a)pyrene (BaP), a PAH with five benzene rings and with well-known carcinogenic effects, are explored. Chrysene and benzo(a)anthracene are chosen as starting structures to examine the routes in which two PAHs with four aromatic rings become more toxic just by an additional benzene ring. HACA (hydrogen abstraction acetylene addition), HAERA (hydrogen abstraction ethynyl radical addition) and DA (Diels-Alder) mechanism-based BaP formation pathways are investigated. The mechanisms included H abstractions, additions of acetylenes, ethynyls and hydrogens, ring closures, and hydrogen eliminations. To select the best computational method to study the reactions, homolytic bond dissociation energies of naphthalene and acenaphthylene are computed and compared to experimental values. The lowest deviations (2.2 kJ/mol and 1.6 kJ/mol) between the available experimental and calculated BDE values are achieved by using the ωB97X-D/6-311++G(d,p) level of theory. Thus, this is proved to be suitable to z analyze the reactions. It is found that the rate-determining steps are in a range between 60.92 kJ/mol and 64.48 kJ/mol for the HAERA and HACA mechanisms as well. For the Diels-Alder mechanism, the highest barrier heights are 220.07 kJ/mol and 164.61 kJ/mol for Chr[DA] and BaA[DA], respectively. In the HACA pathway the most exoergic reaction step occurs at the cyclisation in the BaA[HACA]2 route with around -184 kJ/mol. The most exoergic reaction step in the case of the HAERA mechanism is the ethynyl radical addition and the corresponding relative energy is lower than -523 kJ/mol. Since in the Diels-Alder pathways higher energy barriers are identified, the formation of benzo(a)pyrene can be considered more likely through the HACA and HAERA mechanisms. By comparing the chrysene and benzo(a)anthracene routes within a specific reaction mechanism, except the Diels-Alder-type mechanisms, there are no significant differences, which is not surprising as the starting structures are similar, and that in the Chr-BaA comparison the position of the terminal benzene ring is not expected to have a significant influence on the energetics of the radical centers.

3.3. Benzo(a)pyrene formation - MAC mechanism

The formation of benzo(a)pyrene through HACA, HAERA, and DA mechanisms was presented in the previous chapter. However, the formation of benzo(a)pyrene besides the use of acetylene and ethynyl radicals can be achieved with the addition of methyl radicals as well. In this chapter two methyl addition cyclization (MAC) mechanism-based benzo(a)pyrene formation pathways are investigated starting either from the armchair positions of Chr or BaA (**Figure 32**). Both reaction routes include 25 structures: 13 intermediate structures and 12 transition state structures. The intermediate species found in the reaction pathways are denoted alphabetically with lower- and upper case letters (Benzo(a)anthracene = "**a**"; Chrysene = "**A**", **Figure 32**). The transition state structures between successive intermediates such as A and B are denoted as a TS having A and B together in subscript (TS_{AB}). In order to determine the energy level of the reactants, intermediates, transition states and products the Gaussian 09 program package is used [188]. For geometry optimizations, two density functional theory (DFT) methods are applied, the Becke three parameter hybrid method with Lee–Yang–Parr correlation functional approximation (B3LYP) for preliminary calculations and the highly effective Minnesota hybrid meta exchange correlation functional (M06-2X). B3LYP is used in combination with a valence double-ζ basis set including diffuse and polarization functions on heavy atoms and polarization functions for hydrogen (6-31+G(d,p)), while M06-2X calculations are carried out by using the 6-311++G(d,p) basis set [233], [234]. The structures are pre-optimized at the B3LYP/6-31+G(d,p) level of theory. Then, the M06-2X calculations are performed with the default (99 radial shells and 590 angular points per shell) and a finetuned integration grid (99 radial shells and 974 angular points per shell) as well. Both functionals proved to be successful in the study of various aspects of PAHs [61], [235]. However, it is revealed recently, that M06-2X in some cases underestimates activation energies [213]. Therefore, activation energy values obtained by using the two functionals are compared for verification

DOI: 10.14750/ME.2022.010

purposes. Critical stationary points are characterized by frequency calculations at both levels of theory.

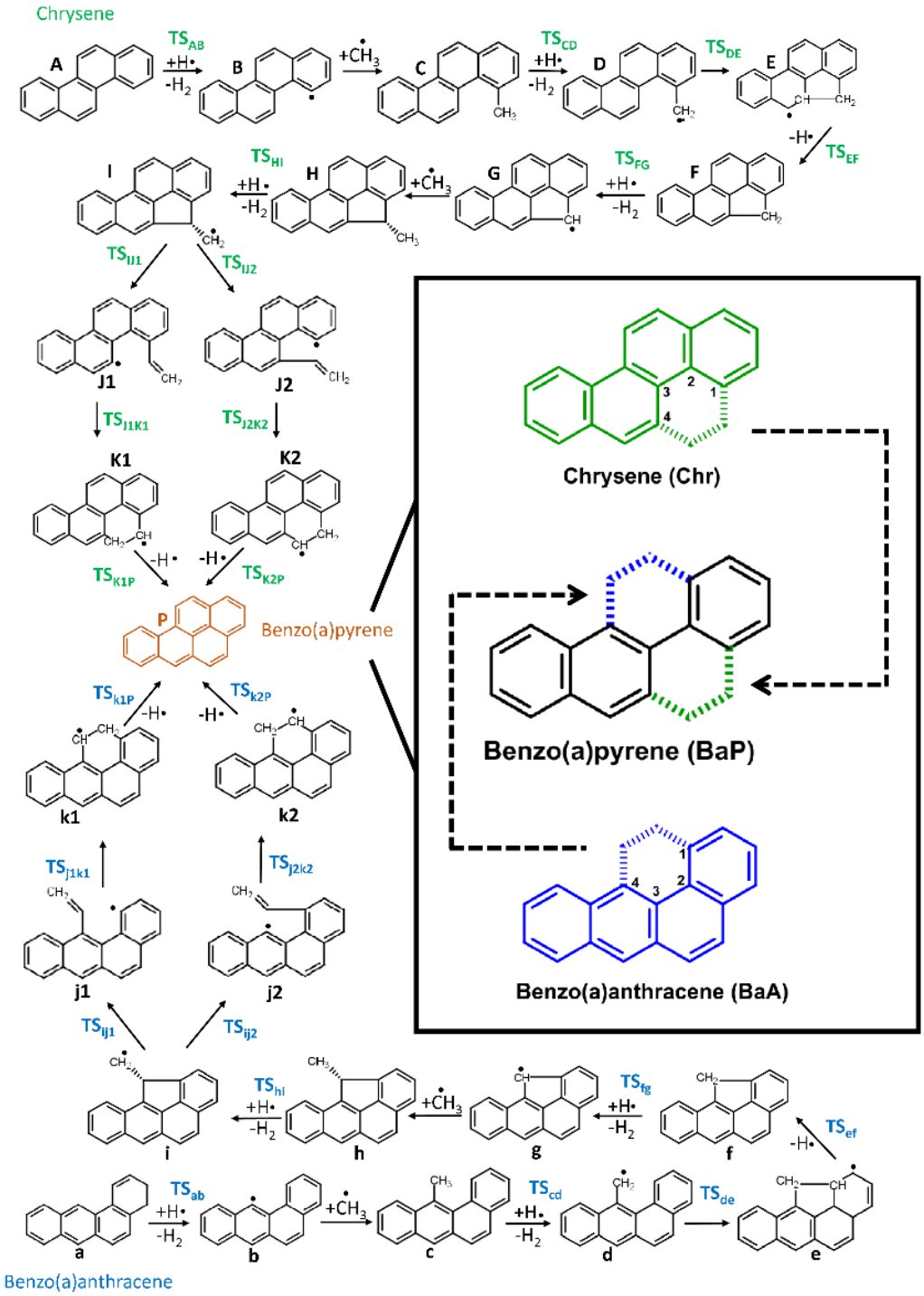

Figure 32 *Reaction pathways of the formation of benzo(a)pyrene ("P") starting from chrysene ("A") or benzo(a)anthracene ("a"). 2D structures of chrysene, benzo(a)pyrene, benzo(a)anthracene is highlighted along with the carbon atoms, which are involved in the new ring formations.*

In addition, to verify that the computed transition states (first-order saddle points) connected the desired starting materials and products (local minima), intrinsic reaction coordinate (IRC) analysis [236] is carried out at the M06-2X/6-311++G(d,p) level of theory.

3.3.1. Balance and validation

The reaction and activation energies as well as the relative energies of the studied molecules are calculated. The reference levels of the two benzo(a)pyrene formation reaction channels corresponded to chrysene (Chr) and benzo(a)anthracene (BaA) with four additional hydrogen atoms (4H•) and two methyl radicals (2•CH_3), which served as reaction partners. Atomic balance is considered and the number of carbon and hydrogen atoms are kept the same by using additional species (hydrogen atoms, hydrogen molecules and methyl radicals) in each step of benzo(a)pyrene formation (**Figure 33**).

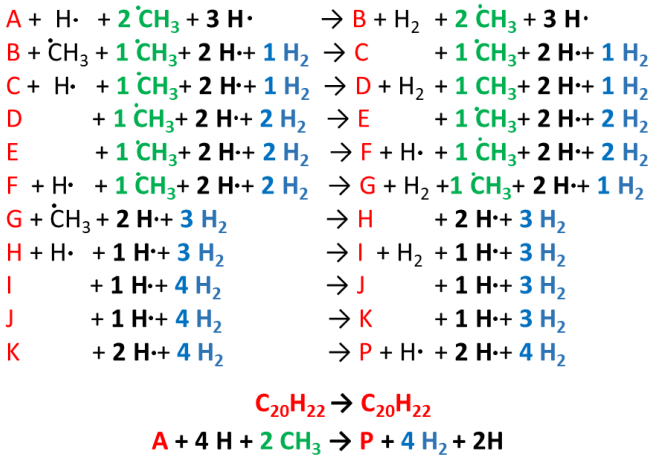

Figure 33 *Atomic balance considered and the number of carbon and hydrogen atoms kept the same by using additional species (hydrogen atoms, hydrogen molecules and methyl radicals) in each step of benzo(a)pyrene formation.*

In order to validate geometric parameters, the obtained results have been compared to experimental values. The results are well in line with the experimental values [237], [238], having a relative error of less than 2% on average for chrysene for both levels of theories (**Table 5** and **Table 6, Figure 34**). However, in the case of benzo(a)pyrene,

the relative errors are 0.5% and 4.1% on average for M06-2X and B3LYP functionals, respectively.

Table 5 *The experimental and computed bond lengths values of chrysene and the relative errors for both levels of theories.*

Bonds in benzo(a)pyrene	Experimental values (Å)	Calc M06-2X/6-311++G(d,p) (Å)	Relative error (%)	Calc B3LYP/6-31+G(d,p) (Å)	Relative error (%)
C1-C2	1.352	1.357	0.4	1.433	6.0
C2-C3	1.441	1.429	0.8	1.367	5.0
C3-C4	1.412	1.405	0.5	1.430	1.3
C4-C5	1.375	1.381	0.4	1.411	2.6
C5-C6	1.378	1.396	1.3	1.389	0.8
C6-C7	1.402	1.391	0.8	1.401	0.1
C7-C8	1.433	1.445	0.8	1.400	2.3
C8-C9	1.342	1.347	0.0	1.443	7.5
C9-C10	1.446	1.446	0.0	1.358	6.1
C10-C11	1.361	1.374	1.0	1.443	6.1
C11-C12	1.418	1.413	0.4	1.385	2.3
C12-C13	1.425	1.420	0.4	1.416	0.7
C13-C14	1.374	1.367	0.5	1.424	3.7
C14-C15	1.397	1.412	1.1	1.376	1.5
C15-C16	1.364	1.370	0.4	1.416	3.8
C16-C17	1.418	1.419	0.1	1.416	0.2
C17-C18	1.436	1.438	0.1	1.422	1.0
C18-C19	1.393	1.407	1.0	1.444	3.6
C19-C20	1.419	1.429	0.7	1.432	0.9
C1-C18	1.423	1.432	0.6	1.433	0.7
C3-C20	1.417	1.416	0.1	1.427	0.7
C7-C20	1.415	1.422	0.5	1.431	1.1
C10-C19	1.444	1.436	0.6	1.443	0.1
C12-C17	1.410	1.422	1.6	1.435	2.5

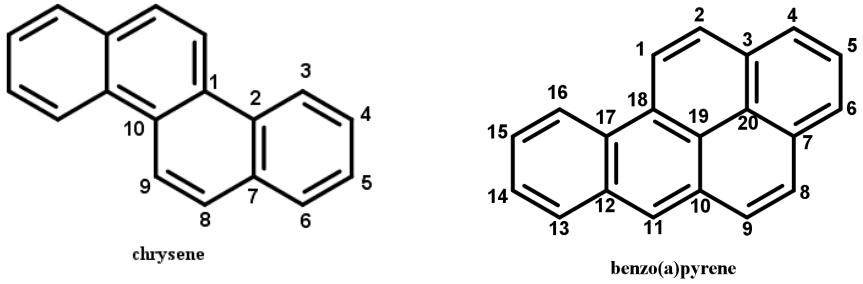

Figure 34 *Atom labeling scheme used in Table 2 and 3 for chrysene and benzo(a)pyrene respectively.*

Table 6 *The experimental and computed bond lengths values of chrysene and the relative errors for both levels of theory*

Bonds in chrysene	Experimental values [237] (Å)	Calc M06-2X/6-311++G(d,p) (Å)	Relative error (%)	Calc B3LYP/6-31+G(d,p) (Å)	Relative error (%)
C1-C2	1.409	1.450	2.9	1.454	2.9
C2-C3	1.433	1.415	1.6	1.419	1.6
C3-C4	1.423	1.375	3.7	1.382	2.9
C4-C5	1.387	1.407	0.9	1.410	1.7
C5-C6	1.392	1.372	1.6	1.380	0.9
C6-C7	1.435	1.413	1.7	1.417	1.3
C8-C9	1.410	1.426	0.7	1.427	1.2
C9-C10	1.403	1.356	3.8	1.365	2.7
C10-C1	1.402	1.405	0.2	1.418	1.1
C2-C7	1.390	1.415	1.4	1.428	2.7

In addition, to verify the method selection, homolytic bond dissociation energies (BDE) of naphthalene, which is the simplest PAH, are computed and the calculated values are compared to the experimental data [239]. The calculated and experimentally measured BDEs are in good agreement with each other as the deviation (BDE_{exp} - BDE_{calc}) is only 1.72 kJ/mol and 3.8 kJ/mol for B3LYP/6-31+G(d,p) (**Table 2**) and M06-2X/6-311++G(d,p), respectively. Thus, the selected model chemistries are reliable and could be used to compute thermochemical parameters of polycyclic aromatic hydrocarbons.

3.3.2. Analysis of the reaction routes

The structural parameters of the transition states such as the bond lengths and angles are collected in **Table 7.** Representative transition state structures (**TS_{ab}**, **TS_{cd}**, **TS_{FG}**, **TS_{J2K2}**) along with the geometrical parameters are depicted in **Figure 35**.

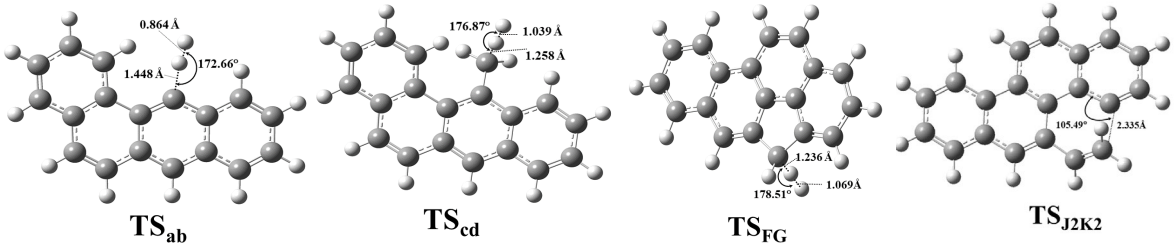

Figure 35 *Representative transition state structures of benzo(a)pyrene formation starting from benzo(a)anthracene (TS_{ab} and TS_{cd}) and chrysene (TS_{FG} and TS_{J2K2}) are located at the M06-2X/6-311++G(d,p) level of theory using a finetuned integration grid (99 radial shells and 974 angular points per shell) and depicted along with interatomic distances and bond angle.*

DOI: 10.14750/ME.2022.010

Table 7 *Structural parameters (bond lengths, angles) of transition state structures of benzo(a)pyren mechanisms starting from benzo(a)anthracene (BaA→BaP) or chrysene (Chr→BaP). The structures ar 311++G(d,p) level of theory at 298.15 K and 1 atm.*

Reaction Type	Transition State	Angles			Bond length (Å)			
			BaA → BaP	Chr → BaP	H-H (BaA→ BaP)	H-H (Chr→ BaP)	C-H (BaA→ BaP)	C-H (Chr→
Hydrogen abstraction	TS_{ab} /TS_{AB}	C-H-H	172.66°	169.44°	0.864	0.868	1.448	1.43
	TS_{cd} /TS_{CD}	C-H-H	176.87°	176.73°	1.039	1.017	1.258	1.26
	TS_{fg} /TS_{FG}	C-H-H	177.87°	178.52°	1.069	1.069	1.237	1.23
	TS_{hi} /TS_{HI}	C-H-H	172.32°	171.84°	0.911	0.910	1.376	1.37
Hydrogen dissociation	TS_{ef} /TS_{EF}	C-C-H	92.90°	97.72°	-	-	1.788	1.80
	TS_{k1P} /TS_{K1P}	H-C-H	84.24°	84.68°	-	-	1.892	1.90
	TS_{k2P} /TS_{K2P}	H-C-H	82.43°	84.12°	-	-	1.878	1.90
	TS_{de} /TS_{DE}	C-C-C	91.37°	91.04°	-	-	-	-
Ring Opening/ Ring Closure	TS_{ij1} /TS_{IJ1}	C-C-C	107.98°	110.41°	-	-	-	-
	TS_{ij2} /T_{SIJ2}	C-C-C	110.42°	110.70°	-	-	-	-
	TS_{j1k1} /T_{J1K1}	C-C-C	105.72°	105.62°	-	-	-	-
	TS_{j2k2} /T_{J2K2}	C-C-C	106.00°	105.49°	-	-	-	-

DOI: 10.14750/ME.2022.010

The activation energy values of the reactions are calculated and are enumerated in **Table 8** and **Table 9**. In the case of the chrysene route, the Gibbs free energy of activation values obtained with B3LYP/6-31+G(d,p) is lower (13.0 kJ/mol on average) than those obtained with M06-2X/6-311++G(d,p) in all cases. This is also the case for the benzo(a)anthracene route, except **TS_{ef}** structure, which is higher with 2 kJ/mol than the values obtained with M06-2X/6-311++G(d,p).

Table 8 *Comparison of the activation energy values ($\Delta G^{\ddagger}$, kJ/mol) of benzo(a)pyrene (BaP) formation mechanism starting from chrysene (Chr → BaP) computed at the B3LYP/6-31+G(d,p) [B3LYP] and M06-2X/6-311++G(d,p) [M06-2X] levels of theory. In the latter case, the calculations are performed besides the default integration grid (99 radial shells and 590 angular points per shell) with a finetuned setting as well (99 radial shells and 974 angular points per shell) [M06-2X_gr]. The difference between the activation energies ($\Delta\Delta G^{\ddagger}$, kJ/mol) of [M06-2X vs B3LYP] and [M06-2X_gr vs B3LYP] is also tabulated.*

Chr → BaP	M06-2X	B3LYP	M06-2X_gr	M06-2X vs B3LYP	M06-2X_gr vs B3LYP
	$\Delta G^{\ddagger}$			$\Delta\Delta G^{\ddagger}$	
	kJ/mol				
A - **TS_{AB}** - B	90.71	68.21	92.24	22.49	24.03
C - **TS_{CD}** - D	55.76	30.00	55.62	25.77	25.62
D - **TS_{DE}** - E	115.07	110.70	112.16	4.37	1.46
E - **TS_{EF}** - F	123.47	121.48	122.57	1.98	1.08
F - **TS_{FG}** - G	51.87	27.64	51.71	24.24	24.07
H - **TS_{HI}** - I	73.01	48.43	72.34	24.58	23.91
I - **TS_{IJ1}** - J1	120.41	105.63	121.93	15.06	16.29
I - **TS_{IJ2}** - J2	120.69	105.63	121.93	15.06	16.29
J1 - **TS_{J1K1}** - K1	27.04	20.72	27.42	6.32	6.70
J2 - **TS_{J1K2}** - K2	28.93	21.61	28.70	7.32	7.09
K1 - **TS_{K1P}** - P	152.21	147.48	152.55	4.73	5.07
K2 - **TS_{K2P}** - P	153.46	148.38	153.32	5.08	4.94

DOI: 10.14750/ME.2022.010

Table 9 *Comparison of the activation energy values (ΔG‡, kJ/mol) of benzo(a)pyrene (BaP) formation mechanism starting from benzo(a)anthracene (BaA → BaP) computed at the B3LYP/6-31+G(d,p) [B3LYP] and M06-2X/6-311++G(d,p) [M06-2X] levels of theory. In the latter case, the calculations are performed besides the default integration grid (99 radial shells and 590 angular points per shell) with a finetuned setting as well (99 radial shells and 974 angular points per shell) [M06-2X_gr]. The difference between the activation energies (ΔΔG‡, kJ/mol) of [M06-2X vs B3LYP] and [M06-2X_gr vs B3LYP] is also tabulated.*

BaA → BaP	M06-2X	B3LYP	M06-2X_gr	M06-2X vs B3LYP	M06-2X_gr vs B3LYP
	$\Delta G^{\ddagger}$			$\Delta\Delta G^{\ddagger}$	
	kJ/mol				
a - **TS_{ab}** - b	94.43	71.09	94.50	23.34	23.40
c - **TS_{cd}** - d	52.83	26.69	52.15	26.14	25.46
d - **Ts_{de}** - e	132.92	128.48	132.61	4.44	4.12
e - **Ts_{ef}** - f	114.11	116.27	114.26	2.16	2.01
f - **TS_{fg}** - g	51.70	27.67	51.28	24.03	23.60
h - **TS_{hi}** - i	72.25	48.39	72.15	23.86	23.76
i - **TS_{ij1}** - j1	120.01	104.56	121.76	15.45	17.20
i - **TS_{ij2}** - j2	118.63	99.64	119.71	18.99	20.07
j1 - **TS_{j1k1}** - k1	20.95	14.13	20.64	6.82	6.51
j1 - **TS_{j1k2}** - k2	27.57	21.25	27.40	6.32	6.15
k1 - **TS_{k1P}** - P	149.04	145.39	149.83	3.65	4.43
k2 - **TS_{k2P}** - P	137.57	135.05	137.87	2.52	2.81

In order to evaluate and compare energetically the reaction mechanisms, a potential energy diagram is drawn (**Figure 36**). It clearly shows, that both reaction routes follow a similar trend. Both of the proposed pathways include the alternation of the two essential steps. These are the hydrogen abstractions to create radical sites on PAH structures, which is followed by the methyl addition. The hydrogen abstraction is achieved by either an additional hydrogen atom or by self cleavage of the carbon-hydrogen bonds, which lead to a carbon-centered radical. Then, the addition of a methyl group to the previously formed free radical site can occur.

DOI: 10.14750/ME.2022.010

Table 10 *Relative Gibbs free energy (ΔG, kJ/mol), relative enthalpy (ΔH, kJ/mol), and entropy (S, cal/mol*K) values of benzo(a)pyrene (BaP) formation mechanism starting from chrysene (Chr→BaP) or benzo(a)anthracene (BaA→BaP) computed at the M06-2X/6-311++G(d,p) level of theory using a fine-tuned integration grid (99 radial shells and 974 angular points per shell), at 298.15 K and 1 atm within the harmonic oscillator rigid rotor approximation.*

BaA→BaP	Δ*G*	Δ*H*	*S*	Chr→BaP	Δ*G*	Δ*H*	*S*
a	0.00	0.00	108.46	**A**	0.00	0.00	108.91
TS_{ab}	94.50	67.86	114.51	**TS_{AB}**	92.24	64.50	114.06
b	24.76	30.63	109.44	**B**	21.46	26.89	109.54
c	−307.39	−359.74	113.13	**C**	−313.47	−364.87	114.34
TS_{cd}	−255.24	−336.50	117.34	**TS_{CD}**	−257.86	−339.06	117.84
d	−389.58	−435.92	114.22	**D**	−377.64	−424.03	114.62
TS_{de}	−256.98	−306.65	111.54	**TS_{DE}**	−265.48	−315.72	111.53
e	−358.30	−408.32	111.27	**E**	−372.38	−422.91	111.31
TS_{ef}	−244.05	−294.14	111.21	**TS_{EF}**	−249.81	−300.47	111.21
f	−295.00	−314.47	108.36	**F**	−300.71	−320.71	108.38
TS_{fg}	−243.72	−291.55	113.02	**TS_{FG}**	−248.99	−297.58	112.86
g	−387.31	−401.11	109.19	**G**	−390.87	−405.51	108.96
h	−631.14	−700.50	115.01	**H**	−639.50	−708.80	115.49
TS_{hi}	−558.99	−656.73	119.65	**TS_{HI}**	−567.16	−664.70	120.25
i	−649.59	−710.62	117.95	**I**	−655.24	−715.79	118.78
TS_{ij1}	−527.83	−590.35	117.05	**TS_{IJ1}**	−533.35	−595.99	117.10
TS_{ij2}	−529.88	−592.03	116.76	**TS_{IJ2}**	−533.31	−596.02	117.05
j_1	−545.54	−603.31	120.90	**J_1**	−553.65	−611.28	121.12
j_2	−553.48	−610.83	120.57	**J_2**	−552.85	−610.59	121.03
TS_{j1k1}	−524.89	−587.64	116.58	**TS_{J1K1}**	−526.23	−588.62	117.31
TS_{j2k2}	−526.08	−588.47	116.87	**TS_{J2K2}**	−524.15	−586.46	117.38
k_1	−764.02	−827.12	116.29	**K_1**	−755.42	−818.33	116.88
k_2	−752.55	−818.11	114.32	**K_2**	−756.29	−820.14	116.13
TS_{k1P}	−614.19	−678.89	115.01	**TS_{K1P}**	−602.87	−668.16	114.99
TS_{k2P}	−614.69	−679.93	114.58	**TS_{K2P}**	−602.96	−668.26	114.97
P	−658.89	−694.43	110.99	**P**	−646.93	−683.02	110.99

Based on the structural features of the starting species (”**A**” and ”**a**” structures in **Figure 32**) the growth mechanisms are started by hydrogen abstractions following the attack of external H-atoms from the first and fourth carbon atoms (**Figure 32**) in the case of

DOI: 10.14750/ME.2022.010

chrysene and benzo(a)anthracene, respectively. These steps resulted in **B** and **b** radical intermediates (**Figure 32)** with the following activation energy values: $\Delta G^{\ddagger}$(**TS$_{AB}$**) = 92.2 kJ/mol and $\Delta G^{\ddagger}$(**TS$_{ab}$**) = 94.5kJ/mol (**Table 10**). Furthermore, the reaction energies for these endergonic reactions are 21.5 kJ/mol and 24.8 kJ/mol, in the case of **B** and **b**, respectively (Table 1). The reactions are continued with barrierless additions of methyl groups on the free radical sites of **B** and **b** in order to form methyl-chrysene and methyl-benzo(a)anthracene structures (**C** and **c**). These steps represented the most exergonic phases among the reaction mechanism, having ΔG(**BC**) = −334.9 kJ/mol and ΔG(**bc**) = −332.1 kJ/mol reaction energy values for the Chr and BaA channel, respectively. The reaction routes continued with hydrogen abstractions from the methyl groups of **C** and **c**. These are performed by external H atoms, the activation energies required to obtain **D** and **d** structures are $\Delta G^{\ddagger}$(**TS$_{CD}$**) = 55.6 kJ/mol and $\Delta G^{\ddagger}$(**TS$_{cd}$**) = 52.1 kJ/mol. These activation energy values are 1.7 times lower on average than those required for the **B** and **b** formation from **A** and **a**, due to the difference between the strengths of the C-H bonds in the aromatic structures compared to the aliphatic ones. The reactions are followed by the formations of five-membered ring structures (**E** and **e**) through the attack by the methylene groups at the 4th carbon in chrysene and the first carbon atom in BaA (**Figure 32**). This process occurs after overcoming the necessary Gibbs free energy of activation ($\Delta G^{\ddagger}$(**TS$_{DE}$**) = 112.2 kJ/mol and $\Delta G^{\ddagger}$(**TS$_{de}$**) = 132.6 kJ/mol, for the Chr and BaA route, respectively) (**Figure 36**). In the next step, hydrogen from the fourth and the first carbon atom has been eliminated in the case of chrysene and benzo(a)anthracene pathways respectively, which leads to the formation of the **F** and **f** structures. These endergonic reactions required ΔG**(EF)** = 71.7 kJ/mol and ΔG(**ef**) = 63.3 kJ/mol reaction energies (**Table 10**). For the reaction to proceed further, H abstraction from **F** and **f** molecules had to take place, after overcoming a Gibbs free energy of activation of $\Delta G^{\ddagger}$(**TS$_{FG}$**) = 51.7 kJ/mol and $\Delta G^{\ddagger}$(**TS$_{fg}$**) = 51.3 kJ/mol, reaching the intermediate radical species **G** and **g** with energy lower that 90.2 kJ/mol and 92.3 kJ/mol compared to the previous intermediates (**Figure 36**). At this point of the reaction mechanism, the second barrierless methyl addition occurred. As **G** and **g** are planar, this barrierless methyl

DOI: 10.14750/ME.2022.010

addition could have occurred from both sides of the plane, but it would have led to energetically equivalent species. Therefore, only one process is considered and will be discussed. This step increases the stability of the resulted **H** and **h** intermediate by 240.3 kJ/mol and 252.2 kJ/mol with respect to the previous structures (**G** and **g**). The formation of the **I** and i radical intermediate is attributed to another H abstraction from the methyl group by an external H atom, which requires an activation energy of $\Delta G^{\ddagger}$(**TS$_{HI}$**) = 72.3 kJ/mol and $\Delta G^{\ddagger}$(**TS$_{hi}$**) = 72.2 kJ/mol (**Figure 36**). In the next step, as it is shown in Figure 2, the reaction pathways are split into two routes, to obtain **J1** and **J2** as well as **j1** and **j2** structures by ring openings. The reaction routes continue after simultaneous bond breakings and bond formations. In the case of **J2** and **j1** the ring opening occurs at the first carbon, while in the case of **J1** and **j2** this takes place at the 4th carbon. **TS$_{IJ1}$** has the highest Gibbs free energy of activation values among these steps with $\Delta G^{\ddagger}$(**TS$_{IJ2}$**) = 121.9 kJ/mol. However, the difference between the corresponding Gibbs free energies (**TS$_{IJ1}$**, **TS$_{ij1}$** and **TS$_{IJ1}$**, **TS$_{ij1}$**) is just 1.16 kJ/mol on average. All **J1**, **J2**, **j1** and **j2** structures are formed by endothermic reactions. The fifth six-membered ring is formed in **K1** and **k1** as well as **K2** and **k2** structures, with a 205.7 kJ/mol reaction energy value on average. The most stable structure among the four resulting molecules is **k1** with −764.0 kJ/mol, after overcoming an $\Delta G^{\ddagger}$(**TS$_{j1k1}$**) = 20.6 kJ/mol Gibbs free energy of activation. The highest activation energy values appear on the last step for both routes, with $\Delta G^{\ddagger}$(**TS$_{K2P}$**) = 153.3 kJ/mol and $\Delta G^{\ddagger}$(**TS$_{k1P}$**) = 149.0 kJ/mol for chrysene and benzo(a)anthracene, respectively. As it can be seen, between the two routes of this part of the reaction (**K1** and **K2**; **k1** and **k2**; **Error! Reference source not found.**, the left-hand side of the benzo(a)anthracene pathway is more preferable energetically than the right-hand side (**k1** < **k2**). However, in the chrysene pathway, the opposite occurs, obtaining on the right-hand side a more stable molecule (**J2** < **J1**). The penultimate steps are again H eliminations, through which the final product, benzo(a)pyrene is achieved, with the stability of −646.9 kJ/mol and −658.9 kJ/mol, respectively (**Table 10, Figure 36**).

DOI: 10.14750/ME.2022.010

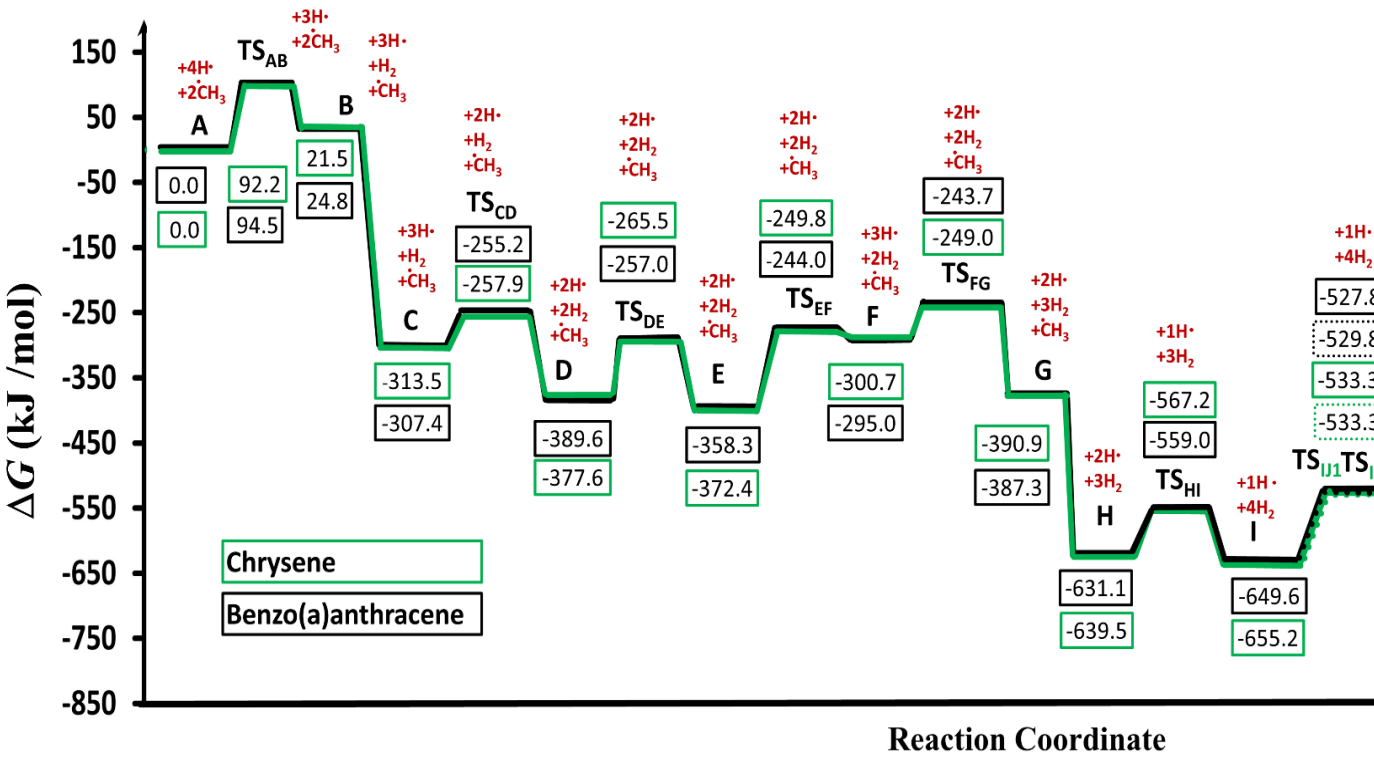

Figure 36 *Gibbs free energy profile of the two reaction pathways leading to the formation of benzo(the M06-2X/6-311++G(d,p) level of theory using a finetuned integration grid (99 radial shells and 97 two reaction pathways are indicated with green and black (solid /dotted) lines, in the case of chrys respectively.*

DOI: 10.14750/ME.2022.010

3.3.3. Conclusion

The formation of the strongly carcinogenic benzo(a)pyrene was studied by applying a newly developed methyl addition/cyclization (MAC) mechanism. Two reaction pathways are proposed starting from chrysene and benzo(a)anthracene (consisting of four aromatic rings), respectively. The reaction routes had the same reaction steps, both included four hydrogen abstractions, two methyl radical additions, three hydrogen atom eliminations, one ring closure and one rearrangement. Energetically the first methyl additions are the most exergonic steps, placing the resultant molecules to –313.5 kJ/mol and –307.4 kJ/mol (**C**, **c**) in case of the chrysene and benzo(a)anthracene, respectively. The two reaction pathways had very similar trends energetically, the difference between the energy levels of the corresponding molecules is just 6.13 kJ/mol on average. The k1 structure in the benzo(a)anthracene → benzo(a)pyrene pathway became the most stable molecule with ΔG = -764.0 kJ/mol. All in all, the formation of benzo(a)pyrene from chrysene and benzo(a)anthracene could be reached with this newly proposed MAC mechanism.

DOI: 10.14750/ME.2022.010

4. Summary

Polycyclic aromatic hydrocarbons (PAH) are harmful chemicals emitted to the environment by incomplete combustion. As the aromatic structure grows, the carcinogenic effect increases, and thus understanding their formation mechanisms is crucial. In this doctoral dissertation, reaction initiation points of the 16 priority PAHs are determined by computing the BDE and C-H bond lengths values. The results are in a range between 342.0 – 485.6 kJ/mol and 1.081 – 1.095 Å, in the case of the BDE and C-H bond lengths, respectively. The obtained results also showed that most of the initiation points are hydrogens in the armchair and peak positions.

In addition, new reaction pathways leading to benzo(a)pyrene, a PAH with well-known carcinogenic effects, are also explored. Starting from armchair positions of both chrysene or benzo(a)anthracene, four types of reaction mechanisms are studied: hydrogen abstraction acetylene addition (HACA), hydrogen abstraction ethynyl radical addition (HAERA), Diels-Alder (DA) and methyl addition cyclization (MAC) processes. A total of 12 reaction pathways are explored, with 50 intermediate and 52 transition state structures. Results show that HAERA is the most, and DA is the least exergonic reaction mechanism for benzo(a)pyrene formation using validated computational chemistry methods. It can be stated, that through this doctoral dissertation a deeper understanding of PAH growth and benzo(a)pyrene formation is achieved.

DOI: 10.14750/ME.2022.010

5. Összefoglalás

A szerves anyagok tökéletlen égése során policiklusos aromás szénhidrogének (PAH-ok) keletkeznek. Ahogy az aromás szerkezet növekszik, a vegyületek rákkeltő hatása fokozódik, ezért nagyon fontos a képződési mechanizmusaik feltárása és megértése. A doktori értekezésem első harmadában 16 ún. „parent" PAH kötésdiszociációs entalpiáit (BDE) vizsgálom és kategorizálom. Az eredmények azt mutatják, hogy a vizsgált molekulák BDE értékei és C-H kötéshosszai a 342,0 - 485,6 kJ/mol és 1,081 - 1,095 Å értékek közé esnek. Az eredmények alapján, a növekedési mechanizmusok lehetséges kezdőpontjait is meghatároztam. Az eredmények azt mutatják, hogy a reakciók az ún. karosszék („armchair") és csúcshelyzetekben („peak") elhelyezkedő hidrogének absztrakciójával kezdődnek.

A doktori disszertációmban az erősen rákkeltő benzo(a)pirén különböző reakció mechanizmusait is feltártam számításos kémiai módszerek alkalmazásával. Hidrogén absztrakció acetilén addíció (HACA), hidrogén absztrakció etinil gyök addíció (HAERA), Diels-Alder (DA) és metil addíciós ciklizáció (MAC) mechanizmusokat vizsgáltam, s ezek összesen 12 reakcióúton, 50 intermeridert és 52 átmeneti állapotot tartalmaznak. Az eredmények azt mutatják, hogy a HAERA a leginkább és a DA a legkevésbé exergonikus reakció útvonal. A számolásokhoz különböző elméleti szinteket alkalmaztam, de csak validált módszerekkel kapott eredmények kerültek tárgyalásra. Összességében elmondható, hogy az alábbi doktori értekezés eredményei elősegítik a PAH-ok, s különösen a benzo(a)pirén, képződésének és növekedésének mélyebb megértését.

DOI: 10.14750/ME.2022.010

6. New scientific results

Based on my computational research, carried out during my Ph.D. studies on the reaction mechanism of polycyclic aromatic hydrocarbons, the following main conclusions are drawn as new scientific results:

1st Thesis

Bond dissociation enthalpies (BDEs) of the 16 priority PAHs are calculated for each unique C-H bond by applying the ωB97X-D/6-311++G(d,p) level of theory and are categorized into seven groups: zig-zag, peak, armchair, penta-bay, anthracene type, aliphatic, and next-to-aliphatic type (**Figure 23**). The BDE and bond length values for the C-H bonds within the 16 priority PAH are in the range between 342.01 – 485.63 kJ/mol and 1.08 – 1.10 Å, respectively. Based on the calculated bond dissociation enthalpy (BDEs) values the potential reaction initiation points are determined on each 16 priority PAHs. The reaction initiation points are in armchair and peak positions for seven and six molecules from the 16 priority PAHs, respectively (**Figure 25**).

2nd Thesis

Benzo(a)pyrene (BaP) formation starting from armchair positions of benzo(a)anthracene (BaA) and chrysene (Chr) are explored by computational methods and a new growth mechanism has been proposed. The mechanism is a hydrogen abstraction ethynyl radical addition process (HAERA) within which two hydrogen abstractions, one ethynyl addition and one hydrogen atom addition occurred. Four possible HAERA reaction pathways are identified and each of these have four transition states and four intermediate structures (**Figure 27**).

DOI: 10.14750/ME.2022.010

3rd Thesis

The hydrogen abstraction acetylene addition mechanism (HACA) has also been considered as a potential growth mechanism leading to benzo(a)pyrene (BaP) and four new reaction pathways explored star ting from benzo(a)anthracene (BaA) and chrysene (Chr), each involving one hydrogen abstraction, one acetylene addition, one cyclization and one hydrogen atom addition (**Figure 28**). The reaction pathways have three transition states and three intermediate structures. In the reaction pathways the barrier heights for the first steps are 60.92 kJ/mol for Chr and 61.17 kJ/mol and 64.48 kJ/mol for the BaA routes, (**Figure 28**, **b**).

4th Thesis

Two Diels-Alder (DA) reaction pathways are proposed and analysed by applying computational methods for the formation of the strongly carcinogenic benzo(a)pyrene (BaP) starting from benzo(a)anthracene (BaA) or chrysene (Chr) and involving one acetylene molecule addition along with one hydrogen molecule elimination. Both reaction routes had 2 transition state structures and one intermediate structure (**Figure 31**). The reaction pathways have 220.07 kJ/mol and 164.61 kJ/mol activation energy values having Chr and BaA as reactants, respectively (**Figure 31**).

5th Thesis

By applying computational methods, a new methyl addition/cyclization (MAC) mechanism leading to the toxic benzo(a)pyrene (BaP) starting from benzo(a)anthracene (BaA) or chrysene (Chr) is proposed (**Figure 32**). The mechanisms include four hydrogen abstractions, two methyl radical additions, three hydrogen atom eliminations, one ring closure, and one rearrangement step. In the studied pathways, methyl additions (intermediate c, C) are the most exoergic steps with –313.5 kJ/mol and –307.4 kJ/mol which occurred in the case of the chrysene and benzo(a)anthracene, respectively. The rate determining steps are 92.2 kJ/mol and 94.5 kJ/mol having Chr and BaA as reactants, respectively (**Figure 36**).

DOI: 10.14750/ME.2022.010

7. Scientific publications

Publications Related to the Subject of the Dissertation

Q1 **Edina Reizer**, Imre G. Csizmadia, Árpád B. Palotás, Béla Viskolcz, and Béla Fiser, "Formation mechanism of benzo(a)pyrene: One of the most carcinogenic polycyclic aromatic hydrocarbons (PAH)," *Molecules*, vol. 24, no. 6, 2019, doi: 10.3390/molecules24061040.
Number of Independent Citations: 10

Q2 **Edina Reizer**, Imre. G. Csizmadia, Károly Nehéz, Béla Viskolcz, and Béla Fiser, "Theoretical investigation of benzo(a)pyrene formation", *Chemical Physics Letters.*, p. 138564, Mar. 2021, doi: 10.1016/j.cplett.2021.138564.
Number of Independent citations: 1

D1 **Edina Reizer,** Béla Viskolcz and Béla Fiser, "Formation and growth mechanisms of polycyclic aromatic hydrocarbons: A mini-review", *Chemosphere* – 2021, doi: 10.1016/j.chemosphere.2021.132793

Edina Reizer, Béla Fiser, "Reaction initiation points of polycyclic aromatic hydrocarbons", *under preparation*, 2021.

Further Publications

Q1 Vanyorek, László, Ádám Prekob, Emőke Sikora, **Edina Reizer**, Gábor Muránszky, Ferenc Kristály, Béla Viskolcz, and Béla Fiser. "Application of carbon nanotube coated aluminosilicate beads as "support on support" catalyst for hydrogenation of nitrobenzene." *Journal of Industrial and Engineering Chemistry* 79 (2019): 307-313.

Number of Independent citations: 5

Presentations and posters

1. Doktoranduszok Fóruma
   Miskolc, Hungary, 2017.11.16.
   Study of atmospheric pollution with aromatic polycyclic hydrocarbons using various bioindicators.
2. 3. MÉB Égéstudományi Konferencia
   Budapest, Hungary, 2017.11.17
   The use of moss, lichen and pine needle for the investigation of PAH molecules in 02the air in six European countries.
3. Műszaki Tudomány az Észak-Kelet Magyarországi Régióban
   Szolnok, Hungary, 2018. 05. 31

DOI: 10.14750/ME.2022.010

Lignit égetése során keletkező policiklikus aromás szénhidrogének (PAH) áttekintése és vizsgálata.

4. 8th Visegrad Symposium on Structural System Biology
   Lučenec, Slovakia, 2018.06.20.
   Computational Study on the formation of benzo(a)pyrene.
5. 5th Anniversary Celebration of Confucius Institute
   Miskolc, Hungary, 2018.10.11.
   Computational Study on the formation of benzo(a)pyrene.
6. 1st Science Unlimited Conferenc - Eötvös Symposium
   Miskolc, Hungary, 2019.05.23.
   A DFT Application for Benzo(a)pyrene Formation.
7. KeMoMo -QSAR Symposium
   Szeged, Hungary, 2019.06.06.
   Mechanistic Studies of Benzo(a)pyrene Formation.
8. 9th Visegrad Symposium on Structural Systems Biology
   Szilvásvárad, Hungary, 2019. 06.18
   Growth Mechanism of Benzo(a)pyrene -A Theoretical Study.
9. Kémiai Előadói Napok
   Szeged, Hungary, 2019. 10. 28.
   A mechanistic investigation of benzo(a)pyrene formation with acetylene additions.
10. Környezetmérnöki Konferencia és Szakmai Nap
    Debrecen, Hungary, 2019. 11. 8.
    A Benzo(a)pirén képződésének vizsgálata metil addíció ciklizáció mechanizmus alkalmazásával.

DOI: 10.14750/ME.2022.010

8. References

[1] G. H. Brundtland, M. Khalid, S. Agnelli, S. Al-Athel, and B. Chidzero, "Our common future," p. New York, 1987.

[2] P. J. Landrigan *et al.*, "The Lancet Commission on pollution and health," *The Lancet*, vol. 391, no. 10119. Lancet Publishing Group, pp. 462–512, Feb. 03, 2018, doi: 10.1016/S0140-6736(17)32345-0.

[3] H. I. Abdel-Shafy and M. S. M. Mansour, "A review on polycyclic aromatic hydrocarbons: Source, environmental impact, effect on human health and remediation," *Egypt. J. Pet.*, vol. 25, no. 1, pp. 107–123, Mar. 2016, doi: 10.1016/j.ejpe.2015.03.011.

[4] A. M. Wagner and A. J. Barker, "Distribution of polycyclic aromatic hydrocarbons (PAHs) from legacy spills at an Alaskan Arctic site underlain by permafrost," *Cold Reg. Sci. Technol.*, vol. 158, pp. 154–165, Feb. 2019, doi: 10.1016/j.coldregions.2018.11.012.

[5] S. Net, R. El-Osmani, E. Prygiel, S. Rabodonirina, D. Dumoulin, and B. Ouddane, "Overview of persistent organic pollution (PAHs, Me-PAHs and PCBs) in freshwater sediments from Northern France," *J. Geochemical Explor.*, vol. 148, pp. 181–188, Jan. 2015, doi: 10.1016/j.gexplo.2014.09.008.

[6] B. M. Sahoo, B. V. V. Ravi Kumar, B. K. Banik, and P. Borah, "Polyaromatic Hydrocarbons (PAHs): Structures, Synthesis and their Biological Profile," *Curr. Org. Synth.*, vol. 17, no. 8, pp. 625–640, Oct. 2020, doi: 10.2174/1570179417666200713182441.

[7] K. Kozak, M. Ruman, K. Kosek, G. Karasiński, Ł. Stachnik, and Ż. Polkowska, "Impact of Volcanic Eruptions on the Occurrence of PAHs Compounds in the Aquatic Ecosystem of the Southern Part of West Spitsbergen (Hornsund Fjord, Svalbard)," *Water*, vol. 9, no. 1, p. 42, Jan. 2017, doi: 10.3390/w9010042.

[8] J. Aurell, B. K. Gullett, and D. Tabor, "Emissions from southeastern U.S. Grasslands and pine savannas: Comparison of aerial and ground field measurements with laboratory burns," *Atmos. Environ.*, vol. 111, pp. 170–178, Jun. 2015, doi: 10.1016/j.atmosenv.2015.03.001.

[9] V. Prakash and S. Singh, "Effect of combustion variables on PAHs emission from incineration of cellulose waste filters from acrylic industry," *Environ. Monit. Assess.*, vol. 163, no. 1–4, pp. 591–598, Apr. 2010, doi: 10.1007/s10661-009-0861-5.

[10] H. Y. Li, P. P. Gao, and H. G. Ni, "Emission characteristics of parent and halogenated PAHs in simulated municipal solid waste incineration," *Sci. Total Environ.*, vol. 665, pp. 11–17, May 2019, doi: 10.1016/j.scitotenv.2019.02.002.

DOI: 10.14750/ME.2022.010

[11] O. Devos, E. Combet, P. Tassel, and L. Paturel, "Exhaust emissions of pahs of passenger cars," *Polycycl. Aromat. Compd.*, vol. 26, no. 1, pp. 69–78, 2006, doi: 10.1080/10406630500519346.

[12] Y. C. Lin, Y. C. Li, S. Shangdiar, F. C. Chou, Y. T. Sheu, and P. C. Cheng, "Assessment of PM2.5 and PAH content in PM2.5 emitted from mobile source gasoline-fueled vehicles in concomitant with the vehicle model and mileages," *Chemosphere*, vol. 226, pp. 502–508, Jul. 2019, doi: 10.1016/j.chemosphere.2019.03.137.

[13] D. N. Inceoğlu, İ. Özbay, and A. Karademir, "VOC and PAH characterization of petroleum coke at maximum thermal decomposition temperature," *Energy Sources, Part A Recover. Util. Environ. Eff.*, vol. 41, no. 11, pp. 1305–1314, Jun. 2019, doi: 10.1080/15567036.2018.1548509.

[14] L. K. Siddens *et al.*, "Polycyclic aromatic hydrocarbons as skin carcinogens: comparison of benzo[a]pyrene, dibenzo[def,p]chrysene and three environmental mixtures in the FVB/N mouse.," *Toxicol. Appl. Pharmacol.*, vol. 264, no. 3, pp. 377–86, Nov. 2012, doi: 10.1016/j.taap.2012.08.014.

[15] B. Moorthy, C. Chu, and D. J. Carlin, "Polycyclic Aromatic Hydrocarbons: From Metabolism to Lung Cancer," *Toxicol. Sci.*, vol. 145, no. 1, pp. 5–15, May 2015, doi: 10.1093/toxsci/kfv040.

[16] J. B. Howard and J. D. Bittner, "Structure of Sooting Flames," in *Soot in Combustion Systems and Its Toxic Properties*, Boston, MA: Springer US, 1983, pp. 57–93.

[17] A. Raj, P. Man, T. Totton, M. Sander, and R. Shirley, "New polycyclic aromatic hydrocarbon (PAH) surface processes to improve the model prediction of the composition of combustion-generated PAHs and soot," *Carbon, Elsevier*, 2010.

[18] V. Chernov, M. J. Thomson, S. B. Dworkin, N. A. Slavinskaya, and U. Riedel, "Soot formation with C1 and C2 fuels using an improved chemical mechanism for PAH growth," *Combust. Flame*, vol. 161, no. 2, pp. 592–601, Feb. 2014, doi: 10.1016/J.COMBUSTFLAME.2013.09.017.

[19] S. Chaudhary and M. D. Milton, "Dicationic imidazolium salts as fluorescent probes for selective detection of Fe3+ion in pure aqueous media," *J. Photochem. Photobiol. A Chem.*, 2018, doi: 10.1016/j.jphotochem.2018.02.003.

[20] P. Selvaraj *et al.*, "A computational study of ethylene–air sooting flames: Effects of large polycyclic aromatic hydrocarbons," *Combust. Flame*, vol. 163, pp. 427–436, Jan. 2016, doi: 10.1016/J.COMBUSTFLAME.2015.10.017.

[21] S. B. Dworkin, Q. Zhang, M. J. Thomson, N. A. Slavinskaya, and U. Riedel, "Application of an enhanced PAH growth model to soot formation in a laminar coflow ethylene/air diffusion flame," *Combust. Flame*, vol. 158, no. 9, pp. 1682–1695, Sep. 2011, doi: 10.1016/J.COMBUSTFLAME.2011.01.013.

[22] H. Richter and J. B. Howard, "Formation of polycyclic aromatic hydrocarbons and

DOI: 10.14750/ME.2022.010

their growth to soot - a review of chemical reaction pathways," *Prog. Energy Combust. Sci.*, vol. 26, no. 4–6, pp. 565–608, Aug. 2000, doi: 10.1016/S0360-1285(00)00009-5.

[23] S. Billet *et al.*, "Genotoxic potential of Polycyclic Aromatic Hydrocarbons-coated onto airborne Particulate Matter (PM2.5) in human lung epithelial A549 cells," *Cancer Lett.*, vol. 270, no. 1, pp. 144–155, Oct. 2008, doi: 10.1016/j.canlet.2008.04.044.

[24] M. Tiwari, S. K. Sahu, and G. G. Pandit, "Distribution of PAHs in different compartment of creek ecosystem: Ecotoxicological concern and human health risk," *Environ. Toxicol. Pharmacol.*, vol. 50, pp. 58–66, Mar. 2017, doi: 10.1016/J.ETAP.2017.01.008.

[25] M. Tiwari, S. K. Sahu, and G. G. Pandit, "Inhalation risk assessment of PAH exposure due to combustion aerosols generated from household fuels," *Aerosol Air Qual. Res.*, vol. 15, no. 2, pp. 582–590, 2015, doi: 10.4209/aaqr.2014.03.0061.

[26] L. Keith and W. Telliard, "Special Report Priority pollutants: I-a perspective view," *Environ. Sci. Technol.*, vol. 13, no. 4, pp. 416–423, Apr. 1979, doi: 10.1021/es60152a601.

[27] L. H. Keith, "The Source of U.S. EPA's Sixteen PAH Priority Pollutants," *Polycycl. Aromat. Compd.*, vol. 35, no. 2–4, pp. 147–160, Mar. 2015, doi: 10.1080/10406638.2014.892886.

[28] J. T. Andersson and C. Achten, "A Critical Look at the 16 EPA PAHs," *Polycycl. Aromat. Compd.*, vol. 35, no. 2–4, pp. 143–146, Mar. 2015, doi: 10.1080/10406638.2015.1005241.

[29] J. T. Andersson and C. Achten, "Time to Say Goodbye to the 16 EPA PAHs? Toward an Up-to-Date Use of PACs for Environmental Purposes," *Polycycl. Aromat. Compd.*, vol. 35, no. 2–4, pp. 330–354, Mar. 2015, doi: 10.1080/10406638.2014.991042.

[30] V. Samburova, B. Zielinska, and A. Khlystov, "Do 16 Polycyclic Aromatic Hydrocarbons Represent PAH Air Toxicity?," *Toxics*, vol. 5, no. 3, p. 17, 2017, doi: 10.3390/toxics5030017.

[31] P. Huetz and V. Poux, "Carcinogenicity of benzo[a]pyrene diol epoxide stereoisomers: A linear free energy relationship study," *J. Mol. Struct. theochem*, vol. 764, no. 1–3, pp. 167–176, May 2006, doi: 10.1016/j.theochem.2006.02.005.

[32] U. S. Department Health and Human Services, "14th Report on Carcinogens, National Toxicology Program," 2016.

[33] J. Dang, X. Shi, J. Hu, J. Chen, Q. Zhang, and W. Wang, "Mechanistic and kinetic studies on OH-initiated atmospheric oxidation degradation of benzo[α]pyrene in the presence of O2 and NOx," *Chemosphere*, vol. 119, pp. 387–393, Jan. 2015, doi: 10.1016/j.chemosphere.2014.07.001.

DOI: 10.14750/ME.2022.010

[34] C. E. Boström *et al.*, "Cancer risk assessment, indicators, and guidelines for polycyclic aromatic hydrocarbons in the ambient air," *Environmental Health Perspectives*, vol. 110, no. SUPPL. 3. Public Health Services, US Dept of Health and Human Services, pp. 451–488, 2002, doi: 10.1289/ehp.110-1241197.

[35] N. Ramírez, A. Cuadras, E. Rovira, R. M. Marcé, and F. Borrull, "Risk assessment related to atmospheric polycyclic aromatic hydrocarbons in gas and particle phases near industrial sites," *Environ. Health Perspect.*, vol. 119, no. 8, pp. 1110–1116, Aug. 2011, doi: 10.1289/ehp.1002855.

[36] "International Agency for Research on Cancer (IARC). Monograph on the Identification of Carcinogenic Hazards to Humans. List of Classifications," vol. 1–123, 2021.

[37] G. I. Agapkina, E. S. Brodskii, and A. A. Shelepchikov, "The Benzo(a)pyrene Total Toxicity Equivalent of Polycyclic Aromatic Hydrocarbons in Soils of Moscow and Assessment of Carcinogenic Risk to Human Beings," *Moscow Univ. Soil Sci. Bull.*, vol. 73, no. 5, pp. 186–194, Dec. 2018, doi: 10.3103/s0147687418050022.

[38] "UNEP, United Nations Environment Programme, 2004. Guidance for a Global Monitoring Programme for Persistent Organic Pollutants."

[39] H. Shen *et al.*, "Global Atmospheric Emissions of Polycyclic Aromatic Hydrocarbons from 1960 to 2008 and Future Predictions," *Environ. Sci. Technol.*, vol. 47, no. 12, pp. 6415–6424, Jun. 2013, doi: 10.1021/es400857z.

[40] F. Gillett, W. Forrest, and K. Merrill, "8-13-micron spectra of NGC 7027, BD+ 30 3639, and NGC 6572.," *Astrophys. J.*, vol. 183, pp. 87–93, 1973.

[41] K. Merrill, B. Soifer, and R. Russell, "The 2-4 micron spectrum of NGC 7027.," *Astrophys. J.*, pp. L37–L39, 1975.

[42] A. Li, "Spitzer's perspective of polycyclic aromatic hydrocarbons in galaxies," *Nat. Astron. 2020 44*, vol. 4, no. 4, pp. 339–351, Mar. 2020, doi: 10.1038/s41550-020-1051-1.

[43] W. D.-F. discussions and undefined 2006, "Polycyclic aromatic hydrocarbons, carbon nanoparticles and the diffuse interstellar bands," *pubs.rsc.org*, Accessed: Aug. 30, 2021. [Online]. Available: https://pubs.rsc.org/en/content/articlehtml/2006/fd/b516323d.

[44] E. Peeters, C. Mackie, A. Candian, and A. G. G. M. Tielens, "A Spectroscopic View on Cosmic PAH Emission," *Acc. Chem. Res.*, vol. 54, no. 8, pp. 1921–1933, Apr. 2021, doi: 10.1021/ACS.ACCOUNTS.0C00747.

[45] A. Li and B. T. Draine, "Infrared Emission from Interstellar Dust. II. The Diffuse Interstellar Medium," *Astrophys. J.*, vol. 554, no. 2, pp. 778–802, Nov. 2000, doi: 10.1086/323147.

DOI: 10.14750/ME.2022.010

[46] B. T. Draine, A. Li, B. T. Draine, and A. Li, "Infrared Emission from Interstellar Dust. IV. The Silicate-Graphite-PAH Model in the Post-Spitzer Era," *ApJ*, vol. 657, no. 2, pp. 810–837, Mar. 2007, doi: 10.1086/511055.

[47] F. J. Lovas *et al.*, "Interstellar chemistry: A strategy for detecting polycyclic aromatic hydrocarbons in space," *J. Am. Chem. Soc.*, vol. 127, no. 12, pp. 4345–4349, Mar. 2005, doi: 10.1021/JA0426239.

[48] S. Thorwirth, P. Theulé, C. A. Gottlieb, M. C. McCarthy, and P. Thaddeus, "Rotational Spectra of Small PAHs: Acenaphthene, Acenaphthylene, Azulene, and Fluorene," *Astrophys. J.*, vol. 662, no. 2, p. 1309, Jun. 2007, doi: 10.1086/518026.

[49] A. Li, "PAHs in Comets: An Overview," *ESO Astrophys. Symp.*, vol. 2009, pp. 161–175, 2009, doi: 10.1007/978-3-540-76959-0_21.

[50] G. Mulas, A. Zonca, S. Casu, and C. Cecchi-Pestellini, "Modeling galactic extinction with dust and 'real' polycyclic aromatic hydrocarbons," *Astrophys. J.*, vol. 207, no. 17pp, p. 7, 2013, doi: 10.1088/0067-0049/207/1/7.

[51] R. P. Lindstedt and G. Skevis, "Benzene formation chemistry in premixed 1,3-butadiene flames," *Symp. Combust.*, vol. 26, no. 1, pp. 703–709, Jan. 1996, doi: 10.1016/S0082-0784(96)80278-5.

[52] E. Wang and J. Ding, "Reaction between the i-C4H5 radical and propargyl radical (C3H3): A theoretical study," *Chem. Phys. Lett.*, vol. 768, p. 138407, Apr. 2021, doi: 10.1016/J.CPLETT.2021.138407.

[53] M. Frenklach, D. W. Clary, W. C. Gardiner, and S. E. Stein, "Detailed kinetic modeling of soot formation in shock-tube pyrolysis of acetylene," *Symp. Combust.*, vol. 20, pp. 887–901, Jan. 1984, doi: 10.1016/S0082-0784(85)80578-6.

[54] B. Jursic and Z. Zdravkovski, "DFT study of the Diels–Alder reactions between ethylene with buta-1,3-diene and cyclopentadiene," *J. Chem. Soc. Perkin Trans. 2*, no. 6, pp. 1223–1226, Jan. 1995, doi: 10.1039/P29950001223.

[55] J. A. Miller and S. J. Klippenstein, "The Recombination of Propargyl Radicals and Other Reactions on a C6H6 Potential," *J. Phys. Chem. A*, vol. 107, no. 39, pp. 7783–7799, 2003, doi: 10.1021/JP030375H.

[56] P. M. Woods, T. J. Millar, A. A. Zijlstra, and E. Herbst, "The Synthesis of Benzene in the Proto-planetary Nebula CRL 618," *Astrophys. J.*, vol. 574, no. 2, p. L167, Jul. 2002, doi: 10.1086/342503.

[57] F. Zhang *et al.*, "Formation of the Phenyl Radical under Single Collision Conditions: A Crossed Molecular Beam and ab Initio Study," *J. Am. Chem. Soc.*, vol. 132, no. 8, pp. 2672–2683, Feb. 2010, doi: 10.1021/ja908559v.

[58] B. Shukla and M. Koshi, "A highly efficient growth mechanism of polycyclic aromatic hydrocarbons," *Phys. Chem. Chem. Phys.*, vol. 12, no. 10, pp. 2427–2437,

DOI: 10.14750/ME.2022.010

Mar. 2010, doi: 10.1039/b919644g.

[59] H. Böhm, H. Jander, and D. Tanke, "PAH growth and soot formation in the pyrolysis of acetylene and benzene at high temperatures and pressures: Modeling and experiment," *Symp. Combust.*, vol. 27, no. 1, pp. 1605–1612, Jan. 1998, doi: 10.1016/S0082-0784(98)80570-5.

[60] E. Georganta, R. Rahman, and A. Raj, "Growth of polycyclic aromatic hydrocarbons (PAHs) by methyl radicals: Pyrene formation from phenanthrene," *Combust. Flame, Elsevier*, vol. 185, pp. 129–141, 2017.

[61] A. Raj, M. J. M. J. Al Rashidi, S. H. Chung, and S. M. Sarathy, "PAH Growth Initiated by Propargyl Addition: Mechanism Development and Computational Kinetics," *J. Phys. Chem. A*, vol. 118, no. 16, pp. 2865–2885, Apr. 2014, doi: 10.1021/jp410704b.

[62] T. Mitra, T. Zhang, A. D. Sediako, and M. J. Thomson, "Understanding the formation and growth of polycyclic aromatic hydrocarbons (PAHs) and young soot from n-dodecane in a sooting laminar coflow diffusion flame," *Combust. Flame*, vol. 202, pp. 33–42, Apr. 2019, doi: 10.1016/J.COMBUSTFLAME.2018.12.010.

[63] A. Scott, W. W. Duley, and G. P. Pinho, "Polycyclic Aromatic Hydrocarbons and Fullerenes as Decomposition Products of Hydrogenated Amorphous Carbon," *Astrophys. J.*, vol. 489, no. 2, p. L193, Oct. 1997, doi: 10.1086/316789.

[64] W. Zhang, Y. Si, J. Zhen, T. Chen, H. Linnartz, and A. G. G. M. Tielens, "Laboratory Photochemistry of Covalently Bonded Fluorene Clusters: Observation of an Interesting PAH Bowl-forming Mechanism," *Astrophys. J.*, vol. 872, no. 1, p. 38, Feb. 2019, doi: 10.3847/1538-4357/aafe10.

[65] A. Raj, R. Tayouo, D. Cha, L. Li, M. A. Ismail, and S. H. Chung, "Thermal fragmentation and deactivation of combustion-generated soot particles," *Combust. Flame*, vol. 161, no. 9, pp. 2446–2457, Sep. 2014, doi: 10.1016/J.COMBUSTFLAME.2014.02.010.

[66] M. B. Colket and D. J. Seery, "Reaction mechanisms for toluene pyrolysis," *Symp. Combust.*, vol. 25, no. 1, pp. 883–891, 1994, doi: 10.1016/S0082-0784(06)80723-X.

[67] N. M. Marinov, W. J. Pitz, C. K. Westbrook, M. J. Castaldi, and S. M. Senkan, "Modeling of Aromatic and Polycyclic Aromatic Hydrocarbon Formation in Premixed Methane and Ethane Flames," *Combust. Sci. Technol.*, vol. 116–117, no. 1–6, pp. 211–287, Aug. 1996, doi: 10.1080/00102209608935550.

[68] H. Wang and M. Frenklach, "A detailed kinetic modeling study of aromatics formation in laminar premixed acetylene and ethylene flames," *Combust. Flame*, vol. 110, no. 1–2, pp. 173–221, Jul. 1997, doi: 10.1016/S0010-2180(97)00068-0.

[69] N. M. Marinov *et al.*, "Aromatic and Polycyclic Aromatic Hydrocarbon Formation in a Laminar Premixed n-Butane Flame," *Combust. Flame*, vol. 114, no. 1–2, pp.

DOI: 10.14750/ME.2022.010

192–213, Jul. 1998, doi: 10.1016/S0010-2180(97)00275-7.

[70] H. Richter, W. J. Grieco, and J. B. Howard, "Formation mechanism of polycyclic aromatic hydrocarbons and fullerenes in premixed benzene flames," *Combust. Flame*, vol. 119, no. 1–2, pp. 1–22, Oct. 1999, doi: 10.1016/S0010-2180(99)00032-2.

[71] A. Violi, A. D'Anna, and A. D'Alessio, "Modeling of particulate formation in combustion and pyrolysis," *Chem. Eng. Sci.*, vol. 54, no. 15–16, pp. 3433–3442, 1999, doi: 10.1016/S0009-2509(98)00460-6.

[72] J. Appel, H. Bockhorn, and M. Frenklach, "Kinetic modeling of soot formation with detailed chemistry and physics: laminar premixed flames of C2 hydrocarbons," *Combust. Flame*, vol. 121, no. 1–2, pp. 122–136, Apr. 2000, doi: 10.1016/S0010-2180(99)00135-2.

[73] A. D'Anna, A. Violi, and A. D'Alessio, "Modeling the rich combustion of aliphatic hydrocarbons," *Combust. Flame*, vol. 121, no. 3, pp. 418–429, Mar. 2000, doi: 10.1016/S0010-2180(99)00163-7.

[74] J. A. Mulholland, M. Lu, and D.-H. Kim, "Pyrolytic growth of polycyclic aromatic hydrocarbons by cyclopentadienyl moieties," *Proc. Combust. Inst.*, vol. 28, no. 2, pp. 2593–2599, Jan. 2000, doi: 10.1016/S0082-0784(00)80677-3.

[75] M. Lu and J. A. Mulholland, "Aromatic hydrocarbon growth from indene," *Chemosphere*, vol. 42, no. 5–7, pp. 625–633, Feb. 2001, doi: 10.1016/S0045-6535(00)00236-8.

[76] M. S. Skjøth-Rasmussen *et al.*, "Formation of polycyclic aromatic hydrocarbons and soot in fuel-rich oxidation of methane in a laminar flow reactor," *Combust. Flame*, vol. 136, no. 1–2, pp. 91–128, Jan. 2004, doi: 10.1016/J.COMBUSTFLAME.2003.09.011.

[77] V. V. Kislov, N. I. Islamova, A. M. Kolker, S. H. Lin, and A. M. Mebel, "Hydrogen abstraction acetylene addition and Diels-Alder mechanisms of PAH formation: A detailed study using first principles calculations," *J. Chem. Theory Comput.*, vol. 1, no. 5, pp. 908–924, Sep. 2005, doi: 10.1021/ct0500491.

[78] D. Wang, A. Violi, D. H. Kim, and J. A. Mullholland, "Formation of Naphthalene, Indene, and Benzene from Cyclopentadiene Pyrolysis: A DFT Study," 2006, doi: 10.1021/JP053628A.

[79] V. Kislov and A. Mebel, "The Formation of Naphthalene, Azulene, and Fulvalene from Cyclic C5 Species in Combustion: An Ab Initio/RRKM Study of 9-H-Fulvalenyl (C5H5−C5H4) Radical Rearrangements," *J. Phys. Chem. A*, 2007, doi: 10.1021/JP0732099.

[80] B. Shukla, A. Susa, A. Miyoshi, and M. Koshi, "In Situ Direct Sampling Mass Spectrometric Study on Formation of Polycyclic Aromatic Hydrocarbons in

DOI: 10.14750/ME.2022.010

Toluene Pyrolysis," 2007, doi: 10.1021/JP071813D.

[81] K. Norinaga, O. Deutschmann, N. Saegusa, and J. Hayashi, "Analysis of pyrolysis products from light hydrocarbons and kinetic modeling for growth of polycyclic aromatic hydrocarbons with detailed chemistry," *J. Anal. Appl. Pyrolysis*, vol. 86, pp. 148–160, 2009, Accessed: Oct. 18, 2019. [Online]. Available: https://www.sciencedirect.com/science/article/pii/S0165237009000801.

[82] N. A. Slavinskaya and P. Frank, "A modelling study of aromatic soot precursors formation in laminar methane and ethene flames," *Combust. Flame*, vol. 156, no. 9, pp. 1705–1722, Sep. 2009, doi: 10.1016/J.COMBUSTFLAME.2009.04.013.

[83] B. Shukla and M. Koshi, "A novel route for PAH growth in HACA based mechanisms," *Combust. Flame*, vol. 159, no. 12, pp. 3589–3596, Dec. 2012, doi: 10.1016/J.COMBUSTFLAME.2012.08.007.

[84] A. Matsugi and A. Miyoshi, "Computational study on the recombination reaction between benzyl and propargyl radicals," *Int. J. Chem. Kinet.*, vol. 44, no. 3, pp. 206–218, Mar. 2012, doi: 10.1002/kin.20625.

[85] D. S. N. Parker *et al.*, "Low temperature formation of naphthalene and its role in the synthesis of PAHs (Polycyclic Aromatic Hydrocarbons) in the interstellar medium," *Proc. Natl. Acad. Sci. U. S. A.*, vol. 109, no. 1, pp. 53–58, Jan. 2012, doi: 10.1073/pnas.1113827108.

[86] N. B. Poddar, "An Experimental Investigation of the Role of Small Hydrocarbons and Combustion-Generated Nanoparticles on the Formation and Growth Reactions of Polycyclic Aromatic Hydrocarbons during the Pyrolysis of a Model-Fuel and Hydrocarbon Gases," Louisiana State University, LSU Doctoral Dissertations. 403., 2012.

[87] A. Raj, I. D. C. Prada, A. A. Amer, and S. H. Chung, "A reaction mechanism for gasoline surrogate fuels for large polycyclic aromatic hydrocarbons," *Combust. Flame*, vol. 159, no. 2, pp. 500–515, Feb. 2012, doi: 10.1016/J.COMBUSTFLAME.2011.08.011.

[88] V. V. Kislov, A. I. Sadovnikov, and A. M. Mebel, "Formation Mechanism of Polycyclic Aromatic Hydrocarbons beyond the Second Aromatic Ring," *J. Phys. Chem. A*, vol. 117, no. 23, pp. 4794–4816, Jun. 2013, doi: 10.1021/jp402481y.

[89] N. E. Sánchez, Á. Millera, R. Bilbao, and M. U. Alzueta, "Polycyclic aromatic hydrocarbons (PAH), soot and light gases formed in the pyrolysis of acetylene at different temperatures: Effect of fuel concentration," *Anal. Appl. Pyrolysis*, vol. 103, pp. 126–133, Sep. 2013, doi: 10.1016/j.jaap.2012.10.027.

[90] Y. Wang, A. Raj, and S. H. Chung, "A PAH growth mechanism and synergistic effect on PAH formation in counterflow diffusion flames," *Combust. Flame*, vol. 160, no. 9, pp. 1667–1676, Sep. 2013, doi: 10.1016/J.COMBUSTFLAME.2013.03.013.

DOI: 10.14750/ME.2022.010

[91] H. Zhou, C. Wu, J. A. Onwudili, A. Meng, Y. Zhang, and P. T. Williams, "Polycyclic aromatic hydrocarbons (PAH) formation from the pyrolysis of different municipal solid waste fractions," *Waste Manag.*, vol. 36, pp. 136–146, Feb. 2015, doi: 10.1016/j.wasman.2014.09.014.

[92] P. Liu, H. Lin, Y. Yang, C. Shao, B. Guan, and Z. Huang, "Investigating the Role of CH2 Radicals in the HACA Mechanism," *J. Phys. Chem. A*, vol. 119, no. 13, pp. 3261–3268, Apr. 2015, doi: 10.1021/jp5124162.

[93] C. Wentrup, H.-W. Winter, and D. Kvaskoff, "C 9 H 8 Pyrolysis. *o* -Tolylacetylene, Indene, 1-Indenyl, and Biindenyls and the Mechanism of Indene Pyrolysis," *J. Phys. Chem. A*, vol. 119, no. 24, pp. 6370–6376, Jun. 2015, doi: 10.1021/acs.jpca.5b03453.

[94] F. Xu, X. Shi, Q. Zhang, and W. Wang, "Mechanism for the growth of polycyclic aromatic hydrocarbons from the reactions of naphthalene with cyclopentadienyl and indenyl.," *Chemosphere*, vol. 162, pp. 345–54, Nov. 2016, doi: 10.1016/j.chemosphere.2016.07.039.

[95] T. Bensabath, H. Monnier, and P. A. Glaude, "Detailed kinetic modeling of the formation of toxic polycyclic aromatic hydrocarbons (PAHs) coming from pyrolysis in low-pressure gas carburizing conditions," *J. Anal. Appl. Pyrolysis*, vol. 122, pp. 342–354, Nov. 2016, doi: 10.1016/j.jaap.2016.09.007.

[96] Y. Z. An *et al.*, "Development of a PAH (polycyclic aromatic hydrocarbon) formation model for gasoline surrogates and its application for GDI (gasoline direct injection) engine CFD (computational fluid dynamics) simulation," *Energy*, vol. 94, pp. 367–379, Jan. 2016, doi: 10.1016/j.energy.2015.11.014.

[97] A. Comandini, S. Abid, and N. Chaumeix, "Polycyclic Aromatic Hydrocarbon Growth by Diradical Cycloaddition/Fragmentation," *J. Phys. Chem. A*, vol. 121, no. 31, pp. 5921–5931, 2017.

[98] N. Hansen, M. Schenk, K. Moshammer, and K. Kohse-Höinghaus, "Investigating repetitive reaction pathways for the formation of polycyclic aromatic hydrocarbons in combustion processes," *Combust. Flame*, vol. 180, pp. 250–261, Jun. 2017, doi: 10.1016/J.COMBUSTFLAME.2016.09.013.

[99] L. Zhu, X. Shi, Y. Sun, Q. Zhang, and W. Wang, "The growth mechanism of polycyclic aromatic hydrocarbons from the reactions of anthracene and phenanthrene with cyclopentadienyl and indenyl.," *Chemosphere*, vol. 189, pp. 265–276, Dec. 2017, doi: 10.1016/j.chemosphere.2017.09.004.

[100] A. M. Mebel, A. Landera, and R. I. Kaiser, "Formation Mechanisms of Naphthalene and Indene: From the Interstellar Medium to Combustion Flames," *J. Phys. Chem. A*, vol. 121, no. 5, pp. 901–926, Feb. 2017, doi: 10.1021/acs.jpca.6b09735.

[101] A. M. Mebel, Y. Georgievskii, A. W. Jasper, and S. J. Klippenstein, "Temperature- and

DOI: 10.14750/ME.2022.010

pressure-dependent rate coefficients for the HACA pathways from benzene to naphthalene," *Proc. Combust. Inst.*, vol. 36, no. 1, pp. 919–926, Jan. 2017, doi: 10.1016/j.proci.2016.07.013.

[102] P. Liu, Z. Li, and W. L. Roberts, "The growth of PAHs and soot in the post-flame region," *Proc. Combust. Inst.*, vol. 37, no. 1, pp. 977–984, Jan. 2018, doi: 10.1016/J.PROCI.2018.05.047.

[103] M. Frenklach, R. I. Singh, and A. M. Mebel, "On the low-temperature limit of HACA," *Proc. Combust. Inst.*, vol. 37, no. 1, pp. 969–976, 2019, doi: 10.1016/j.proci.2018.05.068.

[104] L. Zhao *et al.*, "VUV Photoionization Study of the Formation of the Simplest Polycyclic Aromatic Hydrocarbon: Naphthalene (C10H8)," *J. Phys. Chem. Lett.*, vol. 9, no. 10, pp. 2620–2626, May 2018, doi: 10.1021/acs.jpclett.8b01020.

[105] E. Reizer, I. G. Csizmadia, Á. B. Palotás, B. Viskolcz, and B. Fiser, "Formation mechanism of benzo(a)pyrene: One of the most carcinogenic polycyclic aromatic hydrocarbons (PAH)," *Molecules*, vol. 24, no. 6, 2019, doi: 10.3390/molecules24061040.

[106] H. Jin *et al.*, "A chemical kinetic modeling study of indene pyrolysis," *Combust. Flame*, vol. 206, pp. 1–20, 2019, doi: 10.1016/j.combustflame.2019.04.040.

[107] P. Liu *et al.*, "Computational study of polycyclic aromatic hydrocarbons growth by vinylacetylene addition," *Combust. Flame*, vol. 202, pp. 276–291, Apr. 2019.

[108] L. Zhao *et al.*, "Low-temperature formation of polycyclic aromatic hydrocarbons in Titan's atmosphere," *Nat. Astron.*, no. 2, pp. 973–979, 2019, doi: 10.1038/s41550-018-0585-y.

[109] H. Tao, H.-Y. Wang, W. Ren, and K. C. Lin, "Kinetic mechanism for modeling the temperature effect on PAH formation in pyrolysis of acetylene," *Fuel*, vol. 255, p. 115796, Nov. 2019, doi: 10.1016/J.FUEL.2019.115796.

[110] M. Liu, T. Chu, A. Jocher, M. C. Smith, I. Lengyel, and W. H. Green, "Predicting polycyclic aromatic hydrocarbon formation with an automatically generated mechanism for acetylene pyrolysis," *Int. J. Chem. Kinet.*, vol. 53, no. 1, pp. 27–42, Jan. 2021, doi: 10.1002/kin.21421.

[111] X. Shi, Q. Wang, and A. Violi, "Reaction pathways for the formation of five-membered rings onto polyaromatic hydrocarbon framework," *Fuel*, vol. 283, p. 119023, Jan. 2021, doi: 10.1016/j.fuel.2020.119023.

[112] X. Cheng, Z. Gao, F. Ren, S. Rigopoulos, L. Zhu, and Z. Huang, "Experimental and kinetic modeling study on sooting tendencies of alkylbenzene isomers," *Fuel*, vol. 283, p. 118873, Jan. 2021, doi: 10.1016/j.fuel.2020.118873.

[113] J. D. D. Bittner and J. B. B. Howard, "Composition profiles and reaction mechanisms

DOI: 10.14750/ME.2022.010

in a near-sooting premixed benzene/oxygen/argon flame," *Symp. Combust.*, vol. 18, no. 1, pp. 1105–1116, Jan. 1981, doi: 10.1016/S0082-0784(81)80115-4.

[114] M. Frenklach, D. W. Klarry, and M. K. Ramachandra, "Shock Tube Study of the Fuel Structure Effects on the Chemical Kinetic Mechanisms Responsible for Soot Formation Part II," NASA Contractor Report 174880, Lousiana, 1985.

[115] H. Wang and M. Frenklach, "Calculations of Rate Coefficients for the Chemically Activated Reactions of Acetylene with Vinylic and Aromatic Radicals," *J. Phys. Chem.*, vol. 98, no. 44, pp. 11465–11489, Nov. 1994, doi: 10.1021/j100095a033.

[116] M. Frenklach and H. Wang, "Detailed Modeling of Soot Particle Nucleation and Growth, Twenty-third Symposium on Combustion," *Symp. Combust.*, pp. 1559–1566, 1990, doi: 10.1016/S0082-0784(06)80426-1.

[117] B. Shukla, A. Susa, A. Miyoshi, and M. Koshi, "Role of Phenyl Radicals in the Growth of Polycyclic Aromatic Hydrocarbons," *J. Phys. Chem. A*, vol. 111, pp. 9532–9543, 2008, doi: 10.1021/JP7098398.

[118] V. V. Kislov, N. I. Islamova, A. M. Kolker, S. H. Lin, and A. M. Mebel, "Hydrogen abstraction acetylene addition and Diels-Alder mechanisms of PAH formation: A detailed study using first principles calculations," *J. Chem. Theory Comput.*, vol. 1, no. 5, pp. 908–924, Sep. 2005, doi: 10.1021/ct0500491.

[119] M. Frenklach, "Reaction mechanism of soot formation in flames," *Phys. Chem. Chem. Phys.*, vol. 4, no. 11, pp. 2028–2037, 2002, doi: 10.1039/b110045a.

[120] E. Reizer, I. G. Csizmadia, K. Nehéz, B. Viskolcz, and B. Fiser, "Theoretical investigation of benzo(a)pyrene formation," *Chem. Phys. Lett.*, p. 138564, Mar. 2021, doi: 10.1016/j.cplett.2021.138564.

[121] V. M. Shinde and P. Pradeep, "Detailed gas-phase kinetics and reduced reaction mechanism for methane pyrolysis involved in CVD/CVI processes," *J. Anal. Appl. Pyrolysis*, vol. 154, p. 104998, Mar. 2021, doi: 10.1016/j.jaap.2020.104998.

[122] S. J. Cassady, R. Choudhary, N. H. Pinkowski, J. Shao, D. F. Davidson, and R. K. Hanson, "The thermal decomposition of ethane," *Fuel*, vol. 268, p. 117409, May 2020, doi: 10.1016/j.fuel.2020.117409.

[123] N. A. Slavinskaya, U. Riedel, S. B. Dworkin, and M. J. Thomson, "Detailed numerical modeling of PAH formation and growth in non-premixed ethylene and ethane flames," *Combust. Flame*, vol. 159, no. 3, pp. 979–995, Mar. 2012, doi: 10.1016/J.COMBUSTFLAME.2011.10.005.

[124] T. Li, T. Mitra, C. Chu, Y. Yuan, and M. J. Thomson, "Investigation of PAH and soot formation in a dimethyl ether (DME) laminar coflow diffusion flame," *Combust. Flame*, vol. 223, pp. 437–449, Jan. 2021, doi: 10.1016/j.combustflame.2020.10.019.

DOI: 10.14750/ME.2022.010

[125] W. Sun, A. Hamadi, S. Abid, N. Chaumeix, and A. Comandini, "An experimental and kinetic modeling study of phenylacetylene decomposition and the reactions with acetylene/ethylene under shock tube pyrolysis conditions," *Combust. Flame*, vol. 220, pp. 257–271, Oct. 2020, doi: 10.1016/j.combustflame.2020.06.044.

[126] H. Chu, Y. Ya, X. Nie, F. Qiao, and J. E, "Effects of adding cyclohexane, n-hexane, ethanol, and 2,5-dimethylfuran to fuel on soot formation in laminar coflow n-heptane/iso-octane diffusion flame," *Combust. Flame*, vol. 225, pp. 120–135, Mar. 2021, doi: 10.1016/j.combustflame.2020.10.030.

[127] C. V. Naik *et al.*, "Detailed chemical kinetic mechanism for surrogates of alternative jet fuels," *Combust. Flame*, vol. 158, no. 3, pp. 434–445, Mar. 2011, doi: 10.1016/j.combustflame.2010.09.016.

[128] P. Liu, Z. Li, A. Bennett, H. Lin, S. M. Sarathy, and W. L. Roberts, "The site effect on PAHs formation in HACA-based mass growth process," *Combust. Flame*, vol. 199, pp. 54–68, Jan. 2019.

[129] P. Liu *et al.*, "Chemical Mechanism of Exhaust Gas Recirculation on Polycyclic Aromatic Hydrocarbons Formation Based on Laser-Induced Fluorescence Measurement," *Energy & Fuels*, vol. 32, no. 6, pp. 7112–7124, Jun. 2018, doi: 10.1021/acs.energyfuels.8b00422.

[130] D. S. N. Parker, R. I. Kaiser, B. Bandyopadhyay, O. Kostko, T. P. Troy, and M. Ahmed, "Unexpected Chemistry from the Reaction of Naphthyl and Acetylene at Combustion-Like Temperatures," *Angew. Chemie Int. Ed.*, vol. 54, no. 18, pp. 5421–5424, Apr. 2015, doi: 10.1002/anie.201411987.

[131] J. Thomas Mckinnon and J. B. Howard, "The roles of pah and acetylene in soot nucleation and growth," *Symp. Combust.*, vol. 24, no. 1, pp. 965–971, Jan. 1992, doi: 10.1016/S0082-0784(06)80114-1.

[132] O. T. Dyan, G. I. Borodkin, and P. A. Zaikin, "The Diels-Alder Reaction for the Synthesis of Polycyclic Aromatic Compounds," *European J. Org. Chem.*, vol. 2019, no. 44, pp. 7271–7306, Nov. 2019, doi: 10.1002/ejoc.201901254.

[133] R. D. J. Froese, J. M. Coxon, S. C. West, and K. Morokuma, "Theoretical Studies of Diels−Alder Reactions of Acetylenic Compounds," *J. Org. Chem.*, vol. 62, no. 20, pp. 6991–6996, Oct. 1997, doi: 10.1021/JO970811U.

[134] K. Siegmann and K. Sattler, "Formation mechanism for polycyclic aromatic hydrocarbons in methane flames," *J. Chem. Phys.*, vol. 112, no. 2, pp. 698–709, Jan. 2000, doi: 10.1063/1.480648.

[135] V. V. Kislov, N. I. Islamova, A. M. Kolker, S. H. Lin, and A. M. Mebel, "Hydrogen Abstraction Acetylene Addition and Diels−Alder Mechanisms of PAH Formation: A Detailed Study Using First Principles Calculations," *J. Chem. Theory Comput.*, vol. 1, no. 5, pp. 908–924, Sep. 2005, doi: 10.1021/CT0500491.

DOI: 10.14750/ME.2022.010

[136] L. S. Johansson, B. Leckner, L. Gustavsson, D. Cooper, C. Tullin, and A. Potter, "Emission characteristics of modern and old-type residential boilers fired with wood logs and wood pellets," *Atmos. Environ.*, vol. 38, no. 25, pp. 4183–4195, Aug. 2004, doi: 10.1016/J.ATMOSENV.2004.04.020.

[137] M. M. Pergal, D. Relić, Ž. L. Tešić, and A. R. Popović, "Leaching of polycyclic aromatic hydrocarbons from power plant lignite ash—influence of parameters important for environmental pollution," *Environ. Sci. Pollut. Res.*, vol. 21, no. 5, pp. 3435–3442, Mar. 2014, doi: 10.1007/s11356-013-2314-5.

[138] Y. C. Hsu, S. H. Chang, and M. B. Chang, "Emissions of PAHs, PCDD/Fs, dl-PCBs, chlorophenols and chlorobenzenes from municipal waste incinerator cofiring industrial waste," *Chemosphere*, vol. 280, p. 130645, Oct. 2021, doi: 10.1016/J.CHEMOSPHERE.2021.130645.

[139] K. C. Kalvakala and S. K. Aggarwal, "Effect of Composition and Octane Sensitivity of Gasoline Surrogates on PAH Emissions," *Green Energy Technol.*, pp. 177–198, 2021, doi: 10.1007/978-981-15-5667-8_8.

[140] I. Campos and N. Abrantes, "Forest fires as drivers of contamination of polycyclic aromatic hydrocarbons to the terrestrial and aquatic ecosystems," *Curr. Opin. Environ. Sci. Heal.*, vol. 24, p. 100293, Dec. 2021, doi: 10.1016/J.COESH.2021.100293.

[141] N. Pichler, F. Maria de Souza, V. Ferreira dos Santos, and C. C. Martins, "Polycyclic aromatic hydrocarbons (PAHs) in sediments of the amazon coast: Evidence for localized sources in contrast to massive regional biomass burning," *Environ. Pollut.*, vol. 268, p. 115958, Jan. 2021, doi: 10.1016/J.ENVPOL.2020.115958.

[142] J. E. Silliman, P. A. Meyers, B. J. Eadie, and J. Val Klump, "A hypothesis for the origin of perylene based on its low abundance in sediments of Green Bay, Wisconsin," *Chem. Geol.*, vol. 177, no. 3–4, pp. 309–322, Jul. 2001, doi: 10.1016/S0009-2541(00)00415-0.

[143] B. V Unterreiner, M. Sierka, and R. Ahlrichs, "Reaction pathways for growth of polycyclic aromatic hydrocarbons under combustion conditions, a DFT study," doi: 10.1039/b407279k.

[144] E. S. Oran, "Astrophysical combustion," *Proc. Combust. Inst.*, vol. 30, pp. 1823–1840, 2005, doi: 10.1016/j.proci.2004.08.278.

[145] G. C. Sloan *et al.*, "The Unusual Hydrocarbon Emission from the Early Carbon Star HD 100764: The Connection between Aromatics and Aliphatics," *Astrophys. J.*, vol. 664, no. 2, p. 1144, Aug. 2007, doi: 10.1086/519236.

[146] A. M. Mebel, A. Landera, and R. I. Kaiser, "Formation Mechanisms of Naphthalene and Indene: From the Interstellar Medium to Combustion Flames," *J. Phys. Chem. A*, vol. 121, no. 5, pp. 901–926, Feb. 2017, doi: 10.1021/ACS.JPCA.6B09735.

DOI: 10.14750/ME.2022.010

[147] A. G. G. M. Tielens, "The molecular universe," *Rev. Mod. Phys.*, vol. 85, no. 3, p. 1021, Jul. 2013, doi: 10.1103/RevModPhys.85.1021.

[148] T. Chen and A. Li, "Synthesizing carbon nanotubes in space," *Astron. Astrophys.*, vol. 631, p. A54, Nov. 2019, doi: 10.1051/0004-6361/201935789.

[149] Q. Li, A. Li, B. W. Jiang, and T. Chen, "On carbon nanotubes in the interstellar medium," *Mon. Not. R. Astron. Soc.*, vol. 493, no. 2, pp. 3054–3059, Apr. 2020, doi: 10.1093/MNRAS/STAA467.

[150] L. Vanyorek *et al.*, "Application of carbon nanotube coated aluminosilicate beads as 'support on support' catalyst for hydrogenation of nitrobenzene," *J. Ind. Eng. Chem.*, vol. 79, 2019, doi: 10.1016/j.jiec.2019.07.006.

[151] G. M. Badger, R. G. Buttery, R. W. L. Kimber, G. E. Lewis, A. G. Moritz, and I. M. Napier, "498. The formation of aromatic hydrocarbons at high temperatures. Part I. Introduction," *J. Chem. Soc.*, no. 0, pp. 2449–2452, Jan. 1958, doi: 10.1039/JR9580002449.

[152] J. Yang, L. Zhao, W. Yuan, F. Qi, and Y. Li, "Experimental and kinetic modeling investigation on laminar premixed benzene flames with various equivalence ratios," *Proc. Combust. Inst.*, vol. 35, no. 1, pp. 855–862, Jan. 2015, doi: 10.1016/j.proci.2014.05.085.

[153] O. Féron, F. Langlais, and R. Naslain, "Analysis of the Gas Phase by In Situ FTIR Spectrometry and Mass Spectrometry During the CVD of Pyrocarbon from Propane," *Chem. Vap. Depos.*, vol. 5, no. 1, pp. 1343–1353, 1999, doi: 10.1016/S0008-6223(98)00329-7.

[154] L. Zhao *et al.*, "A Free-Radical Prompted Barrierless Gas-Phase Synthesis of Pentacene," *Angew. Chemie*, vol. 132, no. 28, pp. 11430–11434, Jul. 2020, doi: 10.1002/ANGE.202003402.

[155] Y. S. Kim and R. I. Kaiser, "An infrared spectroscopic study of amorphous and crystalline ices of vinylacetylene and implications for Saturns's satellite Titan," *Astrophys. J. Suppl. Ser.*, vol. 181, no. 2, p. 543, Mar. 2009, doi: 10.1088/0067-0049/181/2/543.

[156] C. S. Contreras and F. Salama, "Laboratory investigations of polycyclic aromatic hydrocarbons of polycyclic aromatic hydrocarbon formation and destruction in the circumstellar outflows of carbon stars," *Astrophys. J. Suppl. Ser.*, vol. 208, no. 1, p. 6, Aug. 2013, doi: 10.1088/0067-0049/208/1/6.

[157] M. Weissman and S. W. Benson, "Pyrolysis of methyl chloride, a pathway in the chlorine-catalyzed polymerization of methane," *Int. J. Chem. Kinet.*, vol. 16, no. 4, pp. 307–333, Apr. 1984, doi: 10.1002/kin.550160403.

[158] B. Shukla, A. Miyoshi, and M. Koshi, "Role of Methyl Radicals in the Growth of PAHs," *J. Am. Soc. Mass Spectrom.*, vol. 21, no. 4, pp. 534–544, Apr. 2010.

DOI: 10.14750/ME.2022.010

[159] X. J. Yang, R. Glaser, A. Li, and J. X. Zhong, "The carriers of the unidentified infrared emission features: Clues from polycyclic aromatic hydrocarbons with aliphatic sidegroups," *New Astron. Rev.*, vol. 77, pp. 1–22, Apr. 2017, doi: 10.1016/J.NEWAR.2017.01.001.

[160] A. M. Mebel, V. V. Kislov, and R. I. Kaiser, "Photoinduced mechanism of formation and growth of polycyclic aromatic hydrocarbons in low-temperature environments via successive ethynyl radical additions," *J. Am. Chem. Soc.*, vol. 130, no. 41, pp. 13618–13629, Oct. 2008, doi: 10.1021/ja804198a.

[161] N. D. Marsh and M. J. Wornat, "Formation pathways of ethynyl-substituted and cyclopenta-fused polycyclic aromatic hydrocarbons," *Proc. Combust. Inst.*, vol. 28, no. 2, pp. 2585–2592, Jan. 2000, doi: 10.1016/S0082-0784(00)80676-1.

[162] K. D. Tucker, M. L. Kutner, and P. Thaddeus, "The ethynl radicak C2H a new interstellar molecule," *Astrophys. J.*, vol. 193, pp. 115–119, 1974.

[163] B. M. Jones *et al.*, "Formation of benzene in the interstellar medium," *Proc. Natl. Acad. Sci.*, vol. 108, no. 2, pp. 452–457, Jan. 2011, doi: 10.1073/PNAS.1012468108.

[164] B. Shukla and M. Koshi, "Comparative study on the growth mechanisms of PAHs," *Combust. Flame*, vol. 158, no. 2, pp. 369–375, Feb. 2011, doi: 10.1016/j.combustflame.2010.09.012.

[165] L. Zhao *et al.*, "Synthesis of Polycyclic Aromatic Hydrocarbons by Phenyl Addition–Dehydrocyclization: The Third Way," *Angew. Chemie Int. Ed.*, vol. 58, no. 48, pp. 17442–17450, Nov. 2019, doi: 10.1002/ANIE.201909876.

[166] Y. Yoon, S. Hörst, R. Hicks, R. Li, J. de G.- Icarus, and undefined 2014, "The role of benzene photolysis in Titan haze formation," *Elsevier*, Accessed: Aug. 26, 2021. [Online]. Available: https://www.sciencedirect.com/science/article/pii/S0019103514000839.

[167] N. Hansen *et al.*, "The importance of fuel dissociation and propargyl+ allyl association for the formation of benzene in a fuel-rich 1-hexene flame," *Phys. Chem. Chem. Phys.*, vol. 12, no. 38, pp. 12112–22, 2010.

[168] A. Matsugi and A. Miyoshi, "Modeling of two- and three-ring aromatics formation in the pyrolysis of toluene," *Proc. Combust. Inst.*, vol. 34, no. 1, pp. 269–277, Jan. 2013, doi: 10.1016/J.PROCI.2012.06.032.

[169] L. Zhao *et al.*, "Gas-phase synthesis of benzene via the propargyl radical self-reaction," *Sci. Adv.*, vol. 7, no. 21, p. eabf0360, May 2021, doi: 10.1126/SCIADV.ABF0360.

[170] A. E. Long *et al.*, "Pressure dependent kinetic analysis of pathways to naphthalene from cyclopentadienyl recombination," *Combust. Flame*, vol. 187, 2018, doi: 10.1016/j.combustflame.2017.09.008.

DOI: 10.14750/ME.2022.010

[171] C. Cavallotti and D. Polino, "On the kinetics of the C5H5 + C5H5 reaction," *Proc. Combust. Inst.*, vol. 34, no. 1, pp. 557–564, Jan. 2013, doi: 10.1016/J.PROCI.2012.05.097.

[172] R. K. Robinson and R. P. Lindstedt, "On the chemical kinetics of cyclopentadiene oxidation," *Combust. Flame*, vol. 158, no. 4, pp. 666–686, Apr. 2011, doi: 10.1016/J.COMBUSTFLAME.2010.12.001.

[173] A. M. Mebel and V. V. Kislov, "Can the C5H5 + C5H 5 → C10H10 → C10H9 + H/C10H8 + H2 Reaction Produce Naphthalene? An Ab Initio/RRKM Study," *J. Phys. Chem. A*, vol. 113, no. 36, pp. 9825–9833, Sep. 2009, doi: 10.1021/jp905931j.

[174] C. F. Melius, M. E. Colvin, N. M. Marinov, W. J. Pit, and S. M. Senkan, "Reaction mechanisms in aromatic hydrocarbon formation involving the C5H5 cyclopentadienyl moiety," *Symp. Combust.*, vol. 26, no. 1, pp. 685–692, Jan. 1996, doi: 10.1016/S0082-0784(96)80276-1.

[175] S. Sharma and W. H. Green, "Computed Rate Coefficients and Product Yields for c -C5H5 + CH3 → Products," *J. Phys. Chem. A*, vol. 113, no. 31, pp. 8871–8882, Aug. 2009, doi: 10.1021/jp900679t.

[176] A. R. Ghildina, D. P. Porfiriev, V. N. Azyazov, and A. M. Mebel, "The mechanism and rate constants for oxidation of indenyl radical C9H7 with molecular oxygen O2: a theoretical study," *Phys. Chem. Chem. Phys.*, vol. 21, no. 17, pp. 8915–8924, Apr. 2019, doi: 10.1039/C9CP01122F.

[177] S. Sinha, R. K. Rahman, and A. Raj, "On the role of resonantly stabilized radicals in polycyclic aromatic hydrocarbon (PAH) formation: Pyrene and fluoranthene formation from benzyl-indenyl addition," *Phys. Chem. Chem. Phys.*, vol. 19, no. 29, 2017, doi: 10.1039/c7cp02539d.

[178] A. R. Ghildina, D. P. Porfiriev, V. N. Azyazov, and A. M. Mebel, "Scission of the Five-Membered Ring in 1- H -Inden-1-one C9H6 O and Indenyl C9H7 in the Reactions with H and O Atoms," *J. Phys. Chem. A*, vol. 123, no. 27, pp. 5741–5752, Jul. 2019, doi: 10.1021/acs.jpca.9b04578.

[179] H. Jin *et al.*, "Experimental and kinetic modeling study of laminar coflow diffusion methane flames doped with 2-butanol," *Proc. Combust. Inst.*, vol. 35, no. 1, pp. 863–871, Jan. 2015, doi: 10.1016/J.PROCI.2014.05.128.

[180] C. Cavallotti, S. Mancarella, R. Rota, and S. Carrà, "Conversion of C5 into C6 Cyclic Species through the Formation of C7 Intermediates," *J. Phys. Chem. A*, vol. 111, no. 9, pp. 3959–3969, 2007, doi: 10.1021/JP067117F.

[181] Y. Georgievskii, J. A. Miller, and S. J. Klippenstein, "Association rate constants for reactions between resonance-stabilized radicals: C3H3 + C3H3, C3H3 + C3H5, and C3H5 + C3H5," *Phys. Chem. Chem. Phys.*, vol. 9, no. 31, pp. 4259–4268, Aug. 2007, doi: 10.1039/B703261G.

DOI: 10.14750/ME.2022.010

[182] A. Galler, J. Canfield, and J. K. Freericks, "Schrodinger's original quantum-mechanical solution for hydrogen," Jul. 2020, Accessed: Mar. 12, 2021. [Online]. Available: http://arxiv.org/abs/2007.14798.

[183] E. Schrödinger, "Quantisierung als Eigenwertproblem," *Ann. Phys.*, vol. 384, pp. 489–527, 1926.

[184] E. Schrödinger, "Quantisierung als Eigenwertproblem," *Ann. Phys.*, vol. 384, pp. 361–376, 1926.

[185] Schrödinger E., "Quantisierung als Eigenwertproblem," *Annelen der Phys.*, vol. 385, pp. 437–490, 1926.

[186] T. Veszprémi, M. Fehér, T. Veszprémi, and M. Fehér, "Fundamentals of Group Theory," in *Quantum Chemistry*, Springer US, 1999, pp. 3–27.

[187] L. S. Cederbaum, "Born-Oppenheimer approximation and beyond for time-dependent electronic processes," *J. Chem. Phys.*, vol. 128, no. 12, p. 124101, Mar. 2008, doi: 10.1063/1.2895043.

[188] M. J. Frisch *et al.*, "Gaussian 03, Revision C.02.," *Gaussian Inc. Wallingford CT*, 2004.

[189] B. Santra, "Density-Functional Theory Exchange-Correlation Functionals for Hydrogen Bonds in Water," Technischen Universitat Berlin, 2010.

[190] D. R. Hartree, "The Wave Mechanics of an Atom with a Non-Coulomb Central Field Part I Theory and Methods," *Math. Proc. Cambridge Philos. Soc.*, vol. 24, no. 1, pp. 89–110, 1928, doi: 10.1017/S0305004100011919.

[191] C. C. J. Roothaan, "New developments in molecular orbital theory," *Rev. Mod. Phys.*, vol. 23, no. 2, pp. 69–89, Apr. 1951, doi: 10.1103/RevModPhys.23.69.

[192] M. Marsman, A. Grüneis, J. Paier, and G. Kresse, "Second-order Møller-Plesset perturbation theory applied to extended systems. I. Within the projector-augmented-wave formalism using a plane wave basis set," *J. Chem. Phys.*, vol. 130, no. 18, p. 184103, May 2009, doi: 10.1063/1.3126249.

[193] C. Møller and M. S. Plesset, "Note on an approximation treatment for many-electron systems," *Phys. Rev.*, vol. 46, no. 7, pp. 618–622, Oct. 1934, doi: 10.1103/PhysRev.46.618.

[194] M. J. Frisch, M. Head-Gordon, and J. A. Pople, "A direct MP2 gradient method," *Chem. Phys. Lett.*, vol. 166, no. 3, pp. 275–280, Feb. 1990, doi: 10.1016/0009-2614(90)80029-D.

[195] P. Hohenberg and W. Kohn, "Inhomogeneous electron gas," *Phys. Rev.*, vol. 136, no. 3B, p. B864, Nov. 1964, doi: 10.1103/PhysRev.136.B864.

[196] J. P. Perdew, "Jacob's ladder of density functional approximations for the exchange-correlation energy," in *AIP Conference Proceedings*, Feb. 2003, vol. 577, no. 1, pp. 1–20, doi: 10.1063/1.1390175.

DOI: 10.14750/ME.2022.010

[197] L. G. Ferreira, V. Ozoliņš, and A. Zunger, "Fitting of accurate interatomic pair potentials for bulk metallic alloys using unrelaxed LDA energies," *Phys. Rev. B - Condens. Matter Mater. Phys.*, vol. 60, no. 3, pp. 1687–1696, Jul. 1999, doi: 10.1103/PhysRevB.60.1687.

[198] D. M. Ceperley and B. J. Alder, "Ground state of the electron gas by a stochastic method," *Phys. Rev. Lett.*, vol. 45, no. 7, pp. 566–569, Aug. 1980, doi: 10.1103/PhysRevLett.45.566.

[199] J. P. Perdew, "Density-functional approximation for the correlation energy of the inhomogeneous electron gas," *Phys. Rev. B*, vol. 33, no. 12, pp. 8822–8824, Jun. 1986, doi: 10.1103/PhysRevB.33.8822.

[200] J. P. Perdew and Y. Wang, "Accurate and simple analytic representation of the electron-gas correlation energy," *Phys. Rev. B*, vol. 45, no. 23, pp. 13244–13249, Jun. 1992, doi: 10.1103/PhysRevB.45.13244.

[201] S. H. Vosko, L. Wilk, and M. Nusair, "Accurate spin-dependent electron liquid correlation energies for local spin density calculations: a critical analysis," *Can. J. Phys.*, vol. 58, no. 8, pp. 1200–1211, Aug. 1980, doi: 10.1139/p80-159.

[202] K. Capelle, "A bird's-eye view of density-functional theory," in *Brazilian Journal of Physics*, 2006, vol. 36, no. 4 A, pp. 1318–1341, doi: 10.1590/s0103-97332006000700035.

[203] J. P. Perdew, K. Burke, and M. Ernzerhof, "Generalized gradient approximation made simple," *Phys. Rev. Lett.*, vol. 77, no. 18, pp. 3865–3868, Oct. 1996, doi: 10.1103/PhysRevLett.77.3865.

[204] A. D. Becke, "Density-functional exchange-energy approximation with correct asymptotic behavior," *Phys. Rev. A*, vol. 38, no. 6, pp. 3098–3100, Sep. 1988, doi: 10.1103/PhysRevA.38.3098.

[205] C. Lee, W. Yang, and R. G. Parr, "Development of the Colle-Salvetti correlation-energy formula into a functional of the electron density," *Phys. Rev. B*, vol. 37, no. 2, p. 785, Jan. 1988, doi: 10.1103/PhysRevB.37.785.

[206] V. N. Staroverov, G. E. Scuseria, J. Tao, and J. P. Perdew, "Comparative assessment of a new nonempirical density functional: Molecules and hydrogen-bonded complexes," *J. Chem. Phys.*, vol. 119, no. 23, pp. 12129–12137, Dec. 2003, doi: 10.1063/1.1626543.

[207] A. D. Becke, "Becke's three parameter hybrid method using the LYP correlation functional," *J. Chem. Phys.*, vol. 98, no. 492, pp. 5648–5652, 1993.

[208] S. Banerjee and D. Bhattacharyya, "Electronic properties of nano-graphene sheets calculated using quantum chemical DFT," *Comput. Mater. Sci.*, vol. 44, no. 1, pp. 41–45, Nov. 2008, doi: 10.1016/J.COMMATSCI.2008.01.044.

DOI: 10.14750/ME.2022.010

[209] I. A. Titaley, D. M. Walden, S. E. Dorn, O. M. Ogba, S. L. Massey Simonich, and P. H. Y. Cheong, "Evaluating Computational and Structural Approaches to Predict Transformation Products of Polycyclic Aromatic Hydrocarbons," *Environ. Sci. Technol.*, vol. 53, no. 3, pp. 1595–1607, Feb. 2019, doi: 10.1021/acs.est.8b05198.

[210] Y. Zhao and G. D. Truhlar, "The M06 suite of density functionals for main group thermochemistry, thermochemical kinetics, noncovalent interactions, excited states, and transition elements: two new functionals and systematic testing of four M06-class functionals and 12 other function," *Theor. Chem. Acc.*, vol. 120, no. 1–3, pp. 215–241, May 2008, doi: 10.1007/s00214-007-0310-x.

[211] H. Lin and D. G. Truhlar, "QM/MM: What have we learned, where are we, and where do we go from here?," in *Theoretical Chemistry Accounts*, Feb. 2007, vol. 117, no. 2, pp. 185–199, doi: 10.1007/s00214-006-0143-z.

[212] M. Nayebzadeh, M. Vahedpour, A. Shiroudi, and J. M. Rius-Bartra, "Kinetics and oxidation mechanism of pyrene initiated by hydroxyl radical. A theoretical investigation," *Chem. Phys.*, vol. 528, p. 110522, Jan. 2020, doi: 10.1016/j.chemphys.2019.110522.

[213] R. Jasiński, "Searching for zwitterionic intermediates in Hetero Diels–Alder reactions between methyl α,p-dinitrocinnamate and vinyl-alkyl ethers," *Comput. Theor. Chem.*, vol. 1046, pp. 93–98, Oct. 2014, doi: 10.1016/J.COMPTC.2014.08.002.

[214] Y. Zhao and D. G. Truhlar, "The Minnesota density functionals and their applications to problems in mineralogy and geochemistry," in *Theoretical and Computational Methods in Mineral Physics: Geophysical Applications*, Walter de Gruyter GmbH, 2018, pp. 19–38.

[215] Y. Zhao, D. T.-T. J. of chemical Physics, and U. 2006, "A new local density functional for main-group thermochemistry, transition metal bonding, thermochemical kinetics, and noncovalent interactions," *aip.scitation.org*, vol. 125, no. 19, 2006, doi: 10.1063/1.2370993.

[216] J. Da Chai and M. Head-Gordon, "Systematic optimization of long-range corrected hybrid density functionals," *J. Chem. Phys.*, vol. 128, no. 8, p. 084106, 2008, doi: 10.1063/1.2834918.

[217] J. Da Chai and M. Head-Gordon, "Long-range corrected hybrid density functionals with damped atom-atom dispersion corrections," *Phys. Chem. Chem. Phys.*, vol. 10, no. 44, pp. 6615–6620, 2008, doi: 10.1039/b810189b.

[218] N. Mardirossian and M. Head-Gordon, "Thirty years of density functional theory in computational chemistry: an overview and extensive assessment of 200 density functionals," *Mol. Phys.*, vol. 115, no. 19, pp. 2315–2372, Oct. 2017, doi: 10.1080/00268976.2017.1333644.

DOI: 10.14750/ME.2022.010

[219] E. R. Davidson and D. Feller, "Basis Set Selection for Molecular Calculations," *Chem. Rev.*, vol. 86, no. 4, pp. 681–696, 1986, doi: 10.1021/cr00074a002.

[220] V. A. Rassolov, M. A. Ratner, J. A. Pople, P. C. Redfern, and L. A. Curtiss, "6-31G* basis set for third-row atoms," *J. Comput. Chem.*, vol. 22, no. 9, pp. 976–984, Jul. 2001, doi: 10.1002/jcc.1058.

[221] A. Schäfer, H. Horn, and R. Ahlrichs, "Fully optimized contracted Gaussian basis sets for atoms Li to Kr," *J. Chem. Phys.*, vol. 97, no. 4, p. 2571, Jun. 1998, doi: 10.1063/1.463096.

[222] A. Schäfer, C. Huber, and R. Ahlrichs, "Fully optimized contracted Gaussian basis sets of triple zeta valence quality for atoms Li to Kr," *J. Chem. Phys.*, vol. 100, no. 8, pp. 5829–5835, 1994, doi: 10.1063/1.467146.

[223] F. Weigend and R. Ahlrichs, "Balanced basis sets of split valence, triple zeta valence and quadruple zeta valence quality for H to Rn: Design and assessment of accuracy," *Phys. Chem. Chem. Phys.*, vol. 7, no. 18, pp. 3297–3305, Aug. 2005, doi: 10.1039/B508541A.

[224] F. Weigend, "Accurate Coulomb-fitting basis sets for H to Rn," *Phys. Chem. Chem. Phys.*, vol. 8, no. 9, pp. 1057–1065, Feb. 2006, doi: 10.1039/B515623H.

[225] R. Benassi, "A proposed modification of CBS-4M model chemistry for application to molecules of increasing molecular size," *Theor. Chem. Acc.*, vol. 106, no. 4, pp. 259–263, Sep. 2001, doi: 10.1007/s002140100274.

[226] E. K. Pokon, M. D. Liptak, S. Feldgus, and G. C. Shields, "Comparison of CBS-QB3, CBS-APNO, and G3 predictions of gas phase deprotonation data," *J. Phys. Chem. A*, vol. 105, no. 45, pp. 10483–10487, Nov. 2001, doi: 10.1021/jp012920p.

[227] S. P. Verevkin, V. V. Turovtsev, I. V. Andreeva, Y. D. Orlov, A. A. Pimerzin, and S. P. Verevkin, "Webbing a network of reliable thermochemistry around lignin building blocks: tri-methoxy-benzenes," *RSC Adv.*, vol. 11, no. 18, pp. 10727–10737, Mar. 2021, doi: 10.1039/d1ra00690h.

[228] S. Grimme, J. Antony, S. Ehrlich, and H. Krieg, "A consistent and accurate ab initio parametrization of density functional dispersion correction (DFT-D) for the 94 elements H-Pu," *J. Chem. Phys.*, vol. 132, no. 15, p. 154104, Apr. 2010, doi: 10.1063/1.3382344.

[229] Yu-Ran Luo, *Comprehensive Handbook of Chemical Bond Energies, ISBN-13:978-0-8493-7366-4*. CRC Press Taylor & Francis Group, 2007.

[230] R. E. Lehr *et al.*, "Bay region theory of polycyclic aromatic hydrocarbon carcinogenesis," *ACS Symp. Ser.*, pp. 63–84, 1985, doi: 10.1021/BK-1985-0283.CH004.

[231] A. D. Becke, "A new mixing of Hartree–Fock and local density-functional theories,"

DOI: 10.14750/ME.2022.010

J. Chem. Phys., vol. 98, no. 2, pp. 1372–1377, Jan. 1993, doi: 10.1063/1.464304.

[232] K. Ishida, K. Morokuma, and A. Komornicki, "The intrinsic reaction coordinate. An ab initio calculation for HNC→HCN and H − +CH 4 →CH 4 +H −," *J. Chem. Phys.*, vol. 66, no. 5, pp. 2153–2156, Mar. 1977, doi: 10.1063/1.434152.

[233] J. A. Montgomery, J. W. Ochterski, and G. A. Petersson, "A complete basis set model chemistry. IV. An improved atomic pair natural orbital method," *J. Chem. Phys.*, vol. 101, no. 7, pp. 5900–5909, Oct. 1994, doi: 10.1063/1.467306.

[234] G. A. Petersson, A. Bennett, T. G. Tensfeldt, M. A. Al-Laham, W. A. Shirley, and J. Mantzaris, "'A complete basis set model chemistry. I. The total energies of closed-shell atoms and hydrides of the first-row atoms,'" *J. Chem. Phys., 89 2193-218.*, 1988.

[235] D. Hou and X. You, "Reaction kinetics of hydrogen abstraction from polycyclic aromatic hydrocarbons by H atoms," *Phys. Chem. Chem. Phys.*, vol. 19, no. 45, pp. 30772–30780, Nov. 2017, doi: 10.1039/C7CP04964A.

[236] C. Gonzales and B. Schlegel, H, "Reaction Path Following in Mass-Wighted Internal Coordinates," *J. Phys. Chem. A*, vol. 90:2154, 1990.

[237] D. M. Burns, I. Iball, and IUCr, "The bond lengths in chrysene," *Acta Crystallogr.*, vol. 9, no. 3, pp. 314–315, Mar. 1956, doi: 10.1107/S0365110X56000851.

[238] C. M. Gittins, E. A. Rohlfing, and C. M. Rohlfing, "Experimental and theoretical characterization of the S1–S0 transition of benzo[a]pyrene," *J. Chem. Phys.*, vol. 105, no. 17, p. 7323, Aug. 1998, doi: 10.1063/1.472591.

[239] D. R. Reed and S. R. Kass, "Experimental determination of the a and b C-H bond dissociation energies in naphthalene," 2000.